RICE UNIVERSITY

HELIUM GAS CHERENKOV DETECTOR

by

AHMAD H. MOHAMMADZADEH

A THESIS SUBMITTED
IN PARTIAL FULFILLMENT OF THE
REQUIREMENTS FOR THE DEGREE

MASTER OF ARTS

RICE

Houston, Texas

June, 1988

RICE UNIVERSITY

HELIUM GAS CHERENKOV DETECTOR

by

AHMAD H. MOHAMMADZADEH

A THESIS SUBMITTED
IN PARTIAL FULFILLMENT OF THE
REQUIREMENTS FOR THE DEGREE

MASTER OF ARTS

APPROVED, THESIS COMMITTEE:

Gerald C. Phillips
Professor of Physics

Hannu E. Miettinen
Associate Professor of Physics

Marjorie D. Corcoran
Associate Professor of Physics

Houston, Texas

June, 1988

ABSTRACT

HELIUM GAS CHERENKOV DETECTOR

by

AHMAD H. MOHAMMADZADEH

We designed and built a large gas Threshold Cherenkov Counter at the Bonner Nuclear Laboratory of Rice University to be used in Fermilab-experiment E-704. We tested and calibrated the detector with an electron beam of 30 GeV/c, at Fermi National Accelerator Laboratory. The efficiency curves for the two different gases Helium and Nitrogen are presented, together with the design, characteristics and performance of the detector. An average collection efficiency of $N_o = 95\ cm^{-1}$ was achieved.

ACKNOWLEDGEMENTS

This thesis is completed only through the help and dedication of my thesis advisor, Professor. G. C. Phillips. I am grateful to him for his timely advice and encouragement. I sincerely thank him for his patience, understanding, and most of all for his genuine kindness. I am also grateful to the other members of my committee, Dr. H. E. Miettinen and Dr. M. D. Corcoran, for reviewing this thesis.

I thank professor J. B. Roberts, Dr. Francesca Nessi, and specially Dr. Marzio Nessi for their assistance in all phases of the work. Special thanks is due to Mr. James Buchanan for designing and building the photomultiplier housing, and Mr. Henry Hinterberger for assisting us with the design of the optics.

I thank my colleagues and all the faculties and staff of the Bonner Nuclear Labratories and Physics Department, for their assistance and cooperations.

At last I wish to thank all members of my family for their courage and support, who give my life meaning far beyond the world of Physics.

TABLE OF CONTENTS

ABSTRACT i

ACKNOWLEDGEMENTS ii

TABLE OF CONTENTS iii

CHAPTER 1: INTRODUCTION 1

CHAPTER 2: PRINCIPLE OF CERENKOV COUNTERS 2

2.1 Cerenkov Light 2

2.2 Cerenkov Light Theory 3

2.3 Relation $I \propto \Theta^2(\frac{1}{\lambda^2})$ 6

2.4 Detection of the Light 7

2.5 Detection Efficiency 8

2.6 Counting Losses 9

2.7 Thershold Cerenkov Detection System 9

2.8 General Description 10

CHAPTER 3: HELIUM GAS CERENKOV DETECTOR CONSTRUCTION DETAILS 11

3.1 Cerenkov Detector Vacuum Vessel 11

3.1.1 Geometry of particle-rays 13

3.1.2 Thin foil 15

3.1.3 Pressure and temperature 17

3.1.4 Mechanical positioning and safety 21

3.2 Mirrors 22

3.2.1 Focal properties and reflectivity 22

3.2.2 Testing 25

3.2.3 Mounting the mirror support plate & the mirrors 30

3.2.4 Alignments and adjustments for C-light 33

3.3 Photomultipliers 35

3.3.1 RCA 8854 specification 36

3.3.2 Base electronics 38

3.3.3 Housing 41

3.3.4 Mounting in the tank 47

3.3.5 Cabling in the tank 49

3.4 Windows 50

3.4.1 Transmisivity 50

3.5 Wavelength Shifters (WLS) 50

3.5.1 Principle of the techniques 52

3.5.2 Materials for WLS 52

3.5.3 Application on photo-tubes 58

3.5.4 Coating the P.M. 59

3.6 Detection Efficiency With & Without WLS. 62

CHAPTER 4: TEST WITH 30 GEV ELECTRONS 65

4.1 Experimental Set-up 65

4.2 Efficiency Measurement 70

4.3 Pulse Height Measurements 72

CHAPTER 5: Experimental Results 74

5.1 Efficiency Vs. Pressure 74

5.2 Pulse Height Distribution Vs. Pressure 77

5.3 Interpretation of Pulse Height Distributions

100

5.3.1 Motivation 100

5.3.2 Means of approach 101

5.3.3 Analysis of the data 102

5.3.4 Conclusions of the P.H.D. study 114

CHAPTER 6: CONCLUSIONS 116

REFERENCES 117

CHAPTER 1

INTRODUCTION

The primary purpose of the design of the Helium gas Cherenkov Counter described in this thesis was for use in the experiment E-704 at Fermilab. The experiment seeks to measure the spin dependence cross sections for inclusive production of charged pions at high X_F. The detector is needed to distinguish between the two charged particles of protons and pions. This purpose is fulfilled by setting the threshold of the detector so that 200 Gev/c through-going protons create no Cherenkov light, but 200 Gev/c pions are detected. The Cherenkov Counter will also be used for the detection of Λ_os which in turn decay into π^- and protons.

Chapter 2 discusses the principle of the Cherenkov Counter. In chapter 3, the construction details of the Rice Helium gas Cherenkov Detection System is presented. Chapter 4 presents the way data was acquired with 30 Gev/c electrons used for calibration. In chapter 5 we present the data and discuss its results which enable one to estimate the number of photoelectrons produced by a through-going charged particle. Chapter 6 includes conclusion and presents the sensitivity of the system.

CHAPTER 2

PRINCIPLE OF CHERENKOV COUNTERS

2.1 CHERENKOV LIGHT.

The discovery of Cherenkov radiation in 1934 by Vavilov[1] and Cherenkov[1] and the subsequent theoretical explanations by Tamm[1] & Frank[1] in 1937 led to a great deal of investigation of the properties of this phenomenon and its applications.

Tamm & Frank developed a classical theory to account for Cherenkov radiation based on the idea that, when high energy charged particles traverse transparent (dielectric) media, part of the light emitted by the excited atoms appears in the form of a coherent wave-front at fixed angle with respect to the trajectory. This phenomenon is known as the Cherenkov effect, after its discoverer. Such radiation is produced whenever the velocity of the particle (βc) exceeds c/n, where c is the speed of light in vacuum and n is the refractive index of the medium. From the Figure (2-1) one sees that the wave-front forms the surface of a cone about the trajectory as axis, such that

$$\text{Cos}\ \theta = \frac{ct/n}{\beta ct} = 1/\beta n = \frac{V_{light}}{V_{particle}}, \qquad \beta > 1/n. \qquad (1.1)$$

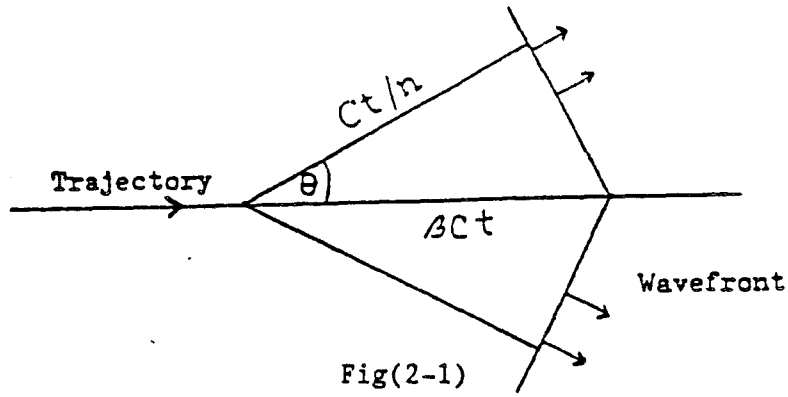

Fig(2-1)

Cherenkov radiation appears as a continuous spectrum.

2.2 CHERENKOV LIGHT THEORY.[1]

If an electron of charge e is moving through a medium along the axis Z with a constant velocity v, the corresponding current density j is equal to

$$j_z = ev\ \delta(x)\delta(y)\delta(z-vt) \qquad (2.1)$$

Where δ denotes Dirac's function. The component j_x and j_y are both zero. Expanding j_z one gets:

$$j_z(\omega) = \frac{e}{2\pi}\, e^{-i\omega z/v}\ \delta(x)\ \delta(y) \qquad (2.2)$$

or, introducing cylindrical co-ordinates ρ and ϕ and z,

$$j_z(\omega) = \frac{e}{4\pi^2\rho}\, e^{-i\omega z/v}\ \delta(\rho). \qquad (2.3)$$

Using the Maxwell equations in the medium and re-writing them as functions of the vector and scalar potentials A and ϕ we get;

$$H_\omega = \mathrm{curl} A_\omega \qquad (2.4)$$

$$\nabla^2 A_\omega + \frac{\omega^2 n^2}{c^2} A_\omega = \frac{-4\pi j_\omega}{c} \qquad (2.5)$$

Now inserting the expression (2.3) into (2.5), and putting

$$A_\rho = A_\phi = 0 \quad \text{and} \quad A_z(\omega) = u(\rho)e^{-i\omega z/v} \tag{2.6}$$

we obtain:

$$\frac{\partial^2}{\partial\rho^2} + \frac{1\partial u}{\rho\partial\rho} + s^2 u = \frac{e}{\pi c\rho}\delta(\rho) \tag{2.7}$$

where;

$$s^2 = \frac{\omega^2}{v^2}(\beta^2 n^2 - 1) = -\sigma^2 \tag{2.8}$$

Thus u is a cylindrical function satisfying the Bessel equation:

$$\frac{\partial^2}{\partial\rho^2} + \frac{1\partial u}{\rho\partial\rho} + s^2 u = 0 \tag{2.9}$$

We now consider two different cases:

An electron moving at low speed, namely at a velocity such that $\beta n<1$. In this case $s^2<0$ and $\sigma^2>0$. The solution of (2.9) vanishing at infinity, is:

$$u = \frac{ie}{2c} H_o^{(1)}(i\sigma\rho) \tag{2.10}$$

where $H_o^{(1)}$ is the Hankle function of the first kind. If $\sigma\rho>>1$, one can use the asymptotic value of $H_o^{(1)}$ and obtain according to (2.6) and (2.10),

$$A_z = \frac{e}{c}\int \frac{\exp[-\sigma\rho+i\omega(t-z/v)]}{\sqrt{2\pi\sigma\rho}}\, d\omega \tag{2.11}$$

thus, in the case of the small velocities, the field of the electron decreases exponentially with ρ, so that at a point remote from the track of the electron, no radiation will be observed.

At high velocities, namely those for which $\beta n>1$, the parameter s in (2.8) is real and the general solution of equations (2.7) and (2.9) represent at infinity, a cylindrical wave. Specifying u in this case

to represent an out- going and not an ingoing wave, we obtain the following solution of (2.9)

$$u = -\frac{ie}{2c} H_o^{(2)} (s\rho), \qquad \text{if} \quad \omega>0 \qquad (2.12)$$

and a complex conjugate if $\omega<0$, s being assumed to be positive. Using the asymptotic value of $H_o^{(2)}$ for $s\rho>>1$, one gets from (2.6) and (2.12):

$$A_z(\omega) = -\frac{e}{c\sqrt{2\pi s\rho}} * \exp[i\omega(t-\frac{z\cos\theta + \rho\sin\theta}{c/n}) + \frac{3}{4}\pi i\ ], \qquad \omega>0.$$

where θ is defined by the coherent relation $\cos\theta = 1/\beta n$. Thus, if $\beta n>1$, a wave is propagated, at infinity, along the direction θ. The electric vector of the wave lies in the meridian plane (z,ρ).

Calculating the field intensity in the wave zone with the aid of (2.4) and (2.5), there are three and only three non-vanishing field vectors, namely:

$$H_\phi = \frac{a}{\sqrt{\rho}} \int\sqrt{s} * \cos\chi * d\omega \qquad (2.13a)$$

$$E_p = -\frac{a}{c\sqrt{\rho}} \int\frac{\sqrt{\beta^2n^2-1}}{\beta^2n^2\sqrt{s}} * \cos\chi * \omega d\omega \qquad (2.13b)$$

$$E_z = \frac{a}{c\sqrt{\rho}} \int(1-\frac{1}{\beta^2n^2}) * \frac{1}{\sqrt{s} * \cos\chi * \omega d\omega} \qquad (2.13c)$$

Where $a = \frac{e}{c}\sqrt{\frac{2}{\pi}}$ and $\chi = \omega[t-\frac{z\cos\theta + \rho\sin\theta}{c/n}] + \frac{\pi}{4}$.

The integrations of (2.13) have to be carried out only over values of ω for which $\beta n(\omega)\geq 1$. The total energy radiated by the electron through the surface of a cylinder of length L whose axis coincides with the line of motion of the electron track, is equal to:

$$W = 2\pi\rho L \int \frac{c}{4\pi} [EH]\, dt \qquad (2.14)$$

using the equations (2.13) and (2.14) enable us arrive at the fundamental equation for the output of radiation, namely

$$\frac{dE}{dL} = \frac{e^2}{c^2} \int_{\beta n>1} (1-\frac{1}{\beta^2 n^2})\ \omega d\omega \qquad (2.15)$$

Since no frequency cut-off has been imposed in deriving this result, the radiation output represented by (2.15) is infinite. In practice, however, a real medium is always dispersive, so that radiation is restricted to those frequency bands for which $n(\omega)>1/\beta$.

2.3 RELATION $I \propto \theta^2(1/\Lambda^2)$

The number of Cherenkov photons N_γ emitted per unit length of a radiator of length L is given by[2]

$$dN_\gamma/dL = 2\pi\alpha Z^2 \int [1-\frac{1}{\beta^2 n^2}]\ d\lambda/\lambda^2 \qquad (3.1)$$

where Ze is the charge of the particle, and λ_1, λ_2 define the limits of the spectral range of the detected radiation. Relation (3.1) shows that most of the Cherenkov light appears at small values of λ, thus blue or ultraviolet light predominates. Neglecting the dependence of n on λ, over a small frequency range, we get

$$N_\gamma = 2\pi\alpha L\ (\frac{1}{\lambda^2_2} - \frac{1}{\lambda^2_1})\ \mathrm{Sin}^2\theta \qquad (3.2)$$

thus; for θ small, $N_\gamma = AL\theta^2$ (3.3)

Where; $A = 2\pi\alpha(\frac{1}{\lambda_2} - \frac{1}{\lambda_1})$

Relation (3.3) indicates the square dependence of the Cherenkov light intensity on Cherenkov angle θ . For the range of spectrum λ_2=200nm and λ_1=500nm the number of Cherenkov-photons N_γ with L in units of Cm is

$$N_\gamma \simeq 1376\ L\ \theta^2 \qquad (3.4)$$

2.4 DETECTION OF THE LIGHT.

Photomultipliers are extensively used as a sensitive light detector providing a charge proportional to light intensity. The photons transmitted through the quartz window and photomultiplier glass hit the photocathode layer which in turn emits electrons by the photoelectric effect. These photoelectrons are electrostatically accelerated and focused onto the first dynode of the electron multiplier. On impact each electron liberates a number of secondary electrons which are, in turn, electrostatically accelerated and focused onto the next dynode. The process is repeated at each subsequent dynode and the secondary electrons from the last dynode are collected at the anode.

The intensity of photoelectrons emitted at the first dynode depends on the energy of the incident light pulse, and they follow individual paths to the second dynode at different points and at different times. Likewise the secondary electrons travel individual paths between the dynodes and anode causing further time dispersion. The photomultiplier output pulse is characterised by its rise time, full width at half maximum and transit time. Typical numbers for

these parameters for the photomultiplier we have used are $2.9 * 10^{-9}$ s, $3.3 * 10^{-9}$ s, and $6.6 * 10^{-8}$ at 3000 volts respectively.

2.5 DETECTION EFFICIENCY[3].

The average number of detected photo-electron in the photomultiplier depends upon the following parameters;

$T(\lambda)$= is the transmission of the radiating medium,

$R(\lambda)$= is the photon collection efficiency,

$q(\lambda)$= is the quantum efficiency of the photocathode,

$A(\lambda)$= is the absorption in the layer of the wavelength shifter on the glass window of the photo-tubes,

$q_e(\lambda)$=is the quantum efficiency for a photon, emitted from the wavelength shifter, that hit the photo-cathode,

$f(\lambda)$ =is the probability that a photon absorbed by the wavelength shifter causes a shifted photon to hit the photo-cathode.

The number of detected photo-electron in the photomultiplier will be

$$N_{p.e.} \approx N_o L \sin^2\theta \qquad (5.1)$$

Where;

$$N_o = 2\pi\alpha \int \frac{d\lambda}{\lambda^2} T(\lambda)\, R(\lambda)\, \{q(\lambda)[1-A(\lambda)]+q_e f A(\lambda)\} \qquad (5.2)$$

In practice the highest reported N_o, (Optical Collection Efficiency) is 168[3]. A high Cherenkov light detection efficiency is achieved in the rice detector by improving the sensitivity to ultraviolet light (up to wavelength λ=180nm), minimizing light losses in the optical

system, using highly reflective mirrors and (RCA-8854) photomultipliers with high quantum efficiency in the UV-region.

2.6 COUNTING LOSSES.

Due to statistical fluctuations in the emission of an average number of photoelectrons ($N_{p.e.}$) from the photocathodes one can define an electronic detection efficiency ε for a counter using a single photomultiplier as

$$\varepsilon = 1 - \mathrm{Exp}[-N_{p.e.}] \ . \qquad (6.1)$$

The values of ε are close to unity, i.e. for N=4.5 photoelectrons the quantity $(1-\varepsilon)$ equals 10^{-2}, and for N=6.9 the $(1-\varepsilon)$ equals 10^{-3}. The useful length L of the Cherenkov counter is a major parameter for the production of photoelectrons, and consequently efficiency ε.

2.7 THRESHOLD CHERENKOV DETECTION SYSTEM.

Threshold Cherenkov counters can be used to discriminate between two relativistic particles of the same momentum P and different masses m_1 & m_2, if the heavier, slower particle (m_2) is just below threshold. In this case, $\beta^2_2 = \frac{1}{n^2}$ where n is the index of refraction of the gas. The gas pressure is adjusted such that only the particle with the fastest [Velocity can produce Cherenkov radiation. After this particle is counted, the index of refraction of the gas is increased by increasing the gas pressure, and each successive particle is counted at its threshold value of index of refraction. Since there are only a few photons per event, photomultipliers with high quantum efficiency

in the UV region are required, and good discrimination for a single-photon event with fast time response are needed.

2.8 GENERAL DESCRIPTION.

The Cherenkov counter structure is shown in Fig(2-2).

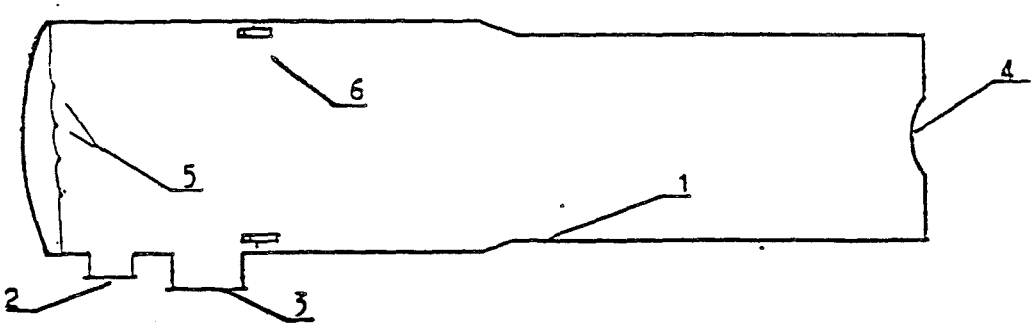

Fig.(2-2)- Cherenkov threshold counter. 1-Steel Vacuum Tank 2-electronic port. 3-Manhole. 4-Thin window. 5-Mirrors. 6-Photomultipliers.

The structure of the counter [Fig(2-2)] is made of two parts for easier construction and transport: a front or "nose" to increase the radiator length and a back which carries the mirrors and photomultipliers fitted with a support to hold the optics in place. The structure, being very large has to be strong enough to avoid deformations that might result in gas leakage and optics misalignment. The inner wall has to be made of material which will not cause contamination by outgassing. A manhole allows access to the optics and a smaller hole makes it possible to run the wires from the photomultiplier to the electronic devices.

CHAPTER 3

HELIUM GAS CHERENKOV DETECTOR CONSTRUCTION DETAILS

3.1 CHERENKOV DETECTOR VACUUM VESSEL

The Rice Cherenkov Counter is a vacuum tank which was fabricated by the Richmond Tank Car Co.[4] of Houston, Texas. This company certified that the tanks confirm to the ASME pressure vessel code and are safe to operate at an external to internal pressure difference of 15 psi at room temperature.

The counter is made of 3/4-inch thick SA 516, steel wall and consists of two 40-feet tanks bolted together to make one 80-foot vessel. One tank is 5 feet in diameter and the other is 6 feet in diameter. At the downstream end of the tank there are an 8-inch port for electronic connections and a 13-inch manhole, which includes the vacuum and gas entry pipes. Figures 3-A and 3-B are photographs of the tank.

Fig.(3-A)- Photograph of the tank taken at MP-9 building at Fermilab.

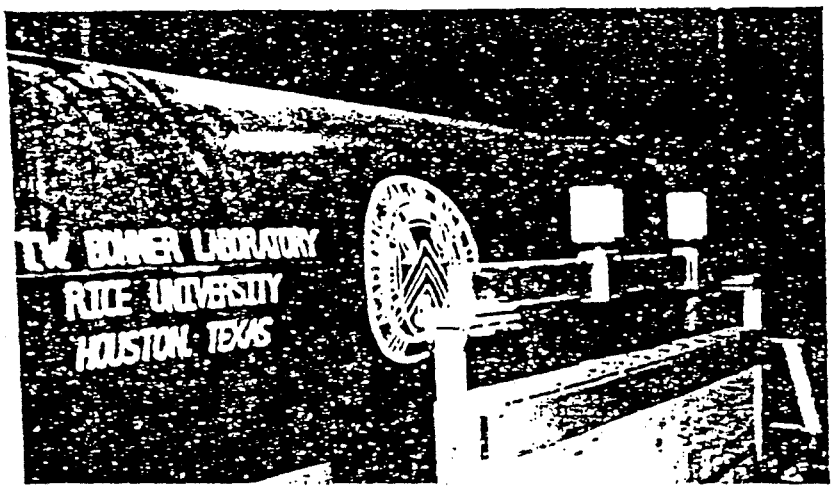

Fig.(3-B)- Photograph taken from inside of the tank.

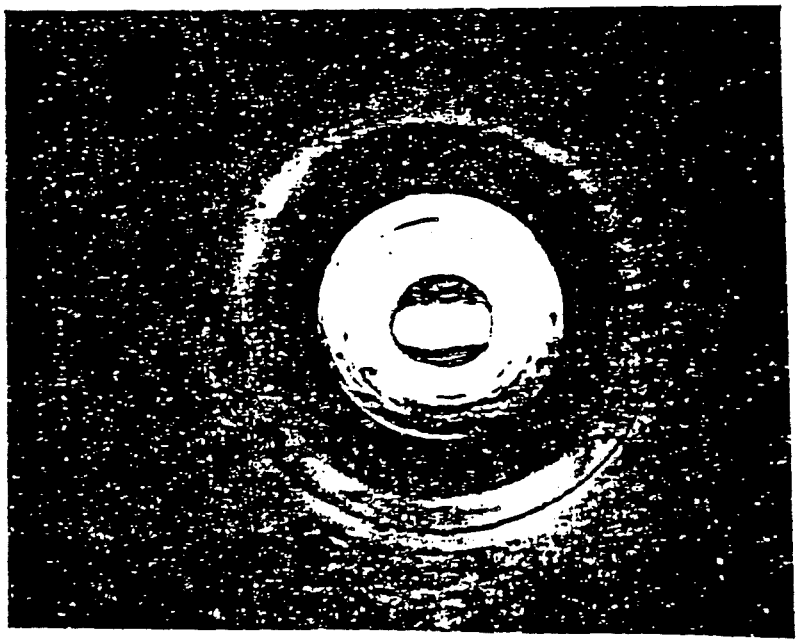

3.1.1 Geometry of the Particle-Rays

The beam used to find the efficiency curve and pulse height distribution of the Rice Cherenkov at MP-9 building, Fermilab where the Rice Cherenkov is set up, was a nominal straight-through beam of 30 GeV. electrons. The momentum of the electron beam was measured by the tagging system 150 feet away from the Cherenkov Counter upstream. Fig. (3-1) shows the electron momentum distribution. The intensity of the test beam received was normally about 10^{12} electron per spill (~20sec. duration, ~60sec. period).

According to the survey engineers at the Fermilab, the 30 GeV. electron beam was at 8′ 2" above the floor, at the downstream end of the tank. We were able to move and locate the Cherenkov tank to the desired position so that the electron beam hit the horizontal center of the 16 mirrors, where the counter is more efficient. The vertical center of the of the Cherenkov mirrors was only 8 feet above the floor for the tests, so that the beam missed the vertical center by 2 inches. This is not a fundamental limitation as explained in section 3.1.4.

Fig.(3-1)- The electron momentum distribution of the test beam in GeV/c.

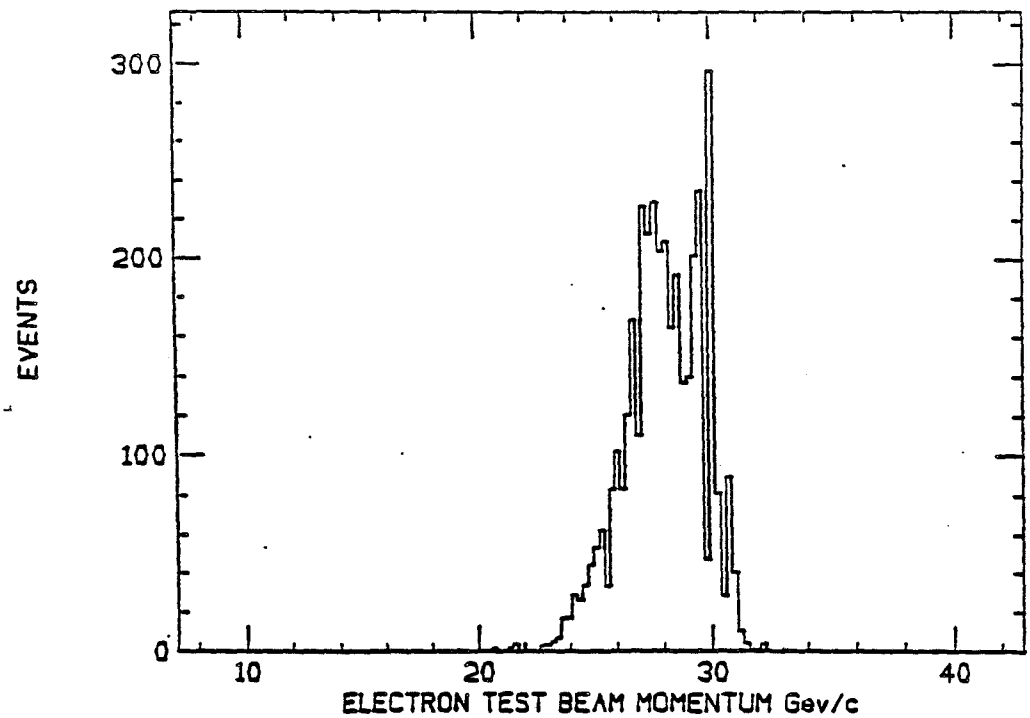

3.1.2 Thin Foil

To decrease the multiple scattering of the high-energy particles as well as their inducing showers and reactions, we installed an 18 mil, type 304 stainless steel 18" by 48" foil at the upstream end of the tank. This replaced the 5-foot diameter, 1.0-inch thick steel tank cover plate.

This thin window was formed pneumatically after being clamped into place and covered by a cover plate to provide a plenum for the injection of compressed air. The cover plate was, of course, removed after forming. Fig. (3-2) shows the thin window assembly. The pressure used to form the window was 62 psi. Since this vacuum vessel will never be operated at an external pressure exceeding one atmosphere or 14.7 psi, the 62 psi used to form the window automatically guarantees a factor of safety of more than 4. This complete procedure was duplicated at fermilab and observed by the Experimental Area Safety Officer, Mr. Bob Scheer. The design of this fabrication and testing system was by Mr. Hank Hinterberger.

Fig.(3-2)- The thin foil assembly.

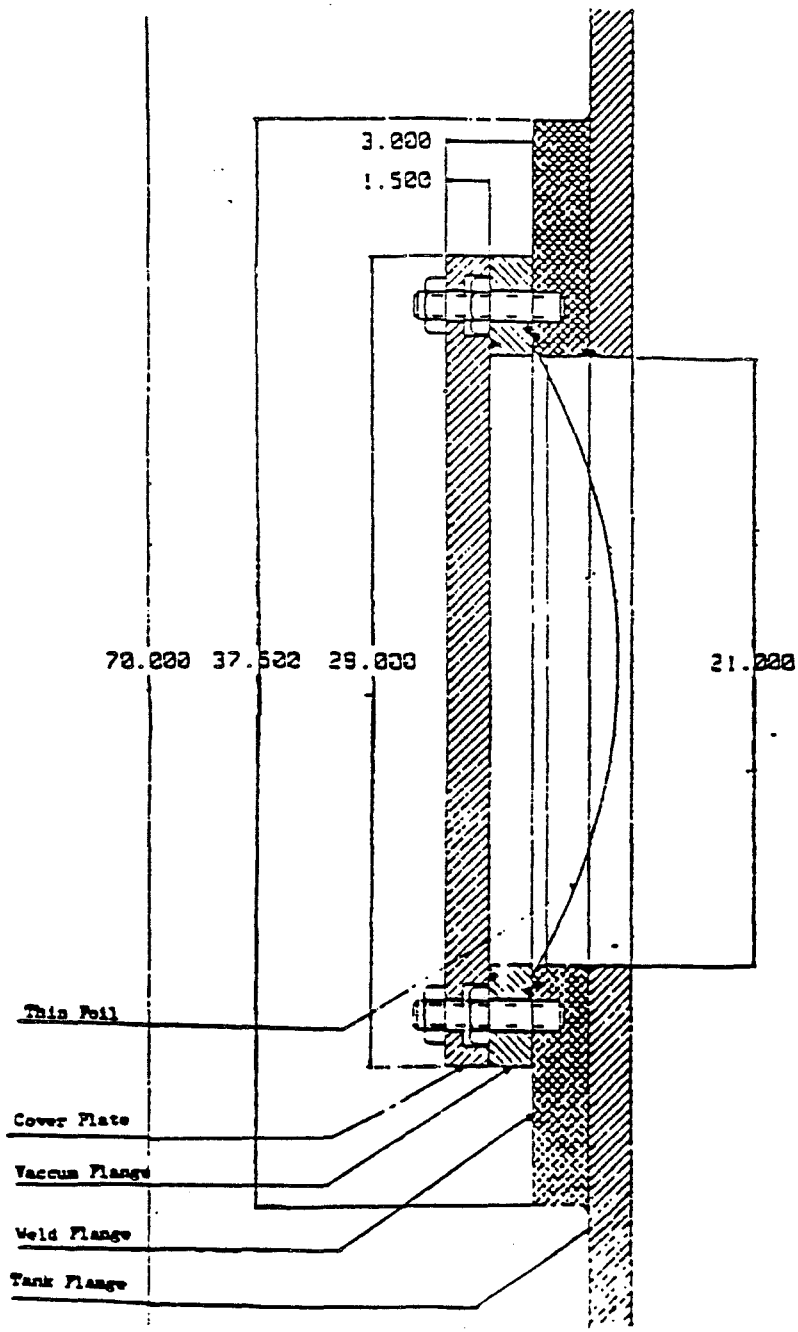

3.1.3 Pressure & Temperature

A gas radiator provides a simple means of changing the refractive index merely by altering the operating pressure. Changing of index of refraction is given by the Lorents Lorenz law:

$$(n^2-1)/(n^2-2) = (R/M)\rho \qquad (3.1)$$

Where R is the molecular refractivity, M is the molecular weight, and ρ is the gas density. For pressures that are not too high, equation (3.1) can be approximated to high accuracy by;

$$(n-1) = (n_o-1)\ P \qquad (3.2)$$

or

$$n = 1+ \eta P \qquad (3.3)$$

Where n_o is the refractive index of the gas for a given wavelength of light, η is n_o-1, at the temperature of the counter and at a pressure of 1 atm. The pressure P, is in atmospheres. The choice of gas depends on the threshold energy required, and this in turn upon the refractive index. For the present application it is necessary to use Helium gas so that the threshold pressure will not be a very small fraction of one atmosphere. Another reason to use helium gas is that the radiating gas must be transparent in UV region and helium gas is outstanding in this regard, with an approximate wavelength cut-off of 60 nm.

To calculate the threshold pressure we set

$$\mathrm{Cos}\theta = 1/\beta n \simeq 1-\theta^2/2 \qquad (3.4)$$

Using equations (3.3) & (3.4), we find

$$\theta^2 = 2\eta_{He}P - \gamma^{-2} \qquad (3.5)$$

threshold; $\theta = 0$

therefore; $$P = 1/2n\gamma^2 \qquad (3.6)$$

Where θ is the threshold angle and P is the pressure in atm. Using the numerical values, $\eta_{He} = 36\times10^{-6}$ and for protons of momentum 200Gev/c, $\gamma\simeq213$, we get

$$P=.305 \text{ atm.} = 231 \text{ mm of Hg.} \qquad (3.7)$$

Using the same procedure we find the expected threshold conditions for the detection of various particles with different energies. Moreover as discussed in section 2.6, by counting loses we can find the efficiency of the counter. Fig. (3-3) shows the predicted efficiency of detection of p^+, K^+, π^+ as functions of the particle energy in GeV, and the chamber pressure of Helium gas in standard atmospheres. The threshold is shown as 0% efficiency. The 90%, 99%, and 99.9% efficiency curves for protons, kaons, pions correspond to the

photomultiplier detecting 2.3, 4.6 and 6.9 photoelectrons.

Fig.(3-3)- The detection efficiency as a function of the energy of the particle.

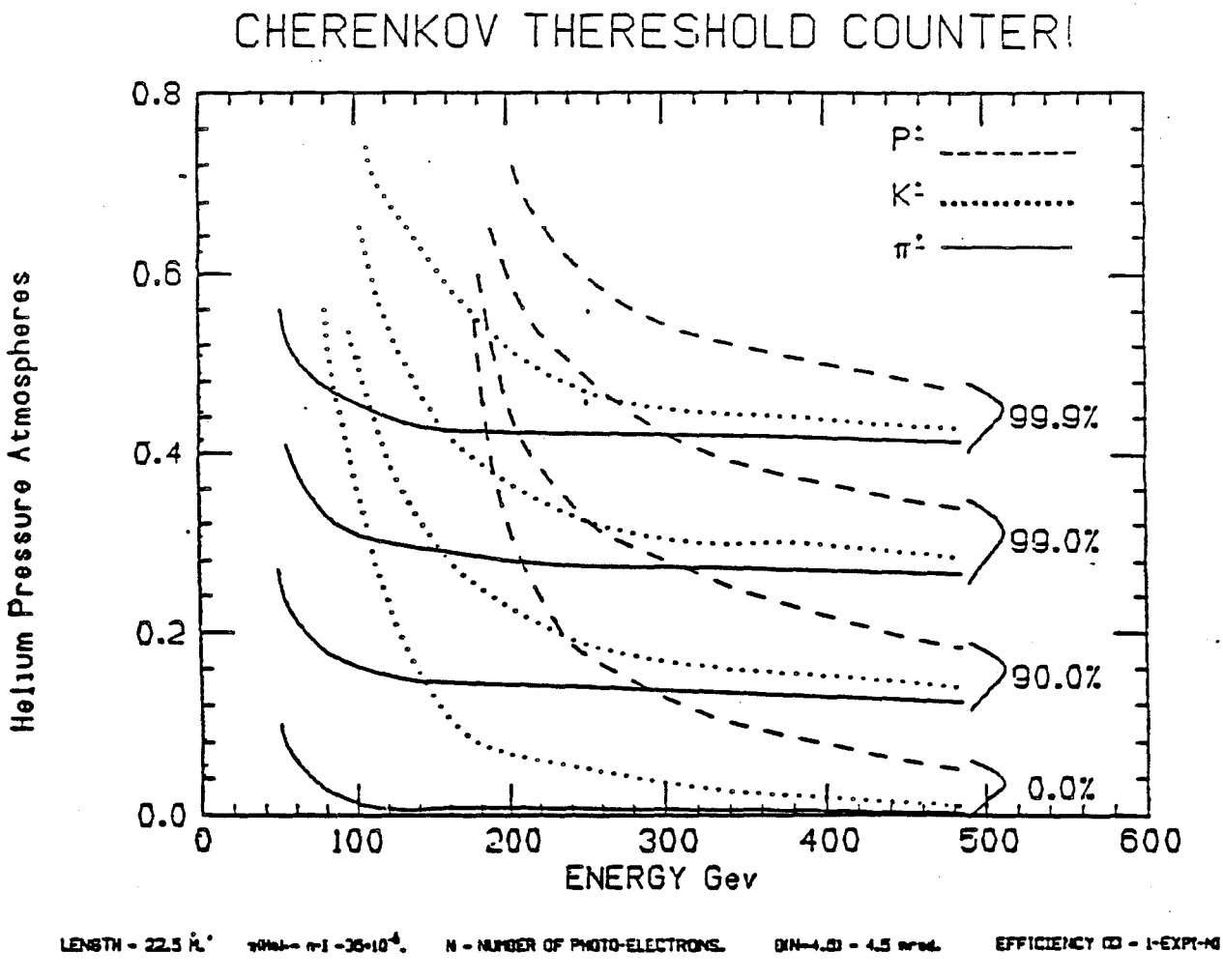

LENGTH = 22.5 M. N = NUMBER OF PHOTO-ELECTRONS. EFFICIENCY

3.1.4 Mechanical Positioning & Safety

To change the position of the tank, the following precautionary measures should be taken:

1-The Cherenkov gas pressure should be changed to one atmosphere, to prevent any implosions.

2-The tank legs must be situated on the prepared square metal-plates at all times. This would help the tank rollers to roll easier at the time of pushing.

3-Before pushing the tank to a different position, most of the tank load must be taken off by using the crane and straps available at MP-9 building, Fermilab.

It is worthwhile to mention that shims on the square metal-plates can also be used to increase the height of the center of the optics from the floor.

3.2 MIRRORS

We used sixteen mirrors that were each coated over an areas of 10" × 10" long and were 3/8" thick, for collection of the Cherenkov light. Each mirror weighed about two pounds and was made of ordinary window glass. The glass was first circle cut, then ground to a spherical concave shape from one side, and it was ground flat on the other side. Later the square substrates were cut to size out of the circular pieces, and the edges were beveled at an angle of 10°. The radius of curvature of mirrors vary from 119.1" to 120.5", which is quite close to the desired radius of 120".

The uncoated mirrors fabricated by S&S Optical Co.[5], were sent to the Evaporated Metal Films Co.[6], for vacuum coatings.

3.2.1 Focal Properties and Reflectivity

The Rice Cherenkov Counter is designed to have spherical mirrors of radius 120±1 inches and good reflective properties in the Ultra-Violet region. Research in the technique of vacuum deposition of Al mirrors coated with thin MgF_2 or LiF protective layers has demonstrated that essentially 80% reflectivities between 1200Å and 2000Å are possible. Above 2000Å, the reflectivity rises to a value of 90% in the visible (see Fig. 3-4). Evaporated Metal Films Co. prepared the mirrors by fast (~1sec.) deposition of Al mirror on a substrate in a very good vacuum (~10^{-7}Torr), followed immediately by the deposition of the protective layer of 250Å of MgF_2. Mirrors not so prepared will usually have bad reflective properties in the UV. It has been observed that such mirrors are stable in air, losing only 2%

reflectivity after one year. The MgF_2 layer is necessary to protect the Al mirror from oxidation and since MgF_2 is transparent down to 1150Å. The reflectivity of the MgF_2 overcoated Al mirrors falls below 1200Å.

Fig.(3-4)- The factory suggested reflectivity of the Al-mirrors as a fuction of wavelength.

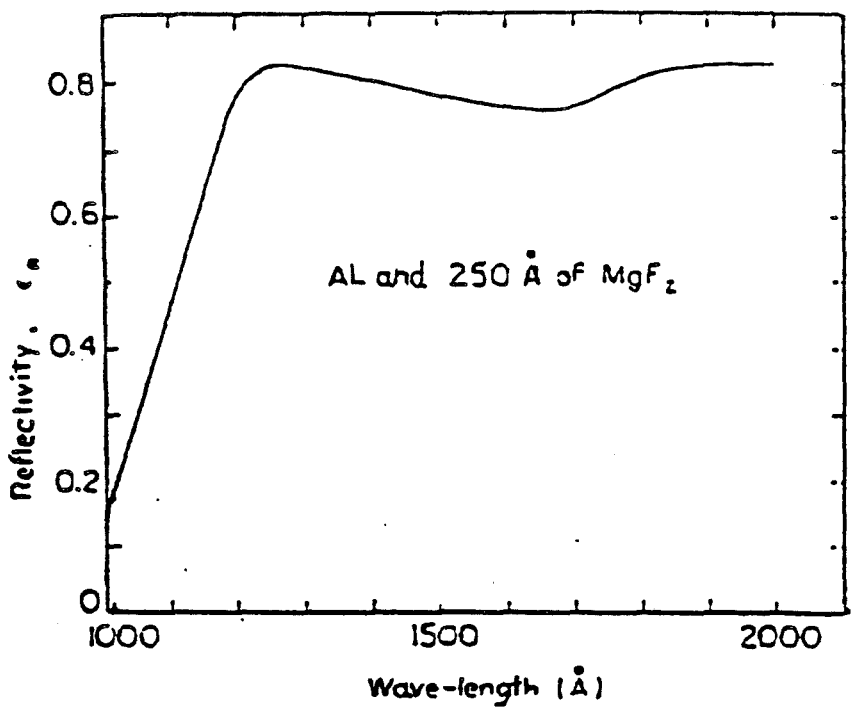

3.2.2 Testing

At Bonner Nuclear Labs, we tested focal properties, reflectivities, distortions and spherical abberations of 10 mirrors. Using the sun as a source, we measured the focal lengths by projecting the image on the wall. The focal lengths measured are indicated in Table 3-1.

MIRROR #	1	2	3	4	5	6	7	8	9	10
FOCAL POINT	119	119.3	118.7	120.5	122.2	120.3	119.4	119.8	118.7	120.3

Table 3-1

To measure the reflectivity of the mirrors versus wavelength of light a laser with three different wavelengths of 193nm, 248.5nm and 350nm was used to aim at 5 different regions of each mirror (the 4 corners & the center). The reflections were focused into a bolometer, an instrument for the detection of a radiant heat by means of the change of resistance of Platinum strips when heated. A temperature change of 10^{-7}°C could be observed. The amount of charge contributed by each reflected pulse was recorded by using an oscilloscope which was connected to the bolometer. We used the same procedure to measure the charge contribution of the undisturbed laser pulses. The reflectivity of each mirror was found by the ratio of the second reading to first. Fig. (3-5) shows the reflectivity of the mirror #1 with three different wavelengths versus the factory suggested

reflectivity (dashed line). Fig. (3-6) & (3-7) show the average reflectivity of 10 mirrors at two different wavelength[Ahs of 193nm and 248.5nm respectively. The measured reflectivities were comparable with the factory suggested reflectivity and were satisfactory.

The spherical abberation was tested by aiming a neon laser beam onto 9 different regions of the mirrors (the corners, center and the sides). The laser was set 100 feet away from the mirror. The 9 image points were marked on grid paper at the focal point of each mirror. A circle of radius 1/4" could confine all the image points, indicating that the spherical abberations of the 10 mirrors tested are insignificant. Moreover, no sign of distortion could be detected by human eye through looking at the images in the mirrors.

Fig.(3-5)- The reflectivity of the 3 different wavelengths, versus the factory suggested reflectivity (dashed curve).

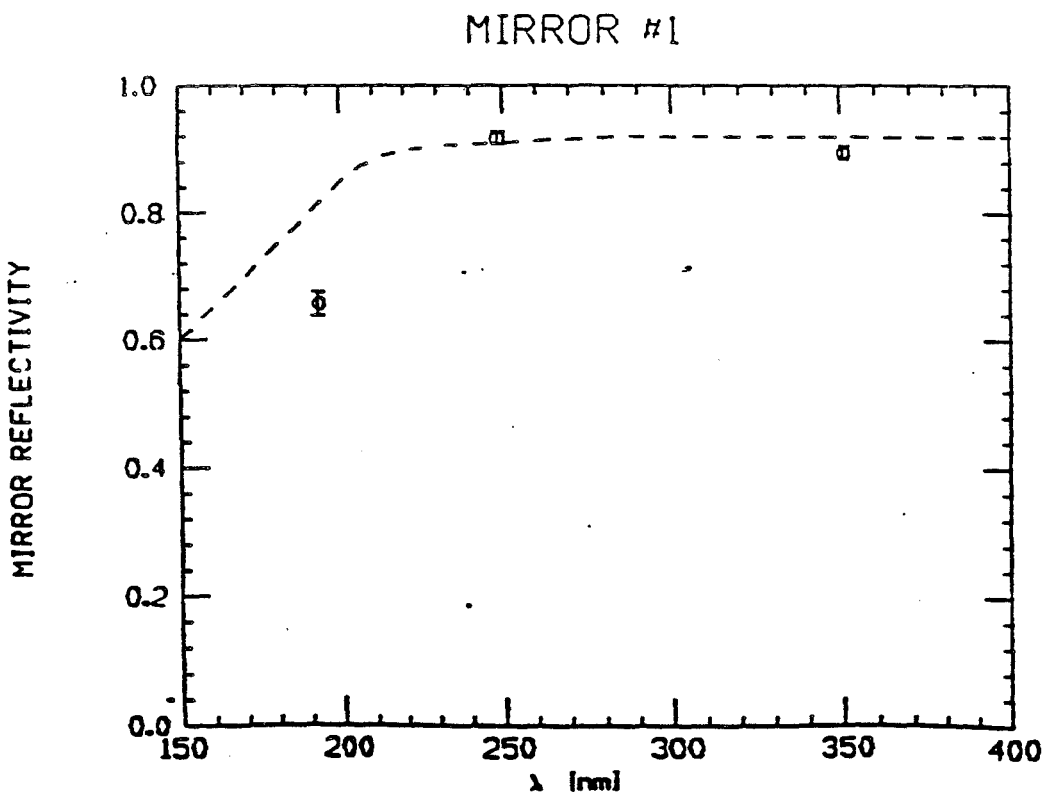

Fig.(3-6)- The average reflectivity of 7 mirrors at λ = 193nm.

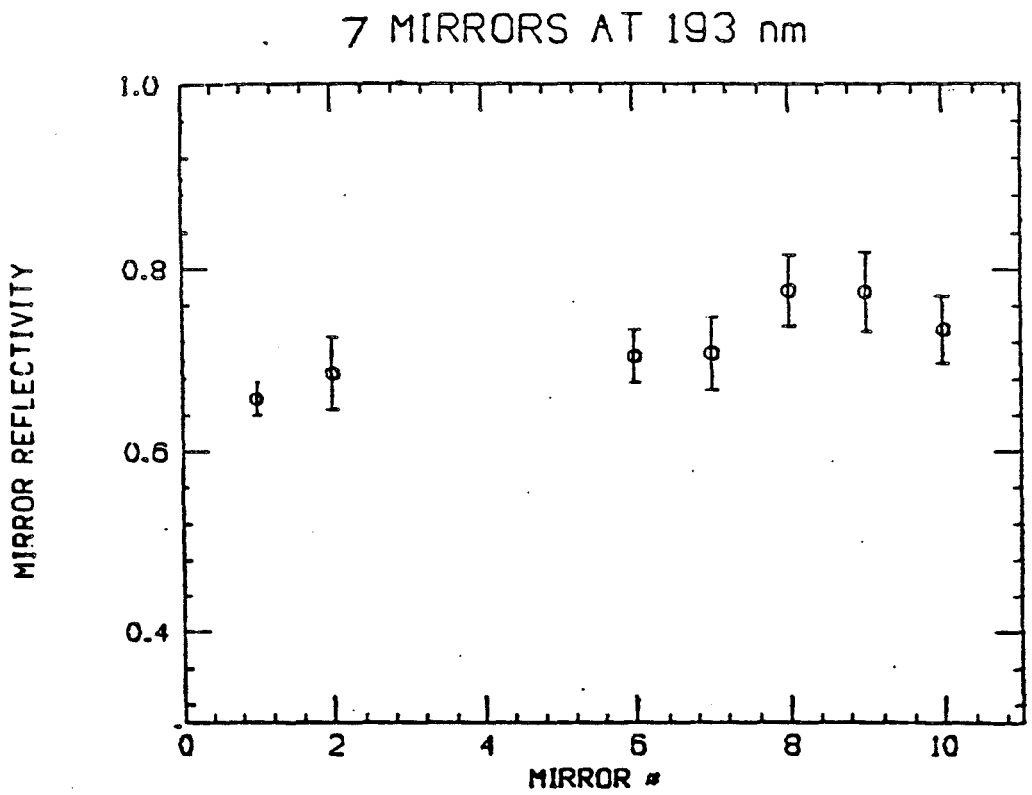

Fig.(3-7)- The average reflectivity of 8 mirrorsa at λ = 248.5nm.

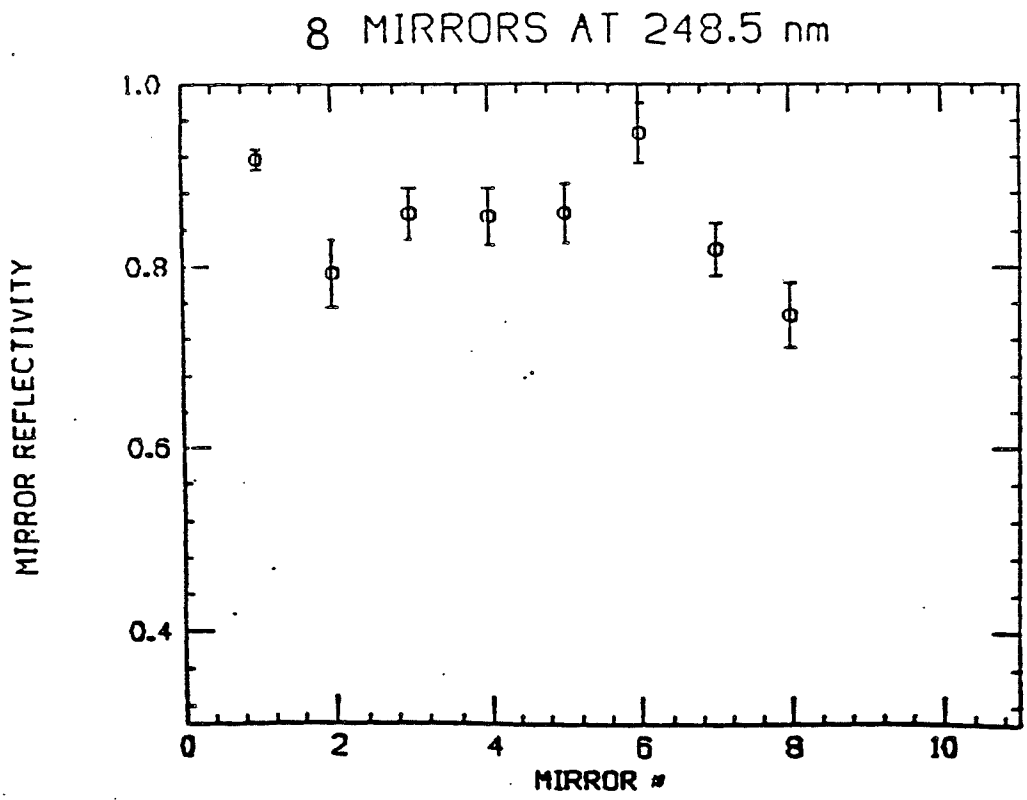

3.2.3 Mounting the Mirror Support Plate & the Mirrors

A 40" × 40", 0.5" thick aluminum plate, the mirror support plate, was installed inside the tank, to hooks on the tank wall by using unistruts. For the purpose of the mass reduction we cut away a few rectangular holes without disturbing the frame structure, as shown in Fig. (3-8). The installed plate is about 1.5 feet away from the downstream end of the vessel. The aluminum plate has 48 holes tapped to fit 10/32" studs. Each stud is 5.0" long and has a 1/4" threaded head which screws into a V-lier, a device that has a ball bearing which swivels (see Fig. 3-9). The V-liers are epoxied at the center of a 3.0" square steel plate with 1/16" thickness, which in turn has a disc magnet 3/8" thick, 1.5" in diameter, epoxied at its center. The design calls for support of each mirror by three studs which form a triangle. On the back of each mirror three, 3.0" square, 1/16" thick steel plates were epoxied, so that the center of each plate coincides with the center of the three support magnets when mirrors are in place. This design allows the mirrors to be accurately positioned. Fig.(3-10) shows the side-view of this set up. Every set of three magnets can hold a mirror in a vertical plane (as shown in Fig. (3-10) which could weigh ~5.5 pounds before it slides downward. Each mirror with its plates weighs only about 2.5 pounds. A safety factor of almost 2 is therefore guaranteed. To enhance the safety factor, we raised the coefficient of frictions by gluing a very fine sand paper (grit 600) on the magnets and the 3.0" square plates. As a result, a safety factor of 4.5 was achieved.

Fig.(3-8)- The picture taken of the mirror suport plate with the studs and magnets in place.

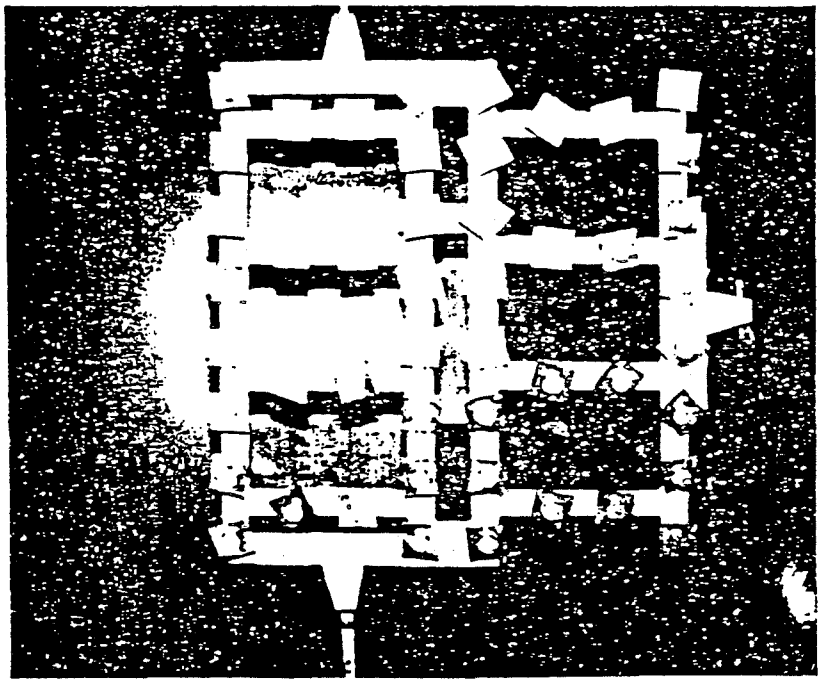

Fig.(3-9)- The Top-View and the Side-View of the V-liers. The V-liers are attached to the studs.

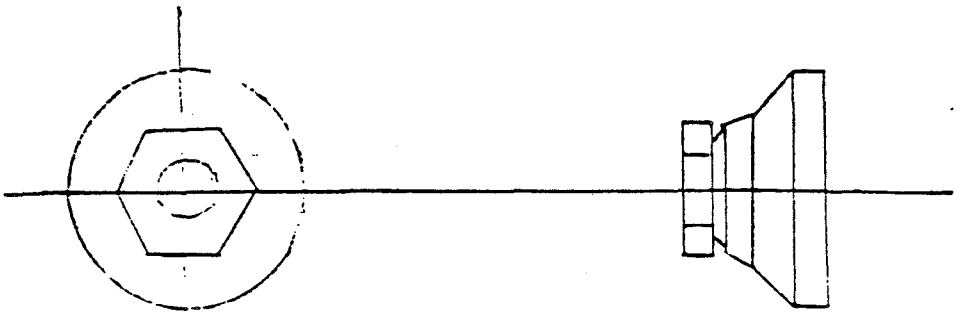

Top-View. **Side-View.**

Fig.(3-10)- The side view of the mirror assembly design

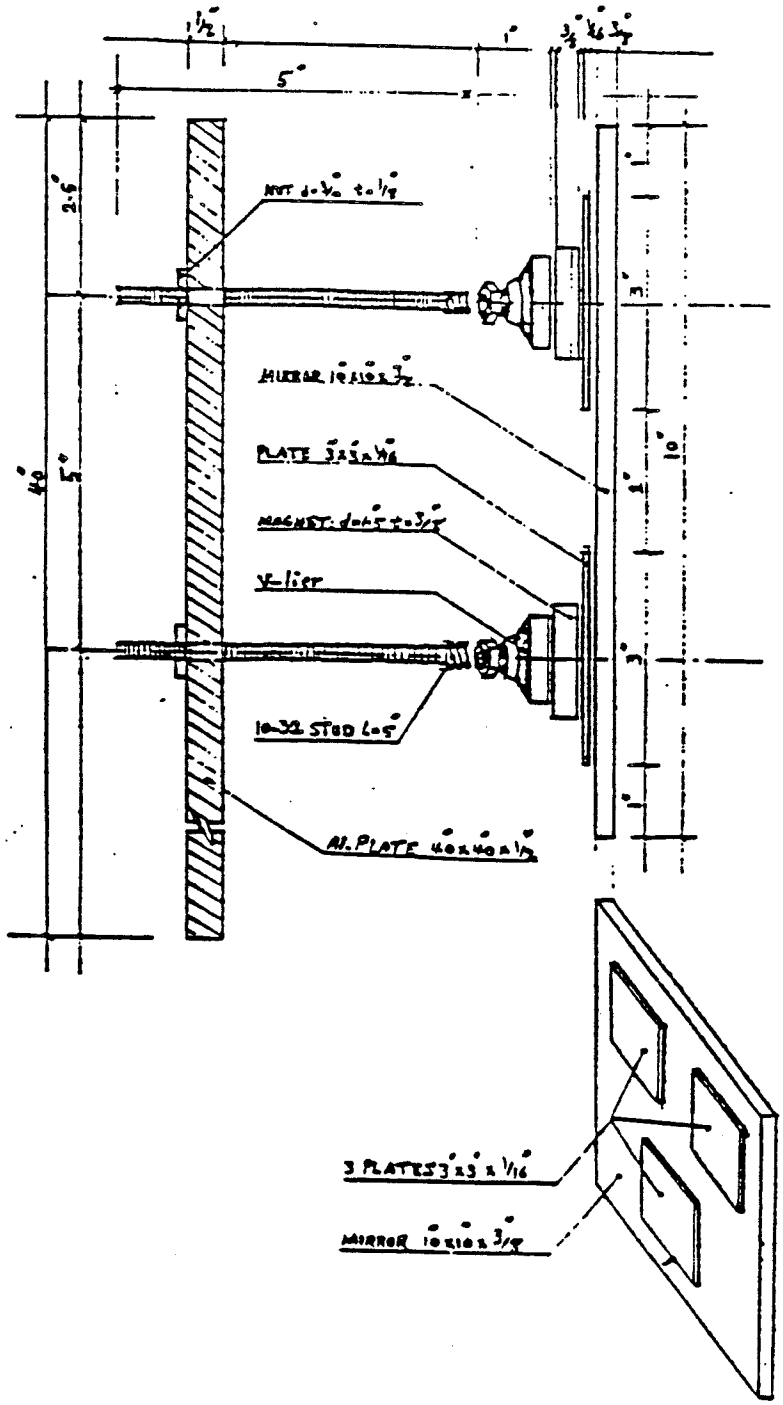

3.2.4 Alignments and Adjustments for C-Light

The size and position of the mirrors to collect the Cherenkov light produced by positively-charged pions in Helium gas was determined by Monte Carlo simulation which was done by Francesca & Marzio Nessi. The result of the simulation and the mirror outline are shown in Fig. (3-11), which shows the mirrors covering an area of 40" × 40" to detect π^+ with $0.3 \leq X_F \leq 0.80$ and P_T up to 2.0 Gev/c.

With the help of a neon laser, every set of four mirrors was adjusted by their studs to form part of a sphere in each quadrant which focuses the Cherenkov light onto the photomultiplier of the corresponding quadrant. The neon laser was positioned at the center of the entrance-thin-foil and directed to illuminate the center of each four-mirror system in turn. The mirrors on all quadrants were also aligned so that there is a minimum gap of 1/16" or less between every two adjacent quadrants.

A Fig.(3-11)- Scatter plot of x-y positions of π^+ (seen upstream). The undeflected beam is the x, while the dashed circle is the magnetically deflected beam spot. The horizental and vertical scales are in centimeters and the 16 mirrors are shown inside the 6-foot diameter tank.

3.3 PHOTOMULTIPLIERS

RCA 8854 5.0" active diameter photomultiplier tubes were selected for the Cherenkov Counter. The properties of the RCA 8854 photomultipliers are described according to its manual as follows:

RCA 8854 is a 5" diameter, 14 stage head-on Quanta-Con photomultiplier having a bialkali photocathode of high quantum efficiency and extremely high-gain cesiated gallium-phosphide first dynode followed by high stability copper berylium dynodes in the succeeding states. The 8854 features high quantum efficiency, ultra-violet response, uniform electron collection from the major portion of the photocathode, fast time response and high current amplification

"The first dynode of the 8854 tube provides up to an order of magnitude increase in secondary emission ratio over conventional dynode materials. This high ratio provides a pulse height resolution capability that permits the discrimination of up to five or more photoelectron events. The extremely high secondary emission ratio of the first dynode is instrumental in providing a decrease in noise induced in signal current by approximately 20%. These characteristics made the 8854 especially suitable for our Cherenkov Counter.

3.3.1 RCA 8854 Specifications

The RCA 8854 Quantum Efficiency (QE), the average number of photoelectrons emitted per incident photon, is 27% at 400nm. Fig.(3-12) shows the spectral response of the RCA 8854.

The Gain, μ, the ratio of the total number of electrons reaching the anode per second, to those emitted from the photo surface is 4×10^7 with E = 2000 Volts. The gain rises with increase of the voltage.

RCA 8854 features good time resolution: The anode pulse rise time, the time required to rise from 10% to 90% of the amplitude, is 2.9×10^{-9} seconds at 3000 Volts, and the electron transit time, the time interval between the arrival of a delta function light pulse at the entrance window of the photomultiplier and the time when the output pulse at the anode reaches the peak amplitude is 6.6×10^{-8} seconds at 3000 Volts. Moreover, the RCA 8854 has a low anode dark current.

Fig.(3-12)- The curve 118 is the absolute sensitivity of the RCA 8854 photomultipliers (Milliamperes/Watt), as a function of wavelength (nm.)

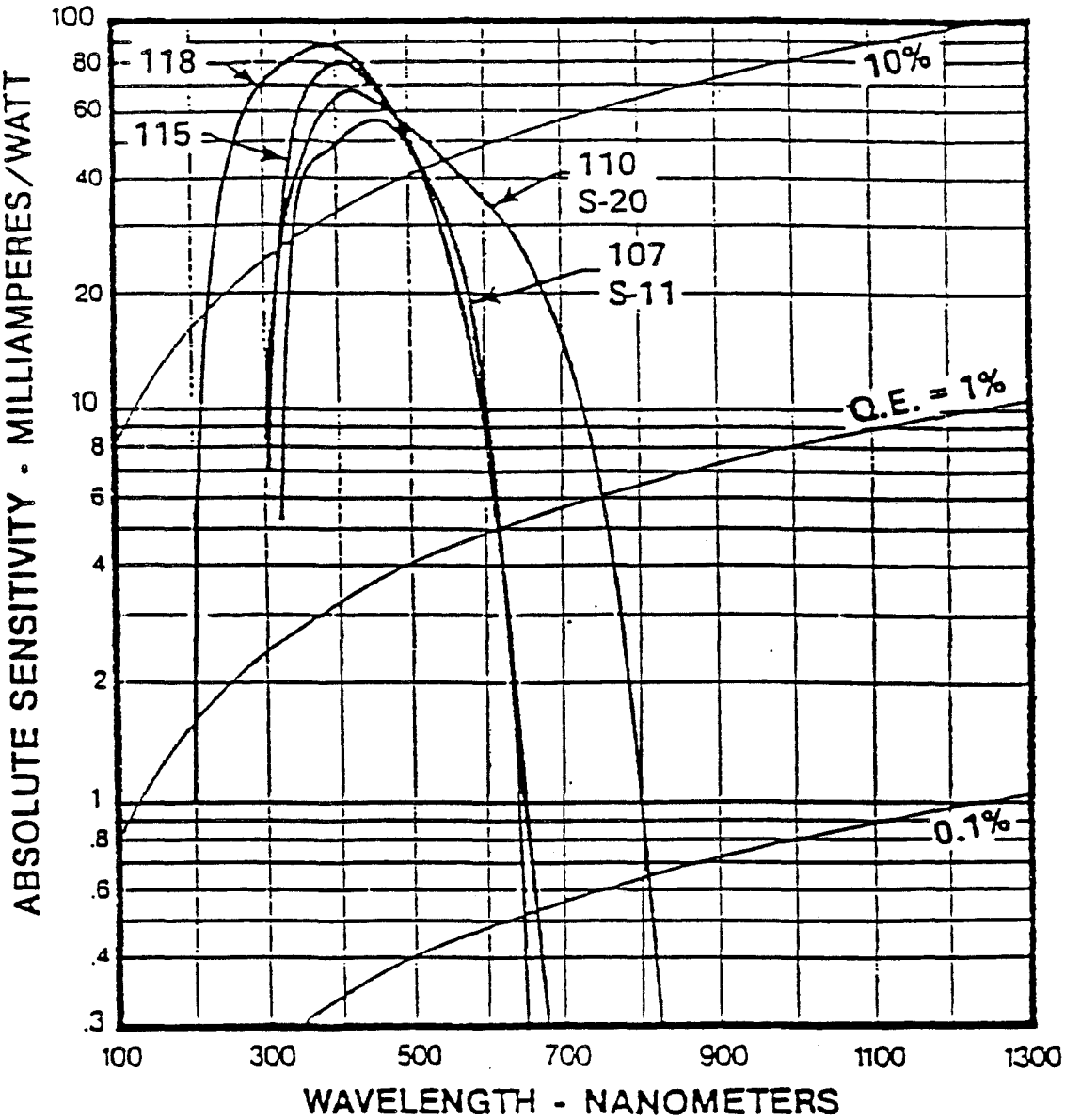

3.3.2 Base electronics

Photomultiplier applications are so diverse that it is often necessary to design a voltage divider chain to satisfy the specific operational requirements. The basic function of the voltage divider circuit consisting of series connected resistors is to provide voltage between each dynode to amplify the electron cascade.

For our application purposes we needed the optimum pulse-height resolution performance. For such a performance we used the factory suggested B-string of the table (3-2). Fig. (3-13) shows the schematic diagram of the voltage divider circuit placed across the high voltage source.

Table 3.2- Voltage distribution for the two different strings of A and B.

Table 3.2		
Voltage Distribution		
Between the following Electrodes: Cathode (K) Dynode (Dy) and Anode (P)	A 5.8% of K-P Voltage (E) Multiplied by:	B* 6.5% of Dy1-P Voltage (E) Multiplied by:
K - Dy1	3	&
Dy1 - Dy2	1	1
Dy2 - Dy3	1	1.5
Dy3 - Dy4	1	1
Dy4 - Dy5	1	1
Dy5 - Dy6	1	1
Dy6 - Dy7	1	1
Dy7 - Dy8	1	1
Dy8 - Dy9	1	1
Dy9 - Dy10	1	1
Dy10 - Dy11	1	1
Dy11 - Dy12	1	1
Dy12 - Dy13	1	1
Dy13 - Dy14	1	1
Dy14 - P	1	1
Dy1 - P	-	14.5
K - P	17	-

* Use distribution B for optimum pulse height resolution performance.

& Cathode to Dynode No 1 Voltage maintained at 650 volts

Fig.(3-13)- The schematic diagram of the voltage divider circuit.

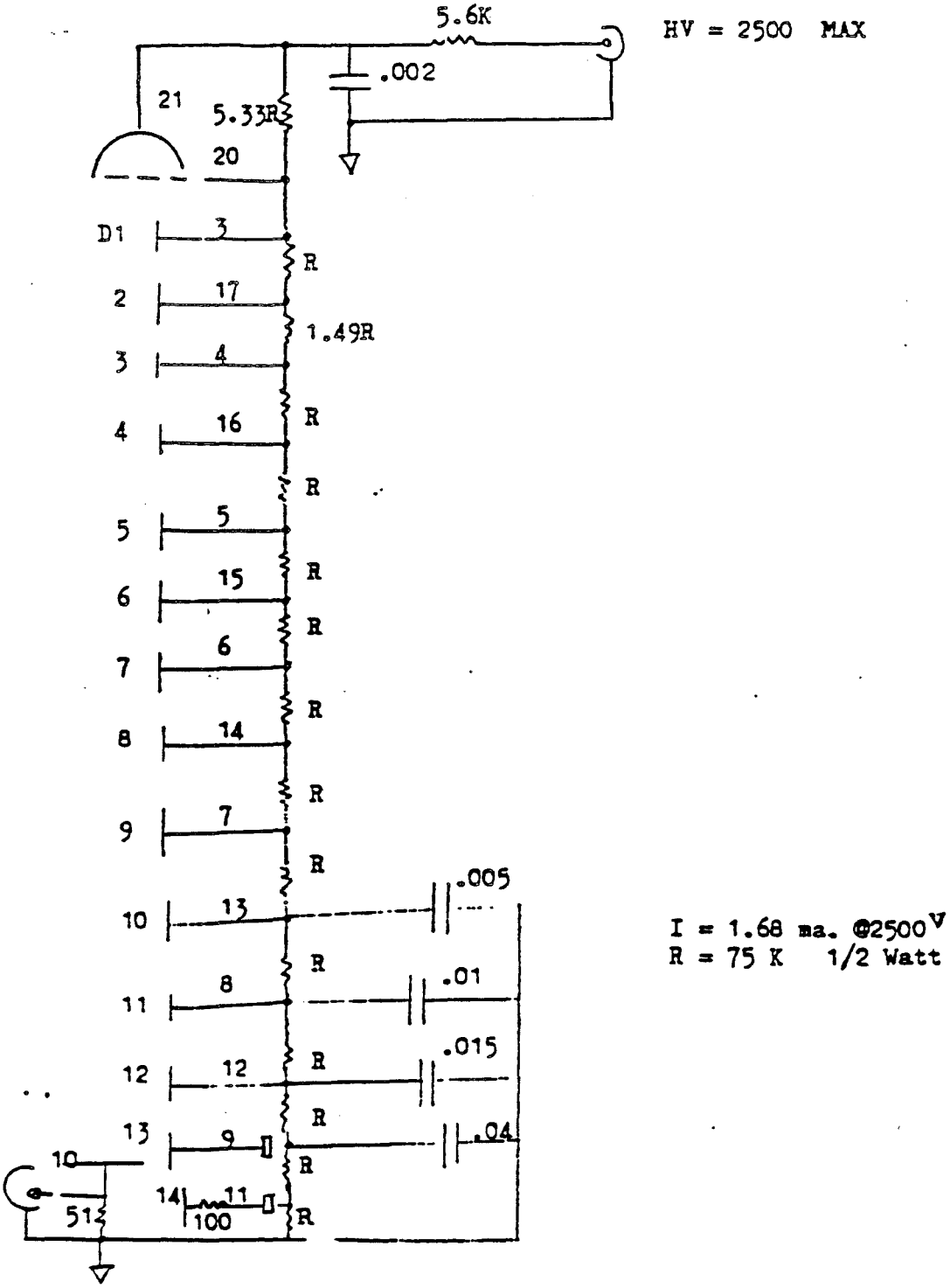

3.3.3 HOUSING

The housing of the four photomultiplier was designed by Mr. James Buchanan. The RCA 8854 photomultiplier tubes were housed in cylindrical cans of 6.065" ID. 0.650" thick and 17.0" long seamless wrought steel pipes. The top end of the cans were sealed off by the quartz windows which were inserted and clamped in place. 1/16" rubber gaskets were used on both sides of the quartz windows. At the bottom end of the cans, the end-plates (Fig. 3-14) were bolted, which in turn were connected to the flexible pipes, not shown in the figures. As shown in Fig. (3-15) the phototubes were pushed forward and held in contact with a nylon (isolating) ring via plexiglass discs by light spring loading applied from the end of the housings (see Fig. 3-16).

The position of the Cherenkov counter with respect to the large magnets at MP-9 building meant that the tubes could be exposed to large magnetic field in addition to the earth's magnetic field. Magnetic shields are essential for reliable and stable operation of photomultiplier tubes which are exposed to magnetic fields, since magnetic fields disturb the electron path from the photocathode, changing the gain characteristics of the tubes. The iron housings are able to shield the high intensity magnetic fields. For low level fields we used Co-netic foil which is primarily used in fields of low intensity in order to utilize its high permeability, and corresponding high attenuation characteristics. Magnetic shields were selected such that 1/16" gap between the Co-netic and glass envelope of the photomultiplier tubes were allowed. An Acrylic cylindrical tube isolated the shielded phototubes, since the Co-netic metal was held at

cathode potential to provide protection against electrostatic interference (see Fig. 3-17).

One has to be careful using photomultiplier tubes around helium in that the envelop is permeable to helium. To avoid this problem, we inserted 1/8" gas tubes in between the Co-netic shield and the phototube in each housing to ventilate the tubes. For the ventilation dry nitrogen gas was used. This gas flow also serve to transport away the heat of the P.M. resistor string across the high voltage.

Fig.(3-14)- The end-plate design of the housing cans.

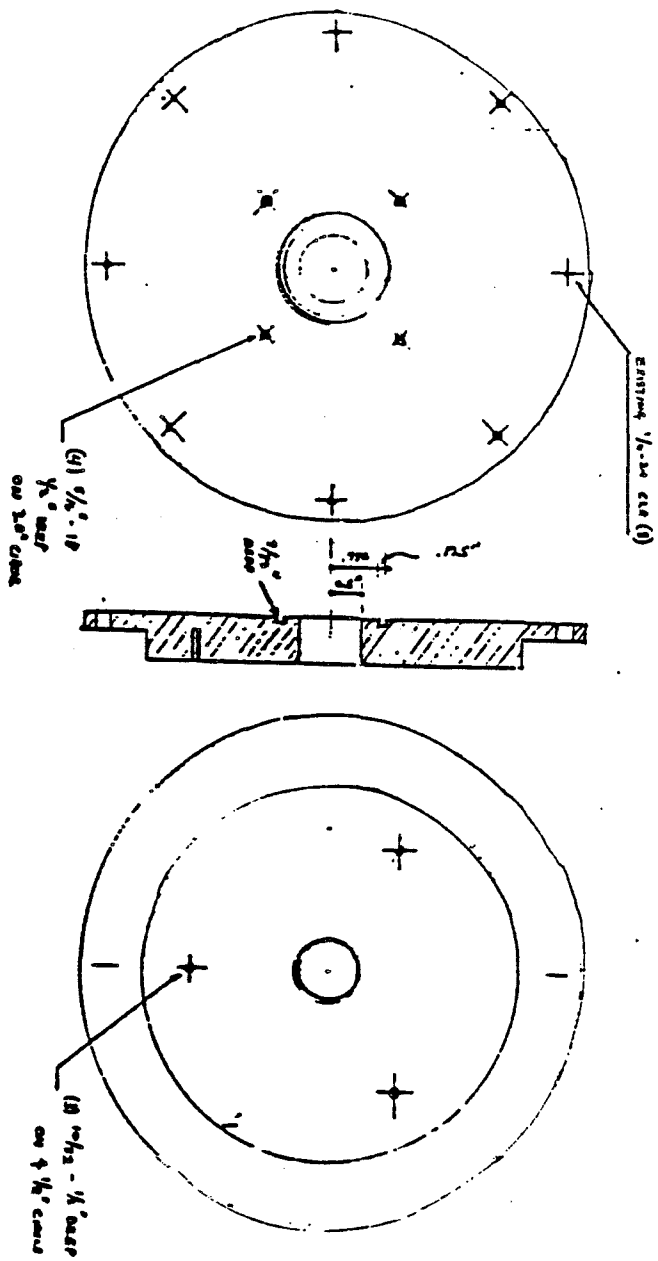

Fig.(3-15)- The photo-tube shown inside the housing can is held in place by a plexiglass disc via light springs.

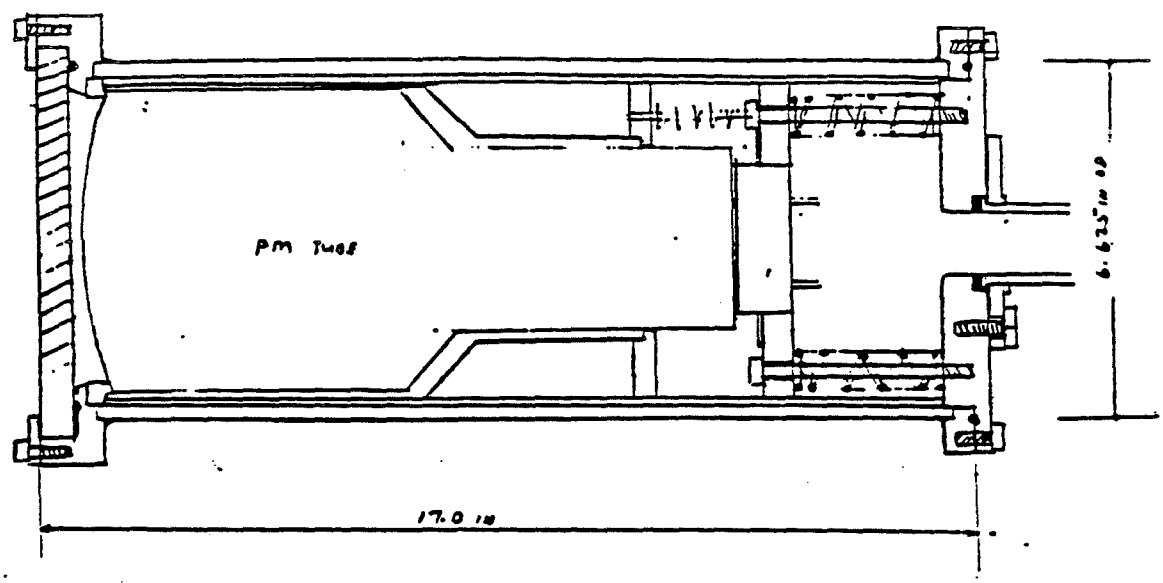

6.625 OD
6.065 ID

Fig.(3-16)- The design of the Nylon ring and the plexiglass discs.

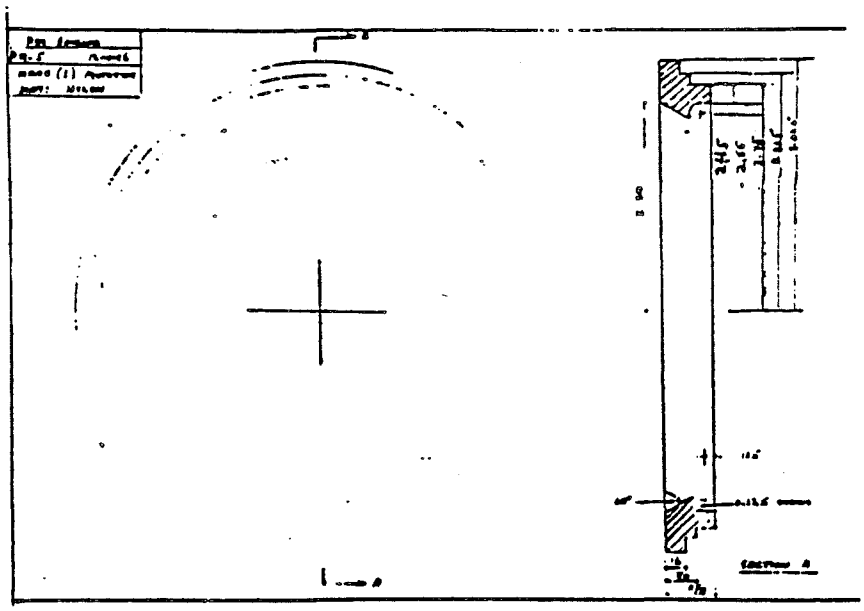

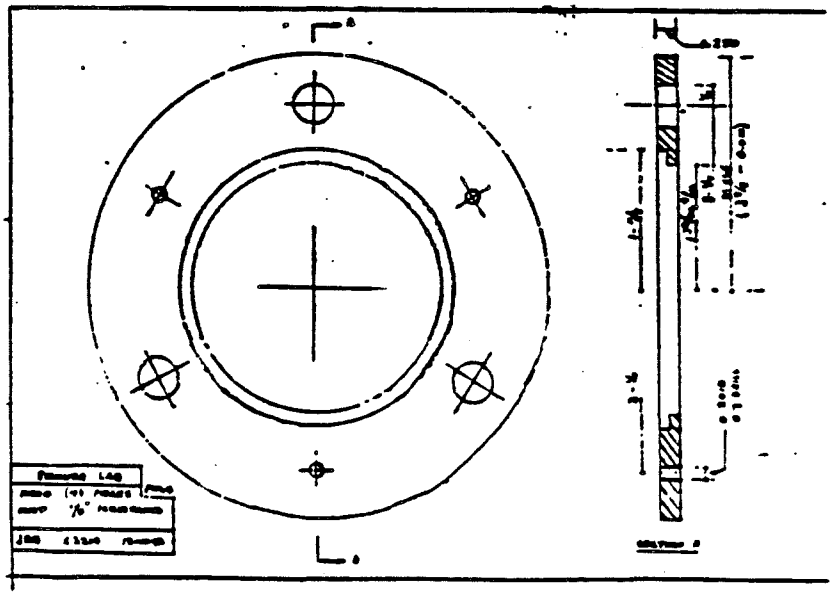

Fig.(3-17)- The deflected design of the housing.

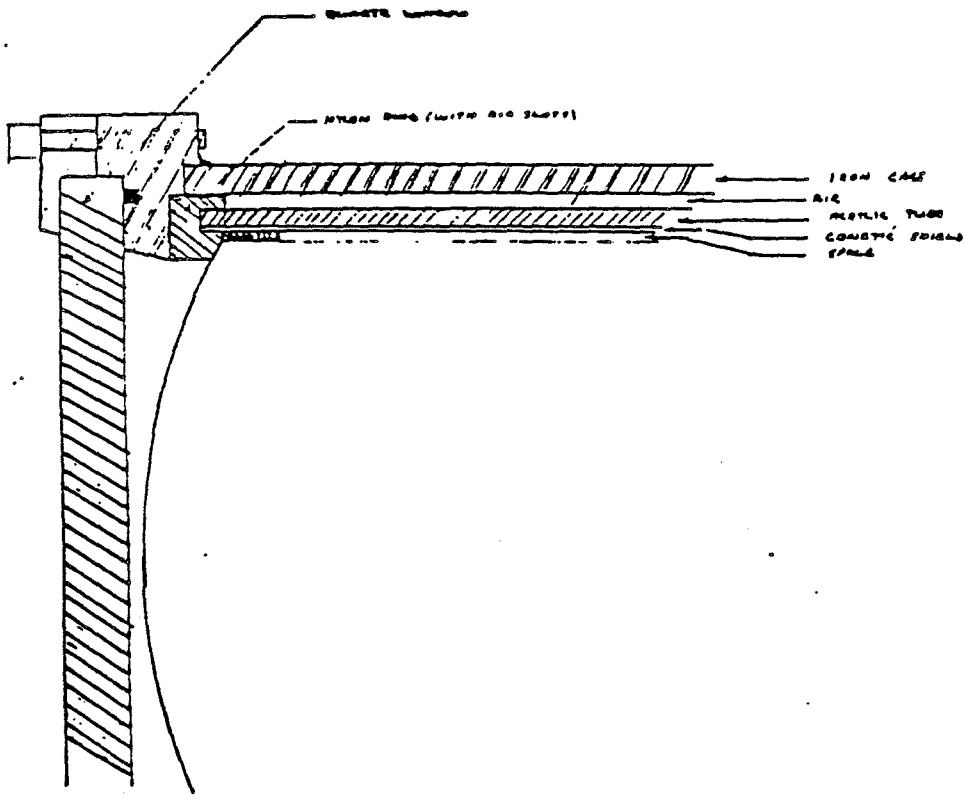

3.3.4 Mounting in the tank

Three pieces of U-channels 4 inches wide and 23 inches long were bent uniformly to form a segment of a circle of radius 36 inches each. All segments had an identical 2" × 8", 0.5" thick plate welded at their ends. The three segments were taken inside the tank and put together with a pair of studs and bolts at each joint to form a circular belt. The belt placed 65 inches away from the mirror frame upstream was expanded via its joints to make contact with the tank wall all around. Two pairs of unistruts 60 inches long were bolted to the fitted belt. The four housed photomultipliers were placed horizontally on the unistruts, and adjusted to the right position before being clamped with pipe clamps. Fig. (3-18) shows a picture taken from this assembly with only three phototube cans in place.

Fig.(3-18)- Photograph taken of installation of three P.M. .

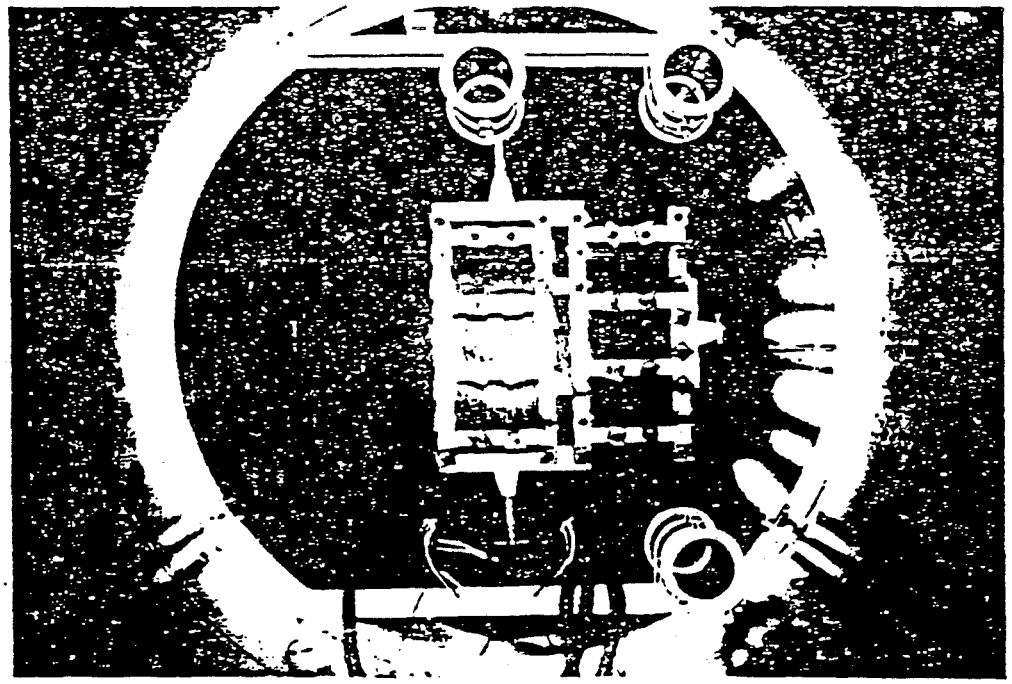

3.3.5 Cabling in the tank

We used 4, 10 feet long, 1.0" ID. flexible pipes. Each pipe had an 3.0" square flat plate welded at its ends. The pipes were connected to the end-plates of the P.M. housing at one end, and to the electronic-port flange at the other end. O-rings were used at both ends to provide vacuum and pressure tight seals. The high voltage cable, the signal cable and a 1/4" gas tube were threaded through each flexible pipe separately, connected to each housed photomultiplier. The flexible pipes were neatly tied to the belt inside the tank to keep the particle rays and the Cherenkov light path clear.

3.4 QUARTZ WINDOWS

The windows were chosen to be quartz because they are much more transparent in the UV region compared to regular window glass. Since the transmissivity of the quartz windows plays an important role in our Cherenkov Counter. The quartz windows were used to prevent the helium gas from diffusing through photomultiplier glass and contaminating the phototube vacuum. Each quarts window is a circular disc, 7.0" in diameter and of 0.5" thickness.

3.4.1 Transmissivity

Once again, we used the same experimental apparatus as we did for measuring the reflectivity of our mirrors.

We aimed the laser at the center of the bolometer surface. The intensity of the undisturbed light pulses were measured via the oscilloscope. Next, we placed the quartz window in between the laser and the bolometer. The intensity of the transmitted light pulses incident on the bolometer was also measured. By comparing the two measurements, we found the transmissivity of each quartz window. Fig. (3-19) shows the average transmissivity of the four quartz windows at three different wavelengths of 193nm; 248.5nm; and 350nm. The dashed curve in Fig. (3-19) is the ideal transmission of the quartz windows suggested by the fabricator[7].

Fig.(3-19)- The transmisssivity of the Quartz Windows at three different wavelengths as a function of wavelength versus the factory suggested transmissivity (dashed curve).

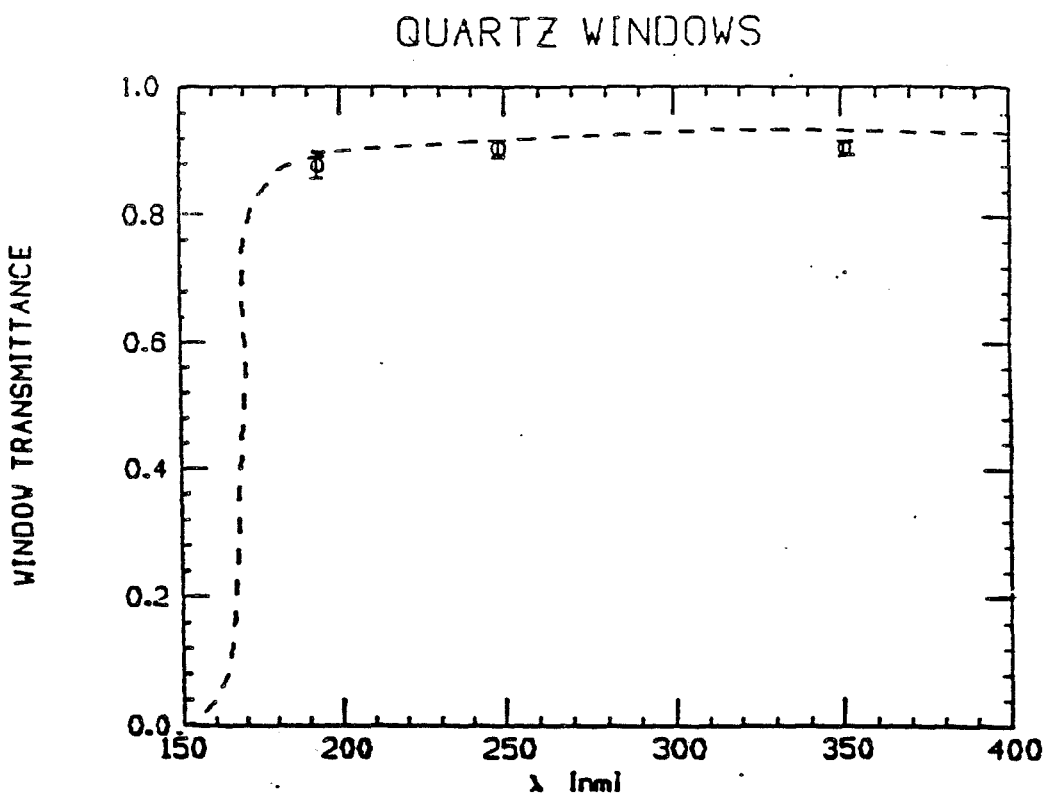

3.5 WAVELENGTH SHIFTERS

Since the Cherenkov yield is proportional to $1/\lambda$, it is useful to be able to extend the response of the photomultiplier tube into the far ultraviolet to increase the light yield, thereby optimizing the response of our Cherenkov counter. One way to make use of this potential light increase is to use wavelength shifters.

3.5.1 Principle of the Techniques

The conversion and concentration of light by fluorescent trapping occurs through absorption of incident light on a suitably doped optically clear medium and re-emission as fluorescence at a longer wavelength, which can be more efficiently detected. The fraction, F, of fluorescent light trapped within a flat plate collector by total internal reflection and propagation to the edge (Fig. 3-20), is given by

$$F_{trapped} = (1-n^{-2})^{1/2} \qquad (5.1)$$

where n is the index of refraction of the doped substrate.

One can achieve full absorption and conversion of the short-wave incident light by doping the films very heavily. Fig. (3-21) shows absorption in a layer of coating we used, for different layer thicknesses, as well as transmission through photomultiplier (RCA 8854) window as a function of wavelength[8]. In Fig. (3-22) the emission spectrum of the coating we used is shown as a function of wavelength[8].

It is possible that the application of the wavelength shifter could improve the UV response of the RCA 8854 considerably. Fig. (3-23) shows an optimistic quantum efficiency improvement of an RCA 8854 photomultiplier with and without WLS.[8]

Fig.(3-20)- Light trapping on WLS. coated substrate. Fluorescence emitted isotopically by the film is trapped in the substrate by total internal reflection for angles greater than the critical angle Θ. Light contained in a cone of solid angle, $\Omega = 2\pi(1-\cos\Theta)$, escapes from substrate through both boundaries.

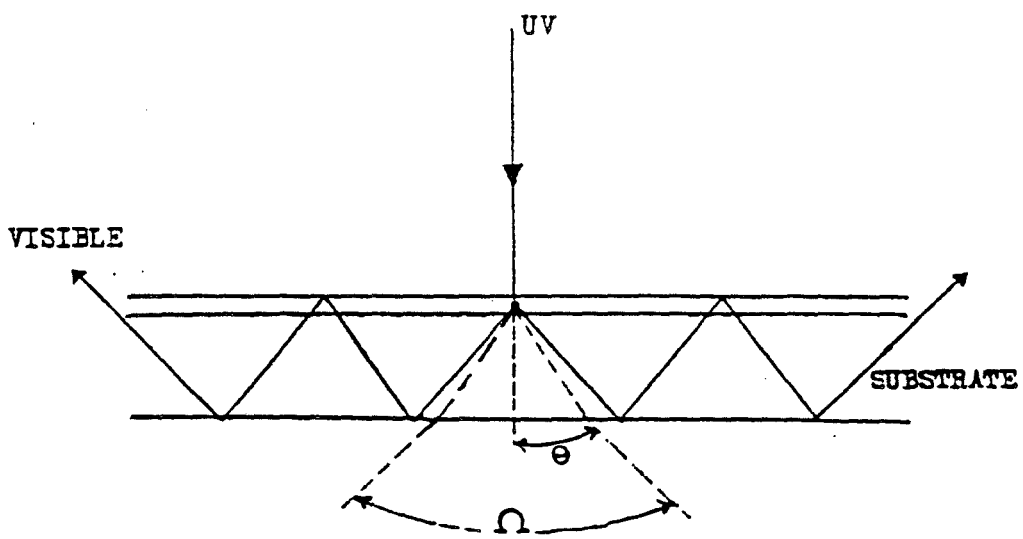

Fig.(3-21)- The absorption in a layer of Paraterphenyl as a function of wavelength[9]. Different curves correspond to different layer thicknesses. The dashed curve gives the transmission through the photomultiplier window (RCA 8854).

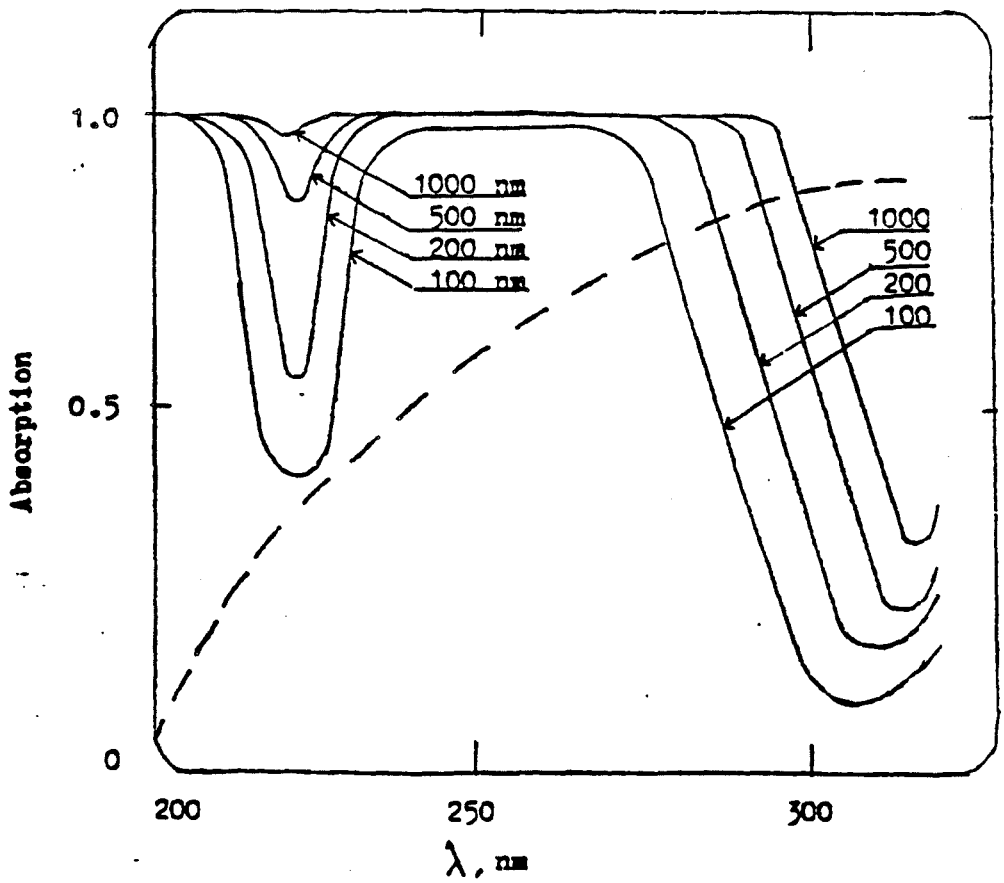

Fig.(3-22)- The emission spectrum as a function of wavelength, for the incident spectrum of $\lambda \approx 220nm-380nm$.

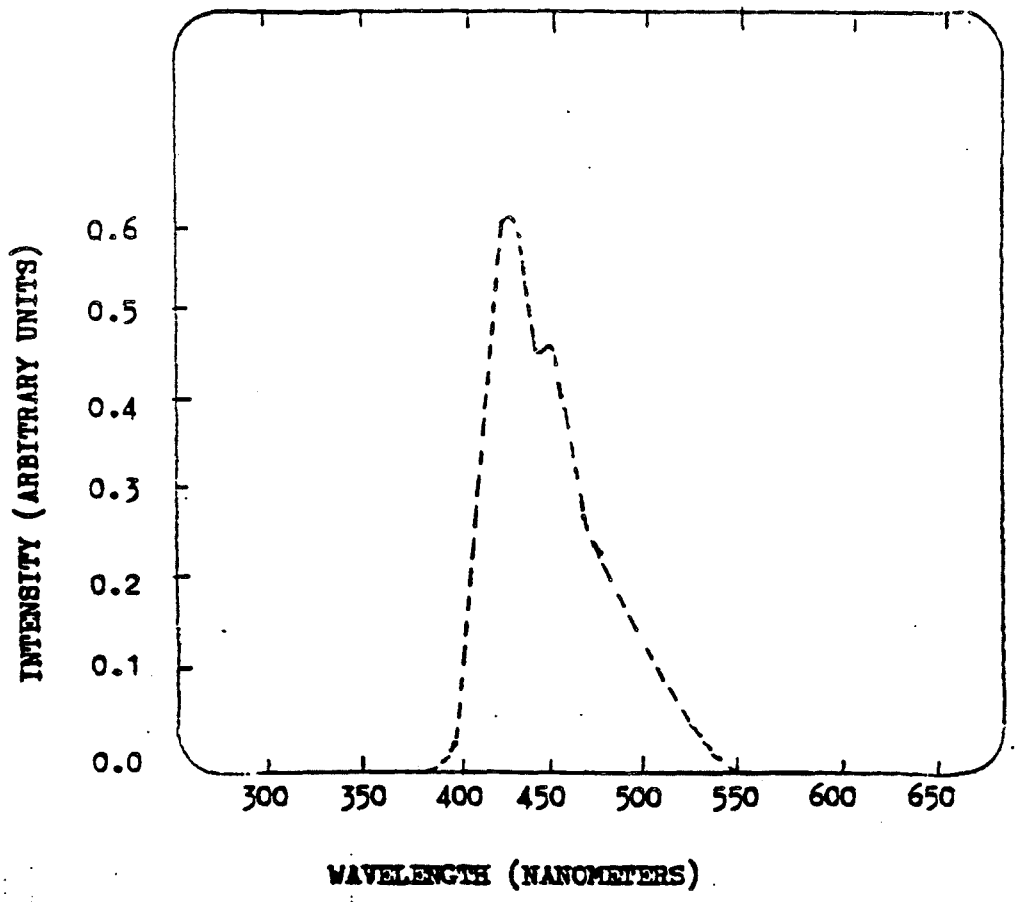

Fig.(3-23)- Estimates of the wavelength dependence of the quantum efficiency of the 8854 phototubes with & without wavelength shifters.

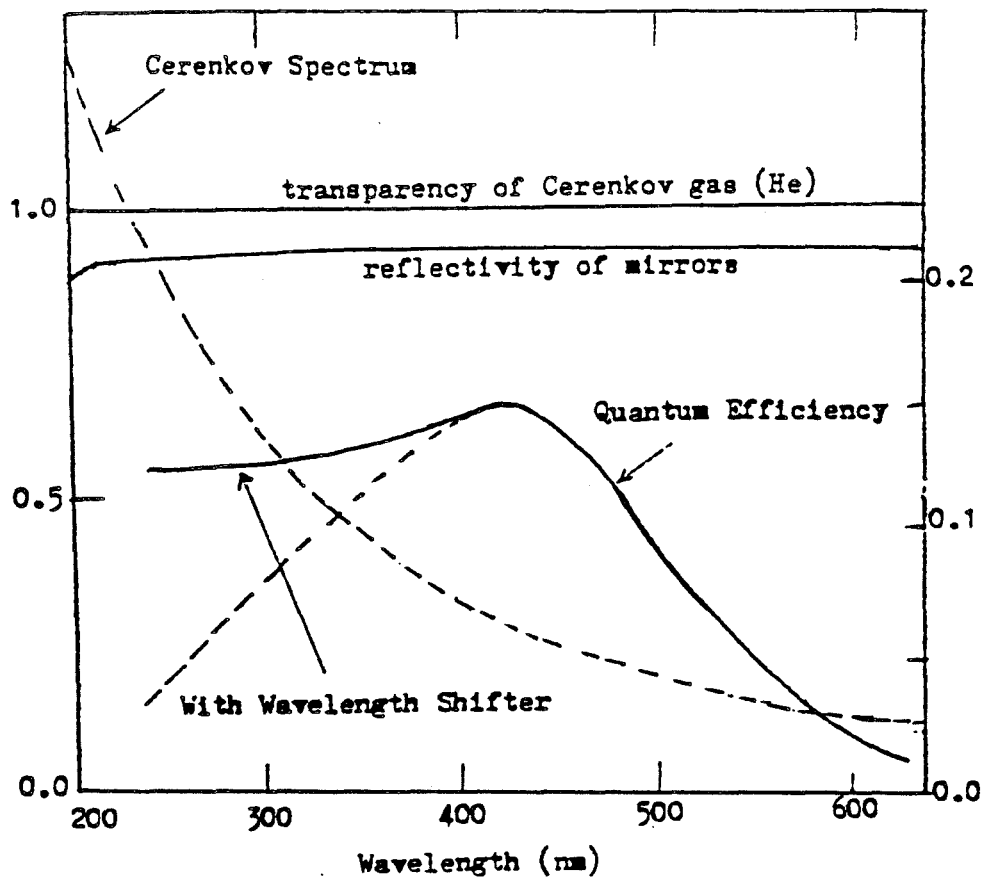

3.5.2 Materials for WLS

Many types of wavelength shifters were investigated. We chose Paraterphenyl (PTP) because it has a short decay time (1 ns), is more stable than Tetraphenyl-butadiene (TPB) and has a high conversion efficiency. For efficient wide band UV to blue conversion, it is necessary to incorporate several UV absorbing dyes with overlapping absorption band into the waveshifter.

Mr. Gary Moss[10] suggested the following recipe for the solution;

6.7 gr PTP, 2 gr bis-MSB and 270 gr Paraloid mixed in one liter Toluene, must be preserved in a glass container for a period of 10 days. Toluene was used because of its high solubility. The amount of plastic (paraloid) could be increased up to a factor of 5 to increase the viscosity and inhibit crystallization of PTP.

For our application, we used 2 gr PTP, 0.6 gr bis-MSB and 80 gr paraloid in 300 cc Toluene.

3.5.3 Coating the P.M.

The conversion films were deposited from liquid solution containing a combination of dyes in Toluene. The phototubes glass were coated by dipping and withdrawal with controlled speed. The axes of the coated tubes were placed vertically in a box and kept dark in a dark incubator for 48 hours to dry. We adjusted the dye concentration such that a single dipping yielded a film of proper thickness. The thickness was about 1000nm. as measured by weighting. For removing the film we used chloroform.

3.5.4 Measurement techniques[11]

The experimental arrangement for measuring the photomultiplier pulse heights is shown schematically in Fig. (3-24). As indicated in Fig. (3-24), the laser pulses, λ=337nm and width of ~3ns, were viewed by an Amprex 2212 photomultiplier in a light-tight room. The coated photomultiplier pulses were measured by a charge sensitive ADC. We removed the coated film of WLS from the face of the photo-tube without disturbing the set up and repeated the measurement once more. Fig. (3-25) shows the one datum at λ=337nm of comparison using or not using the wavelength shifter. The results showed within 5% the same response. The curves of (3-22) and (3-23) show that the wavelength shifter for λ<337nm is unknown but is presumed to be helpful as shown in fig. (3-25).

As shown in Fig. (3-25), the coated photomultiplier is about 5% less efficient for λ=337nm., and we anticipate that the coated P.M. remain less efficient by a few percent for 337nm$\leq\lambda\leq$600nm., since full absorption and conversion of light does not take place. However the performance of the coated P.M. at smaller wavelengths, 200nm$\leq\lambda\leq$300nm, where the uncoated P.M. efficiency is very small is anticipated to be better by far. However, this has not been verified.

Fig.(3-24)- The schematic design of the experimental arrangement for measuring the photomultiplier pulse height.

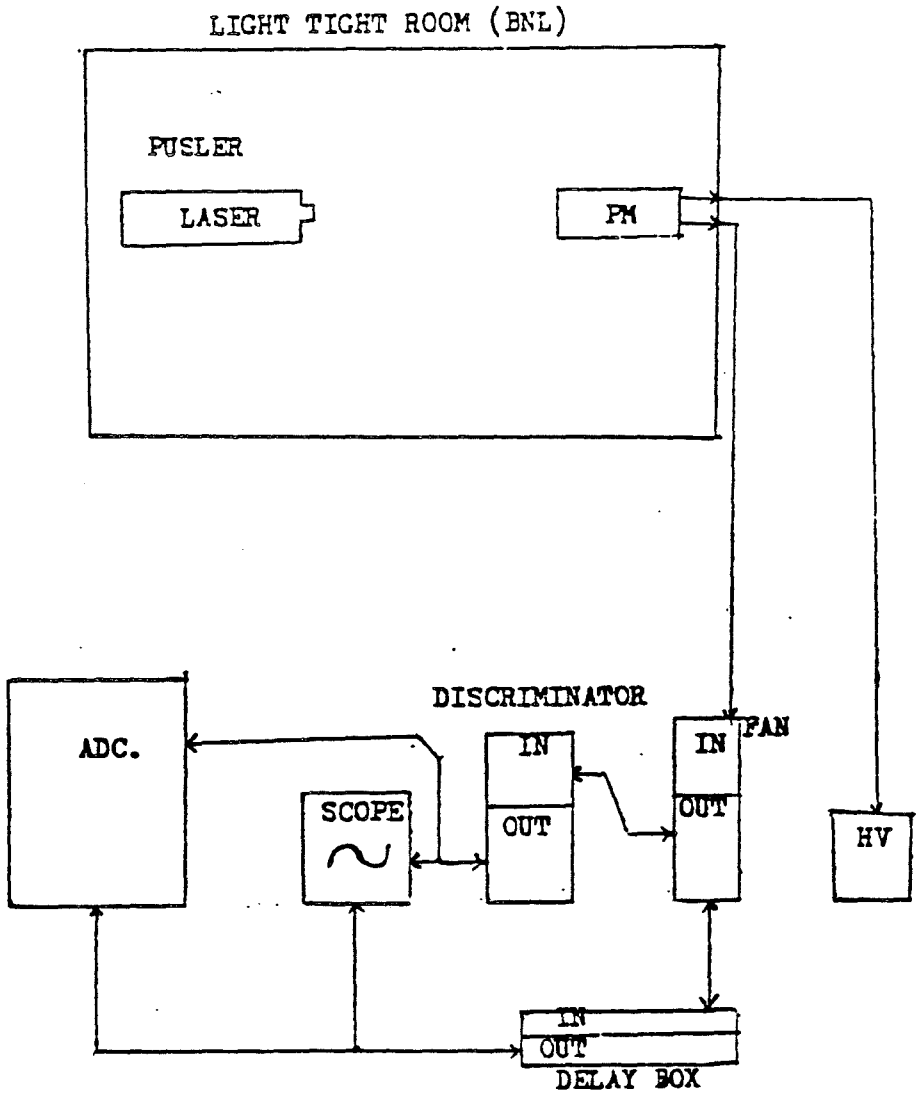

Fig.(3-25)- The estimated relative efficiency responses of the XP2212 photomultiplier with and without the wavelength shifters. The one experimented point is at λ = 337nm.

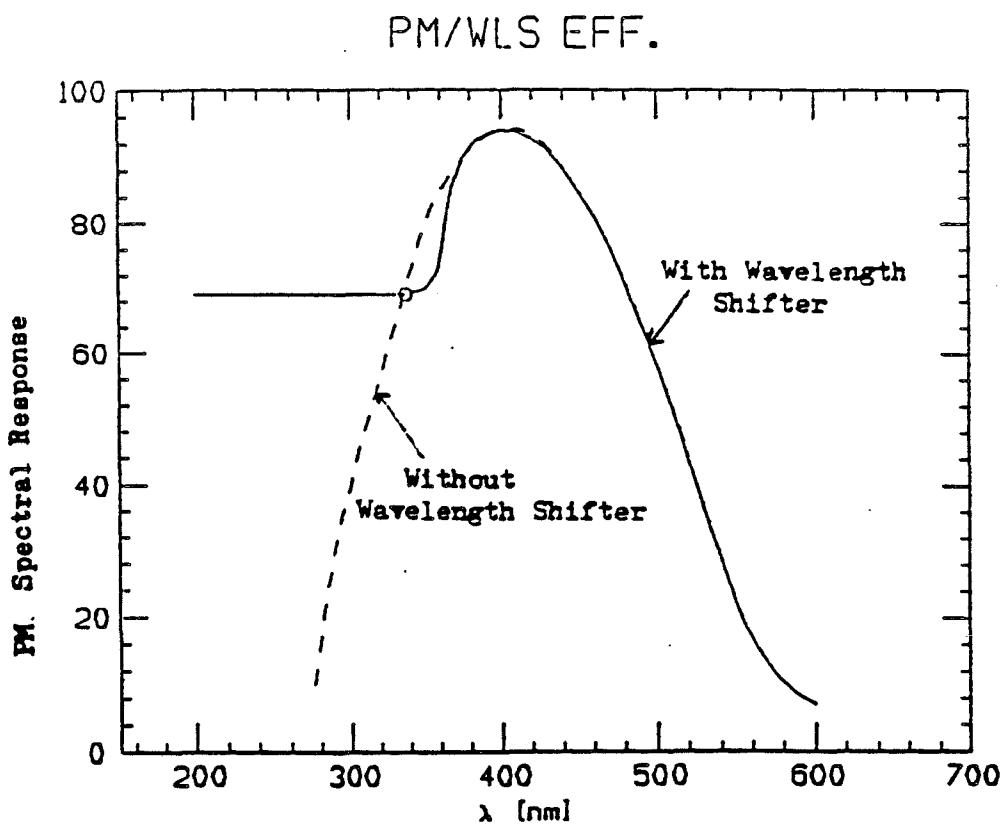

3.6 DETECTION EFFICIENCY

The average number of detected photoelectrons, without W.L.S is given by[12]

$$N_{p.e.} \simeq N_o L\ \theta^2 \qquad (6.1)$$

Where;

$$N_o = 2\pi\alpha \int \frac{d\lambda}{\lambda^2}\, T(\lambda)\ R(\lambda)\ q(\lambda) \qquad (6.2)$$

Using our measured values of the $T(\lambda)$ and $R(\lambda)$, while employing $q(\lambda)$ from reference 13 we have calculated N_o.

To evaluate the integral (6.2), we set λ_1=200nm and λ_2=675nm due to the photocathode spectral response characteristics of the RCA 8854 photo-tubes (see Fig. 3-12). To simplify the evaluation within this spectral range, we substitute the average values of 90%, 85% and 8% for $T(\lambda)$, $R(\lambda)$ and $q(\lambda)$ respectively. The calculated Optical Collection Efficiency, N_o is found to be

$$\text{(uncoated)} \qquad N_o = 98.8 \quad cm^{-1} \qquad (6.3)$$

The average number of detected photoelectrons in the coated photomultiplier is given by[12]

$$N_{p.e.} \simeq N'_o L\ \theta^2 \qquad (6.4)$$

Where;

$$N'_o = 2\pi\alpha \int \frac{d\lambda}{\lambda^2}\, T(\lambda)\ R(\lambda)\ \{q(\lambda)[1-A(\lambda)]+q_e fA(\lambda)\} \qquad (6.5)$$

This equation differs from (6.2) due to the inclusion of the effect of the W.L.S coating. To evaluate the integral (6.5) we set λ_1=185nm, due to wavelength shifter absorption spectra, and λ_2=675nm. We used the average values of 88%, 83% and 10% for $T(\lambda)$, $R(\lambda)$ and $q(\lambda)$ respectively. For the parameters of $A(\lambda)$, q_e and f the average values of 99%, 15% and 74%[3] were used respectively. The calculated Optical Collection Efficiency, N'_o with a coated photomultiplier (using WLS) becomes;

$$N'_o = 146.2 \quad cm^{-1} \qquad (6.6)$$

Thus calculations indicate that, using coated photomultipliers should improve the efficiency of the Cherenkov Counter by better than 47%.

CHAPTER 4

TEST WITH 30 GEV/C ELECTRONS

4.1 EXPERIMENTAL SET-UP

The experimental layout for detecting the Cherenkov light produced by 30 Gev/c electrons alternatively in N_2 and He at partial atmospheric pressures is shown schematically in Fig. (4-1).

Individual incident electrons were detected by the scintillators S_1, S_2, S_{10} and by the beam Cherenkov C_2. The trigger requirement was $C_2S_1S_2S_{10}$. The Rice lead-glass wall, down stream from the S_{10} counter, permitted a detailed study of the electron beam.

The electronics layout is shown in Fig. (4-2). The anode signals c_1, c_2, c_3, c_4 (corresponding to photomultipliers 1 through 4) from the Rice gas Cherenkov detector were fed through low-attenuation cables (RG 258U) to a Lecroy 2249A ADC allowing the input signals to be recorded.

In order to fulfill the trigger requirement we did the following:

The signals from C_2, S_1, S_2 and S_{10} were fed to a 4-fold AND gate (Lecroy 365 level 4) so that if they are all in coincidence, there would be an output signal called the triggered electron signal.

The c_1, c_2, c_3 and c_4 signals were fed to Lecroy 621 high impedance discriminators with their thresholds set at 30mv. Their outputs, 20 nsec square signals, were fed to a 4-fold OR gate (Lecroy 365 level 1) such that if any one or more of the photomultipliers are fired there would be an output signal indicating an event. This output signal and the triggered electron signal were fed to an AND gate (Lecroy 365 level 2) to confirm that the event seen was due to the electron induced trigger, the $C_2S_1S_2S_{10}$ coincidence. With the help of another AND gate and tagging discriminator box we chose only to read the electron events made by ~30 Gev/c electrons as determined by their momentum analysis. At last the good-event signal was fed to the ADC 2249A gate so that the pulse height of these events could be recorded.

The digital gate signal and the analog photo-tube signals should arrive at the ADC at the proper time (see Fig. 4-3).

Fig.(4-1)- Experimental Layout. The beam enters from the left. S_1, S_2 and S_{10} are scintillators, C_2 is beam gas Cherenkov Counter. The Rice counter, C, is filled and tested separately with N_2 and He gas. The Rice lead glass "wall", LG, is the last instrument in the beam.

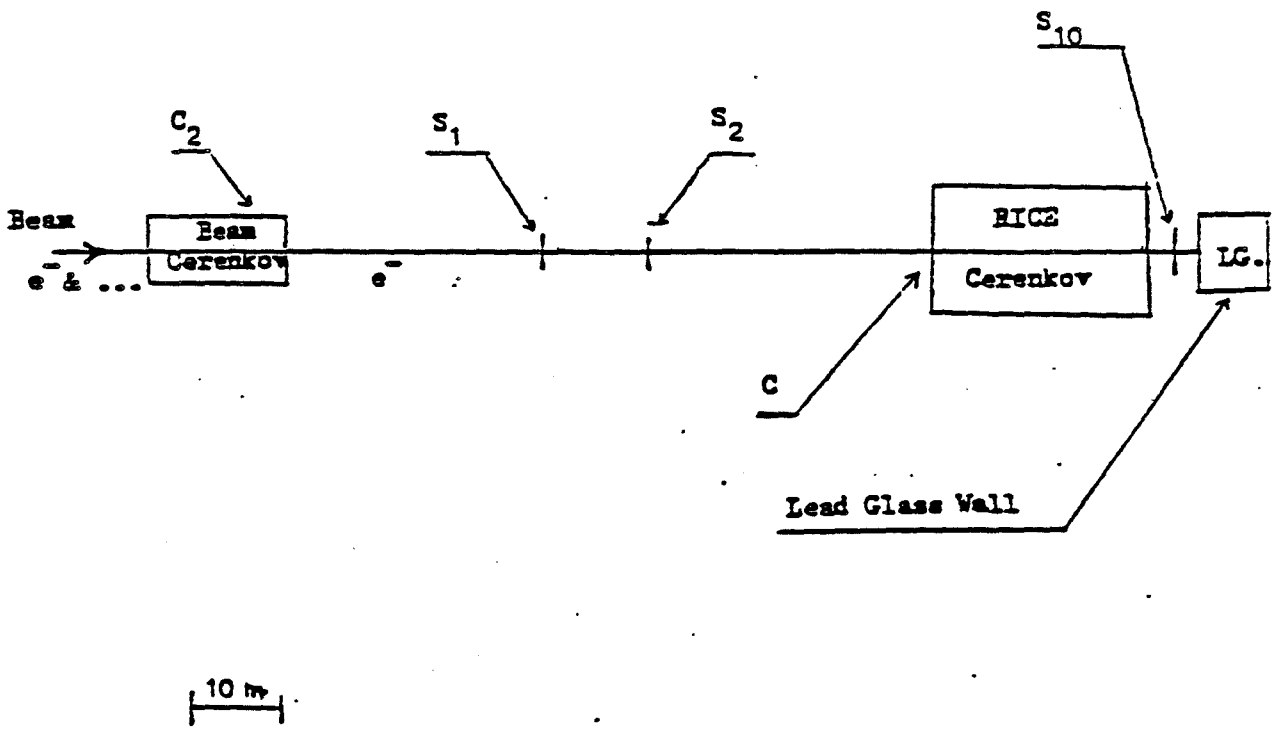

Fig.(4-2)- Electronics Layout.

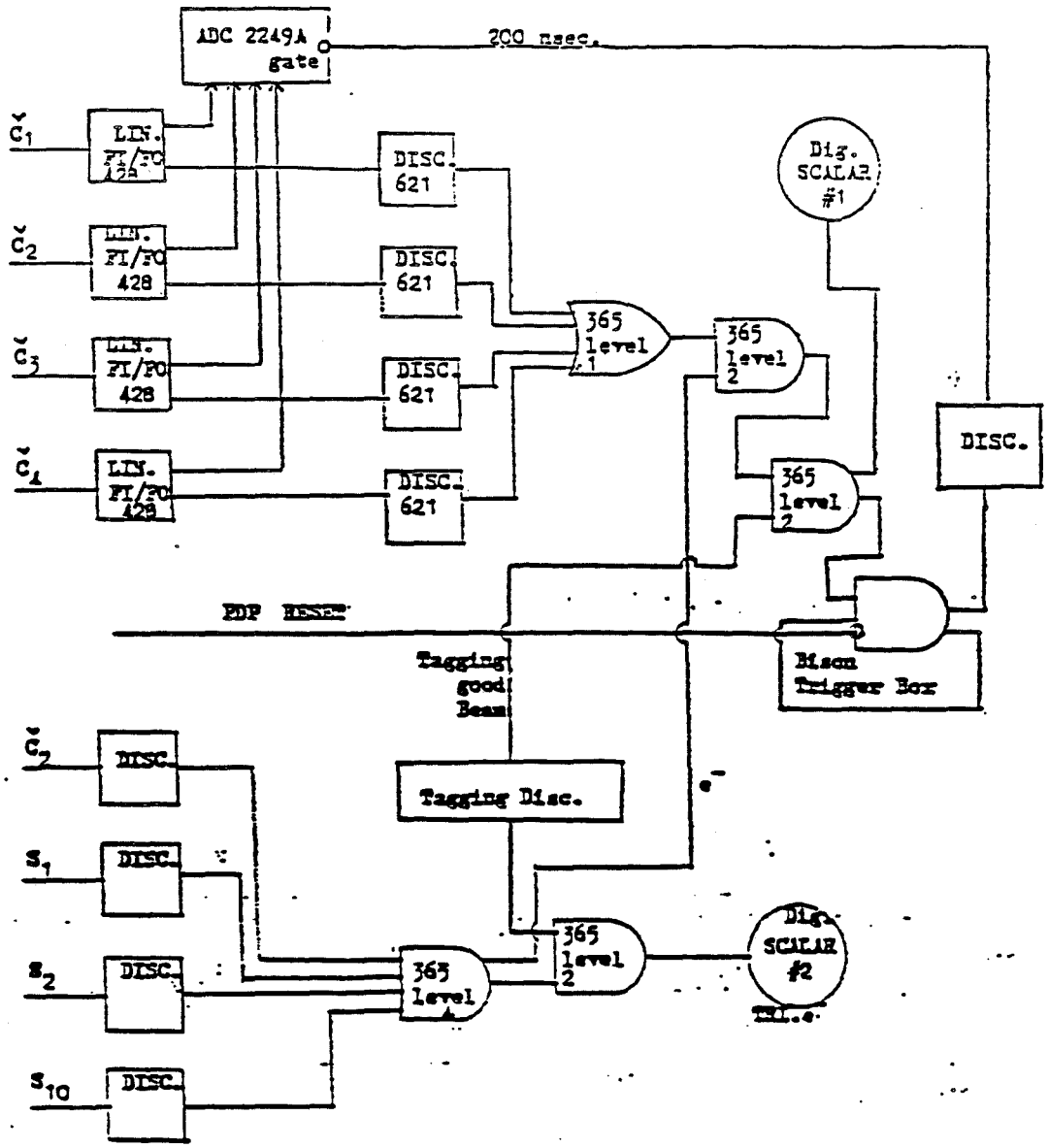

Fig.(4-3)- ADC timing. The oscilloscope scales are 50ns, 50mv and 50ns, 500mv for P.M. (Cherenkov) pulses and ADC gate signal respectively.

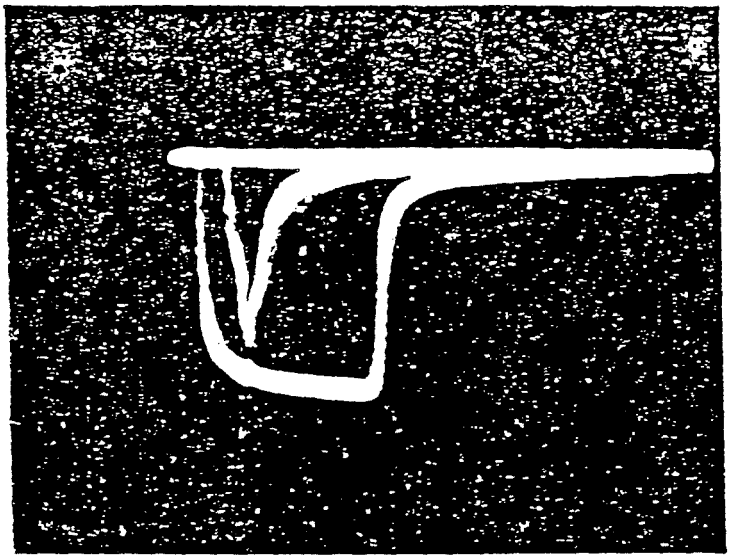

4.2 EFFICIENCY MEASUREMENT

We used 30 Gev/c electrons to measure the efficiency of the Rice gas Cherenkov counter. The measurements were performed with using two different gases, Helium and Nitrogen, separately as Cherenkov gases. An absolute pressure gauge was used to monitor the tank pressure at all times. The control of pressure was made by means of a computer controlled pneumatic regulator.

The efficiency of a Counter is defined as the probability of its detection of the beam particles. To find the efficiency of our Counter we used the two Digital Scalars as shown in Fig. (4-2). As it is explained in section 4.1, Scalar#2 counts the electrons, that we wish to define as our "beam". Scalar#1 counts the number of electrons that the Rice detector responds to. Therefore at a given pressure the efficiency is obtained by

$$\text{Eff} = \frac{\text{Scalar\#1}}{\text{Scalar\#2}}\ 100\% \qquad (2.1)$$

For pressures below threshold, efficiency of the counter is zero. The calculated thresholds for 30 Gev/c electrons for Helium and Nitrogen are 3×10^{-3} mmHg and 25×10^{-3} mmHg respectively. Since the Helium and Nitrogen pressures to attain threshold were so low, no data was taken at threshold with 30 Gev/c electrons.

Due to the design of the optics, the Cherenkov light for a given event could cause more than one photomultiplier to be fired (MULTIPLICITY). The multiplicity was resolved by the nature of the 4-fold OR gate used in the logic design, so that we get only one count when multiplicity occurs.

After taking enough statistics (1000 to 10000 events) for each pressure setting, we found the pressure curves for the two gases of helium and nitrogen. The graphs are presented in the next chapter.

4.3 PULSE HEIGHT MEASUREMENTS

The anode signals C_1, C_2, C_3, C_4, from the photomultipliers were passed through low attenuation cables (RG 258U), And hence into a digital pulse-height analyser, LeCroy 2249A ADC. The operating conditions of the photo-multipliers are discussed in sec.(5-1).

The model 2249A contains twelve complete ADC's in a single-width CAMAC module. Each ADC offers a resolution of ten bits to provide 0.1% resolution over a wide 1024-channel range. The input sensitivity of the model 2249A is 0.25 Pico Coulombs/count for a full scale range of 256 pc. LeCroy 2249A ADC is of the integrating or charge-sensitive type and gives an output (a number) which is proportional to the integral of the input current pulse. The non-linearity and instability of the conversion with time and temperature are small enough in general to present no problem in data acquisition.

The pulse height distributions obtained for helium gas at different pressures are presented in Fig. (5-6) through (5-28). Each figure represents count/channel versus the ADC channel number. Data was obtained on only one of the four-mirror systems, because time limitations precluded placing the beam on the other three mirror systems.

CHAPTER 5

EXPERIMENTAL RESULTS

5.1 EFFICIENCY VS. PRESSURE

The results of the efficiency of the Cherenkov Counter versus pressure, for the two different gases of helium and nitrogen, are shown in Fig. (5-1) and Fig. (5-2) respectively.

The pressure of the gas in the tank was monitored by a Bourdon pressure gauge as well as a Transducer pressure gauge. The mechanical bourdon pressure gauge was calibrated by setting it at one atmosphere for the gas pressure inside the tank when the tank end-plate had been removed. Later the Transduce pressure gauge was calibrated for Helium gas, according to the Bourdon gauge. The Bourdon and the Transducer pressure gauge indicated the same reading at different pressures during the course of the experiment.

The photomultipliers high voltages were all set at 2700 volts for the Helium-Run.

Fig.(5-1)- The absolute efficiency of the Cherenkov Counter versus presure (psi), for the Helium-Run. The P.M.s high voltages were all set at 2700 volts. The threshold of the discriminator was set at 30mV.

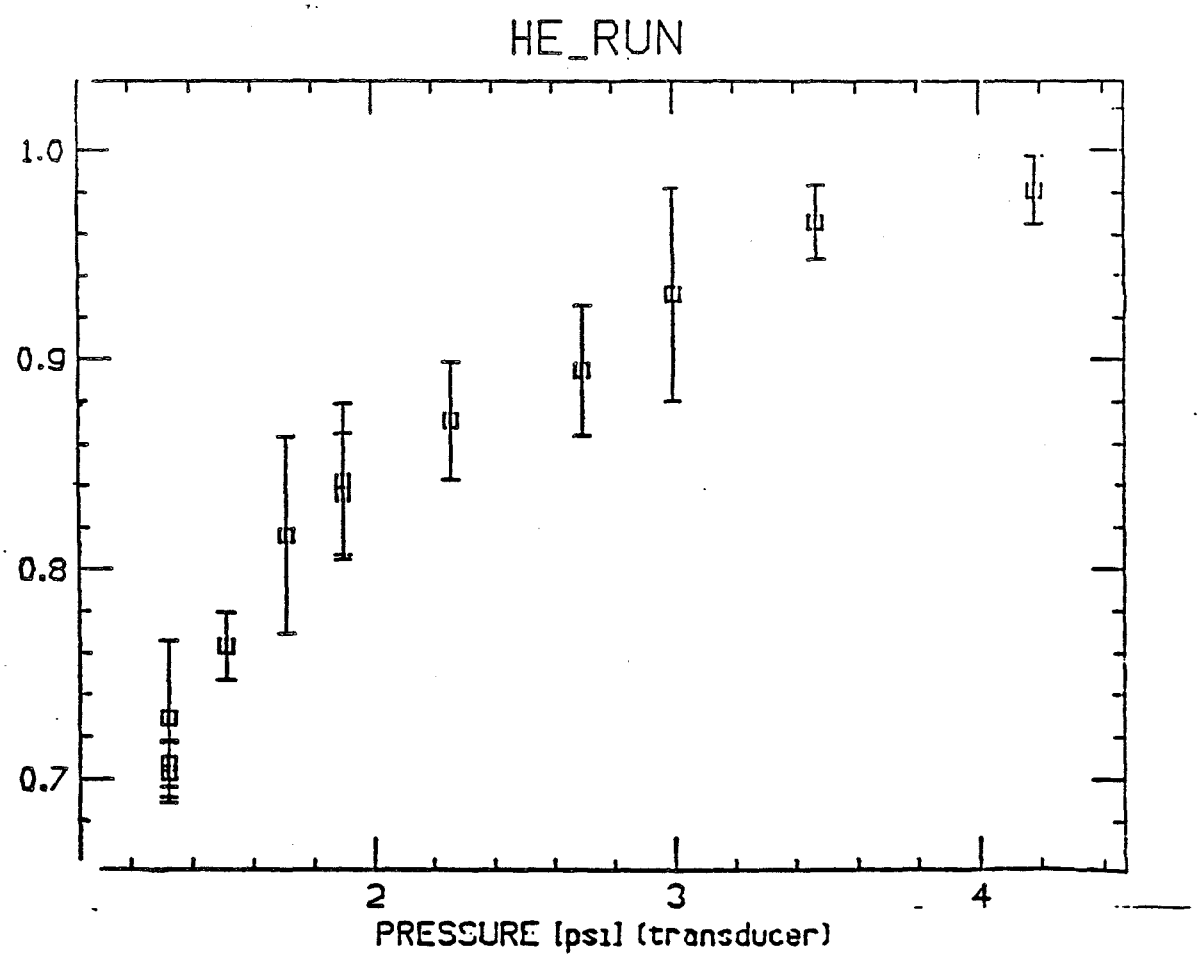

Fig.(5-2)- The absolute efficiency of the Cherenkov Counter versus presure (psi), for the Nitrogen-Run. The P.M.s high voltages were all set at 2600 volts. The threshold of the discriminator was set at 30mV.

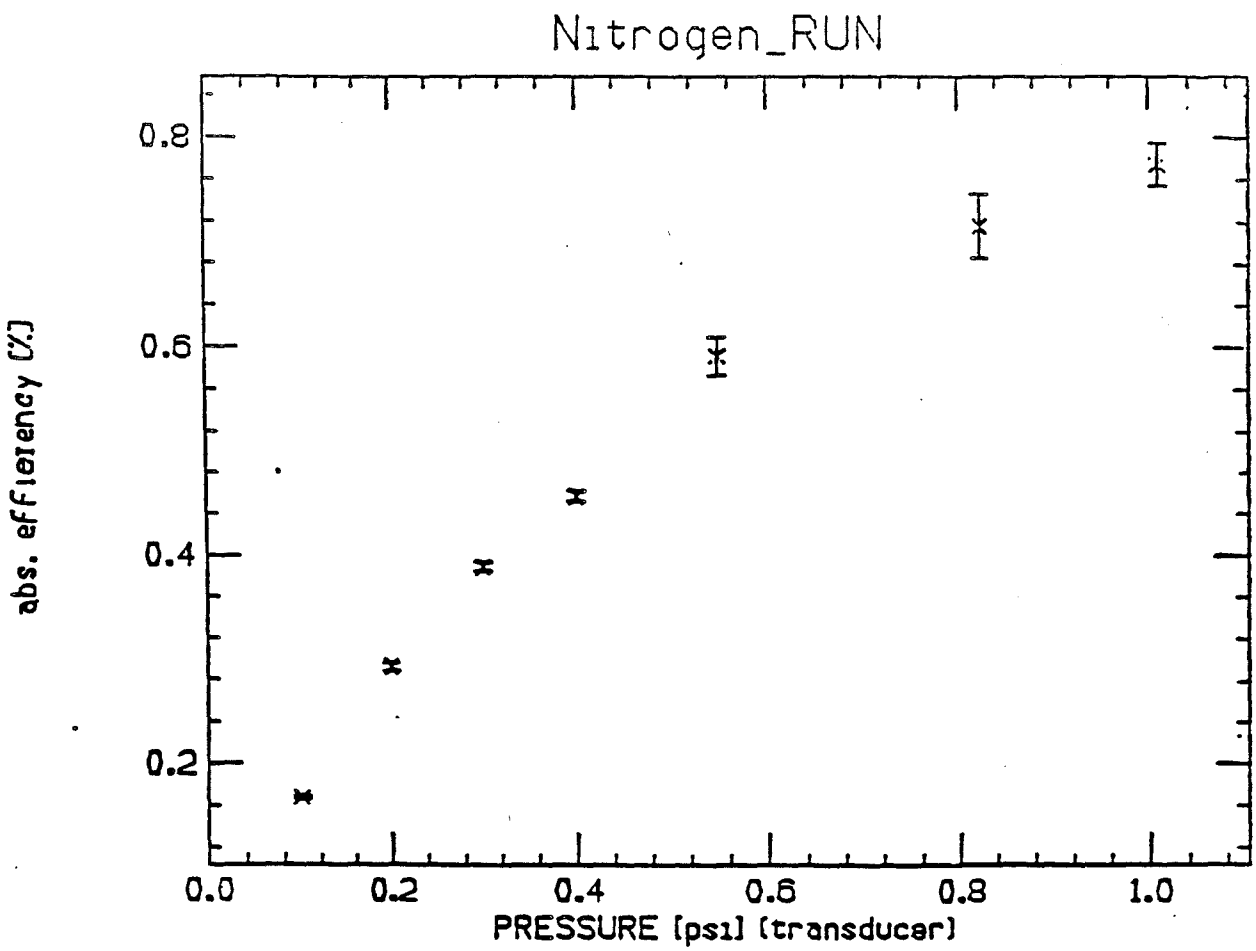

5.2 PULSE HEIGHT DISTRIBUTION VS. PRESSURE

In Fig. (5-3) through Fig. (5-26) we have represented the pulse height distributions obtained with ~30 Gev/c electrons, 30 mv. threshold discrimination, with Helium gas at a different series of indicated pressures. The P.M.'s high voltages were all set at 2700 volts. CER 151, CER 152, CER 153 and CER 154, are representing the responses for the photomultipliers 1, 2, 3, and 4 respectively. The tubes of P.M.#2 and P.M.#4 had been coated with wavelength shifters. For figures (5-3) through (5-24) we have indicated in each figure the pressures at which the pulse height distributions were obtained.

Fig.(5-3)- Helium Gas Pressure = 4.18 psi

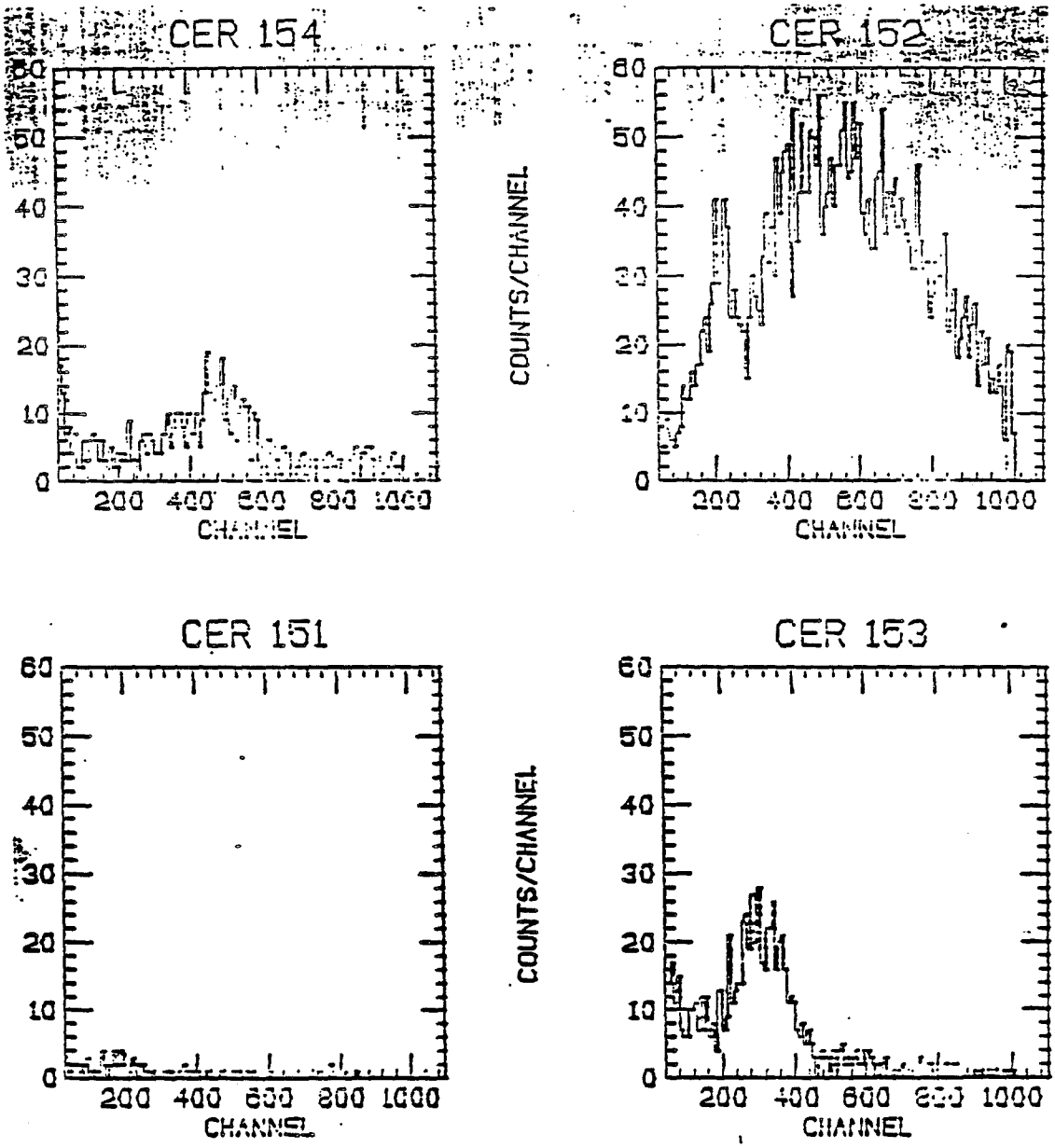

Fig.(5-4)- Helium Gas Pressure = 4.18 psi

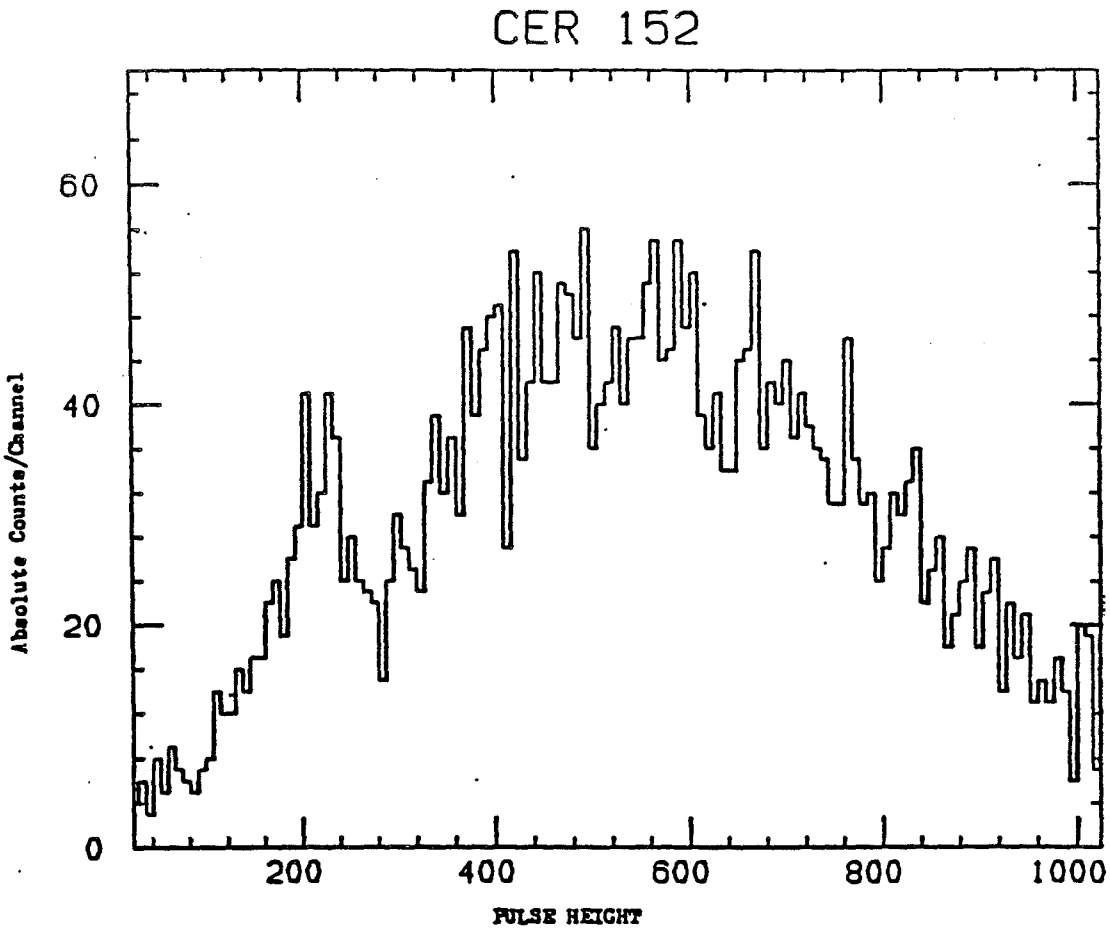

Fig.(5-5)- Helium Gas Pressure = 3.47 psi

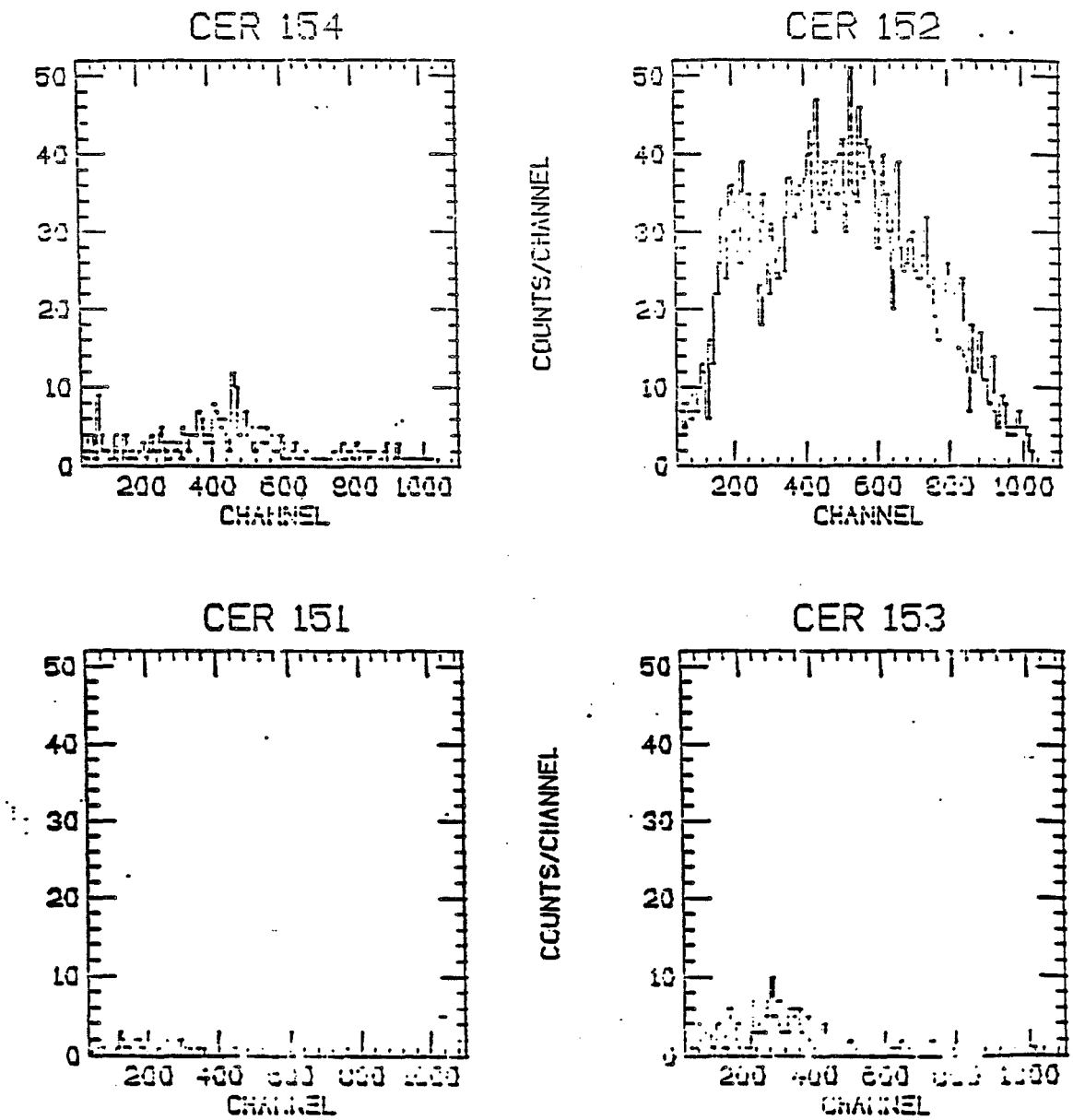

Fig.(5-6)- Helium Gas Pressure = 3.47 psi

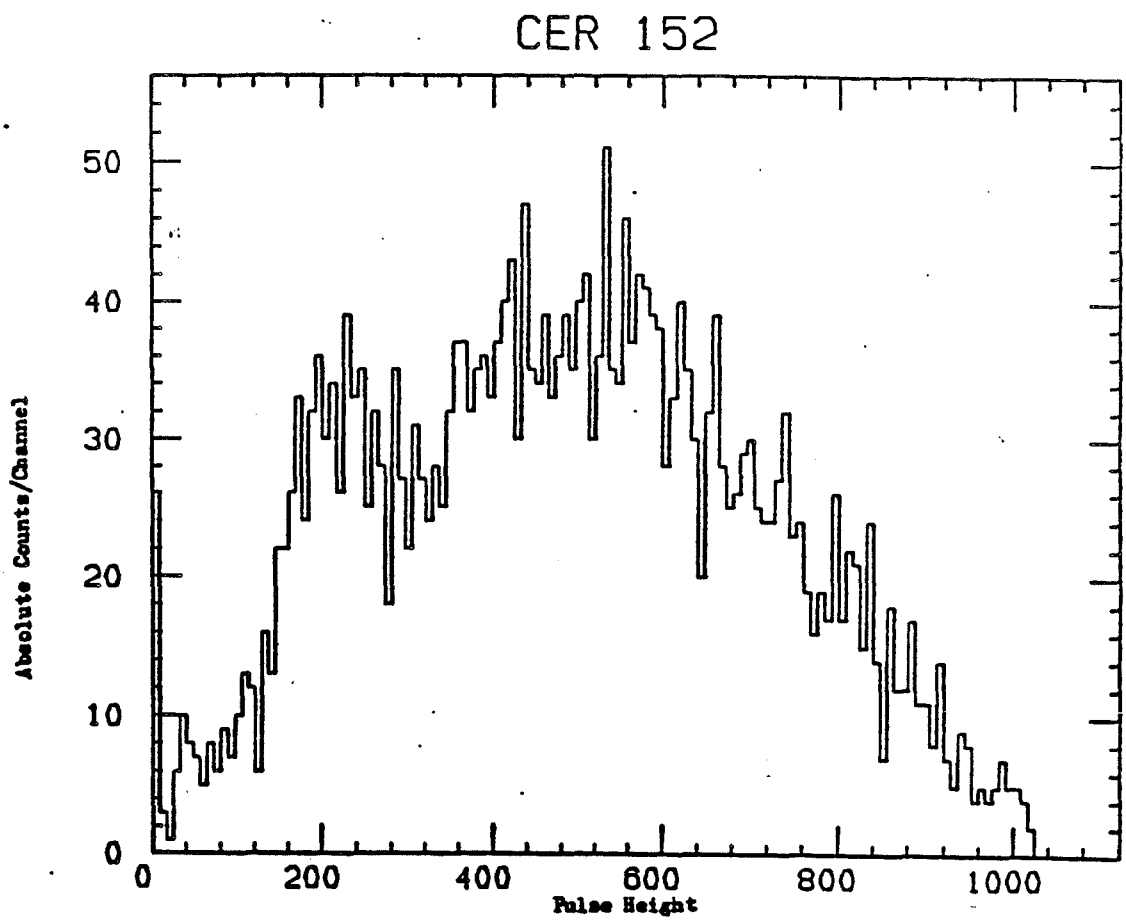

Fig.(5-7)- Helium Gas Pressure = 3.00 psi

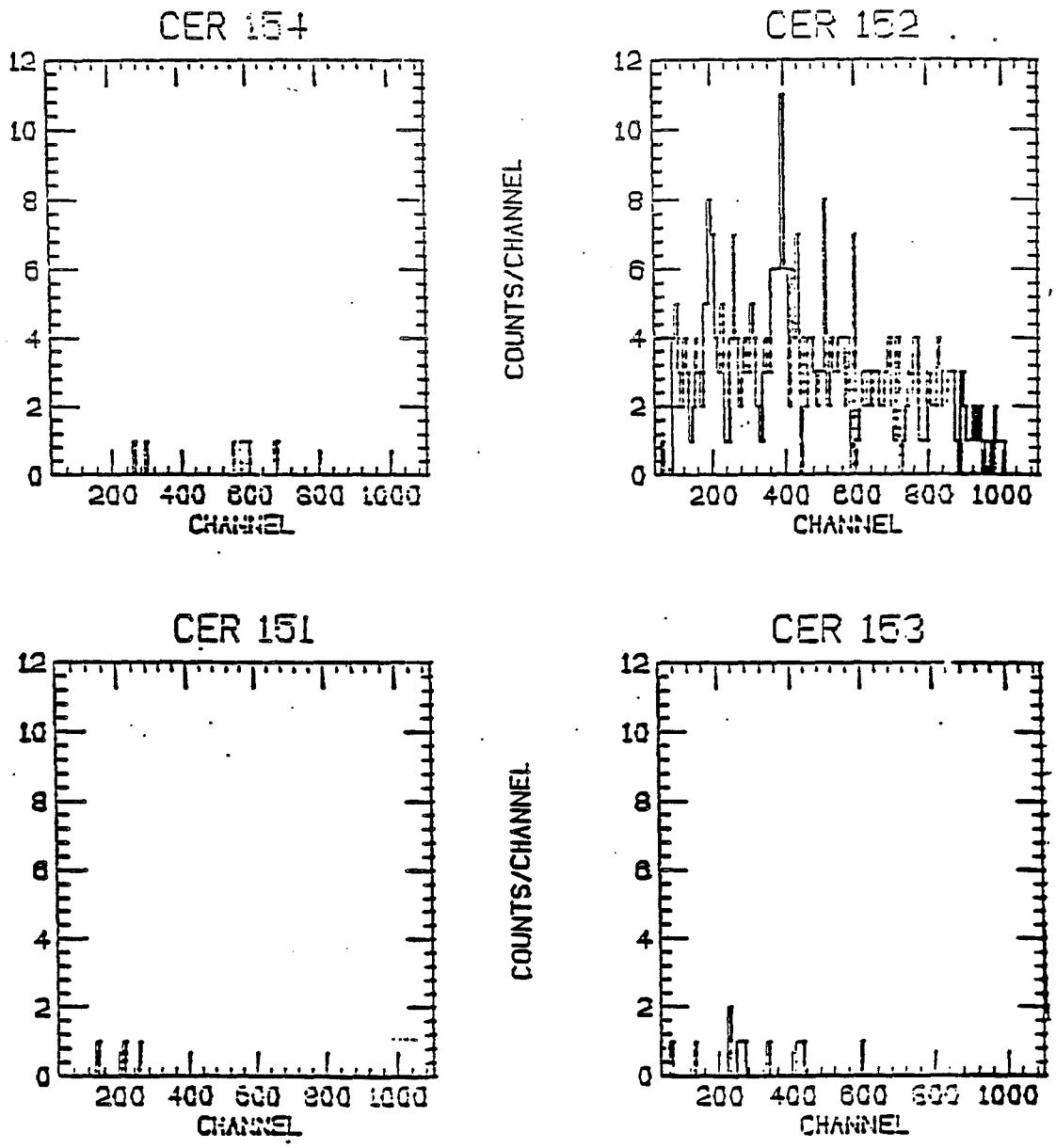

Fig.(5-8)- Helium Gas Pressure = 3.00 psi

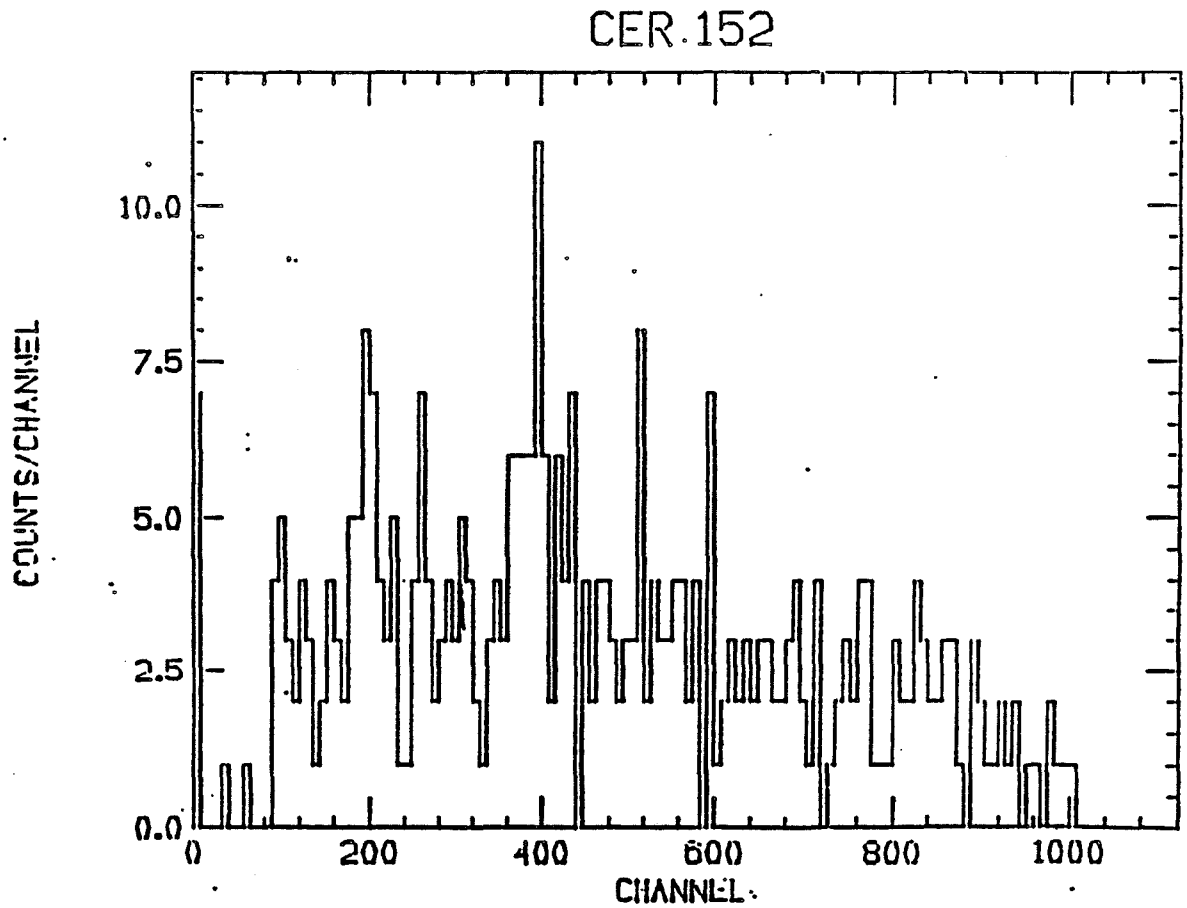

Fig.(5-9)- Helium Gas Pressure = 2.70 psi

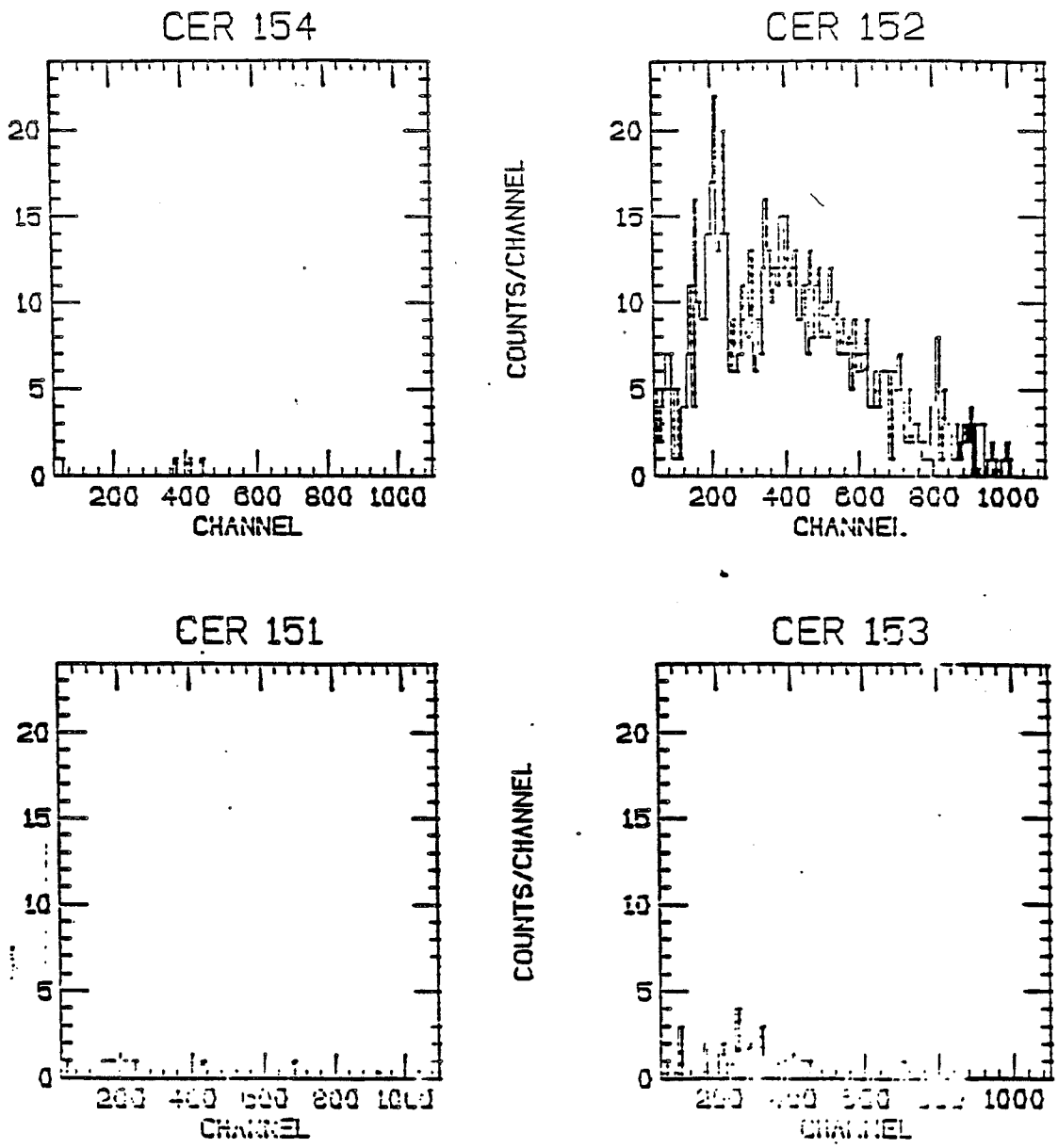

Fig.(5-10)- Helium Gas Pressure = 2.70 psi

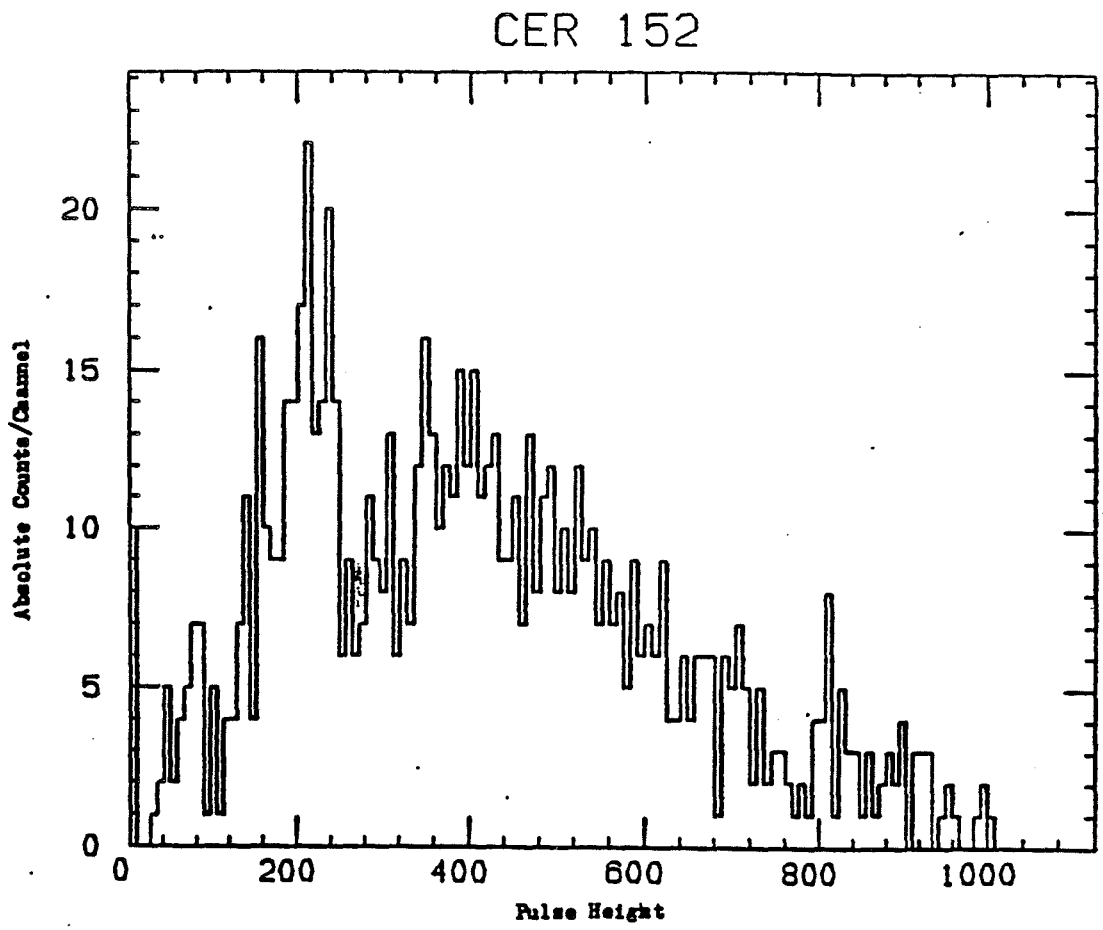

Fig.(5-11)- Helium Gas Pressure = 2.50 psi

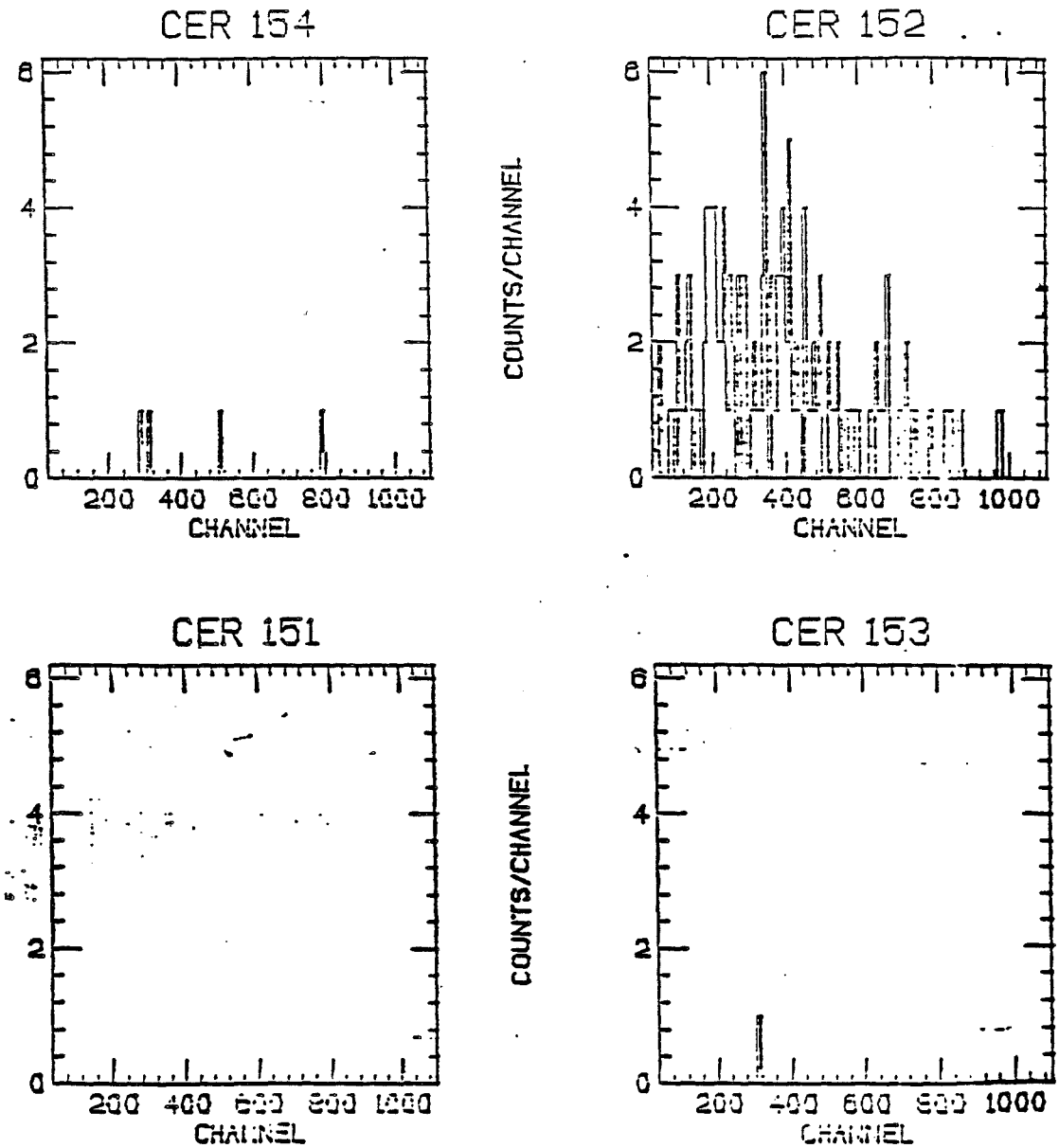

Fig.(5-12)- Helium Gas Pressure = 2.50 psi

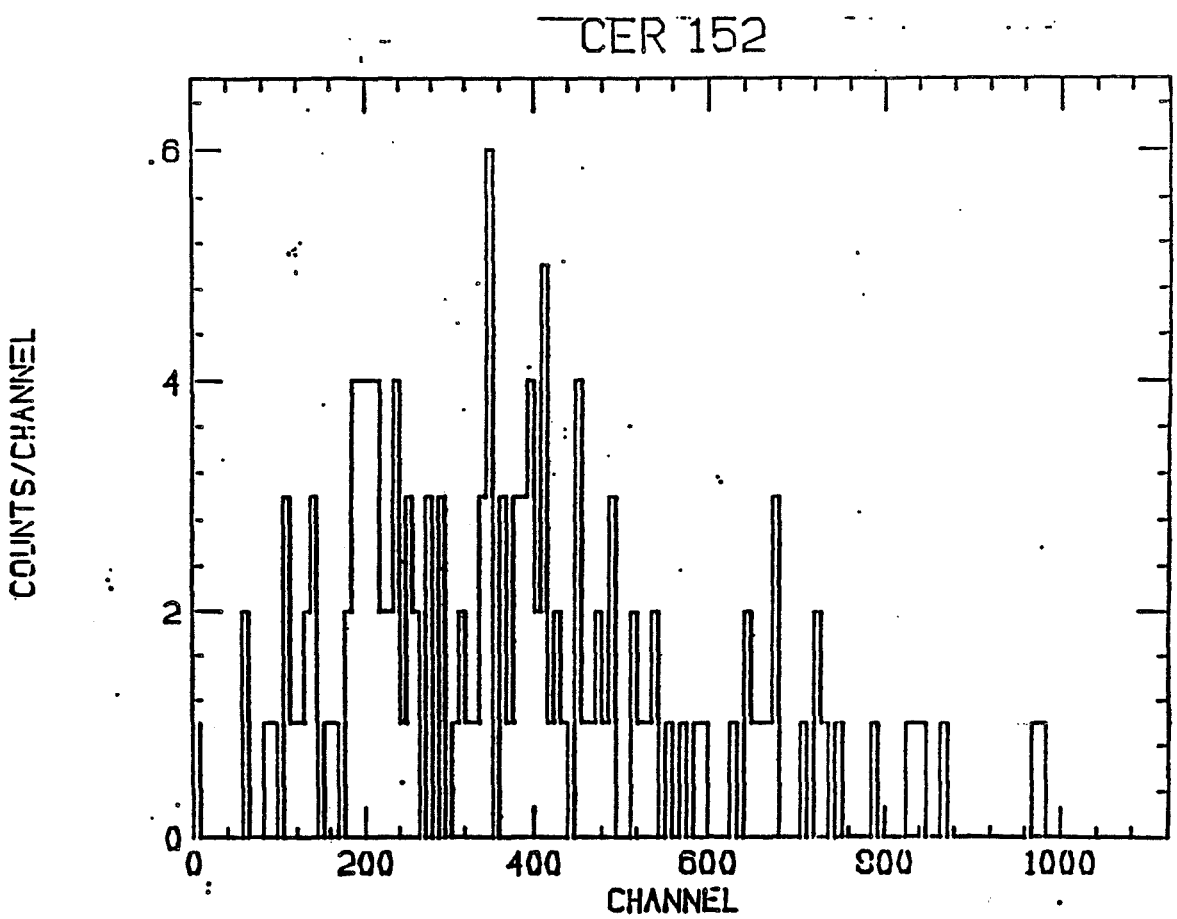

Fig.(5-13)- Helium Gas Pressure = 2.26 psi

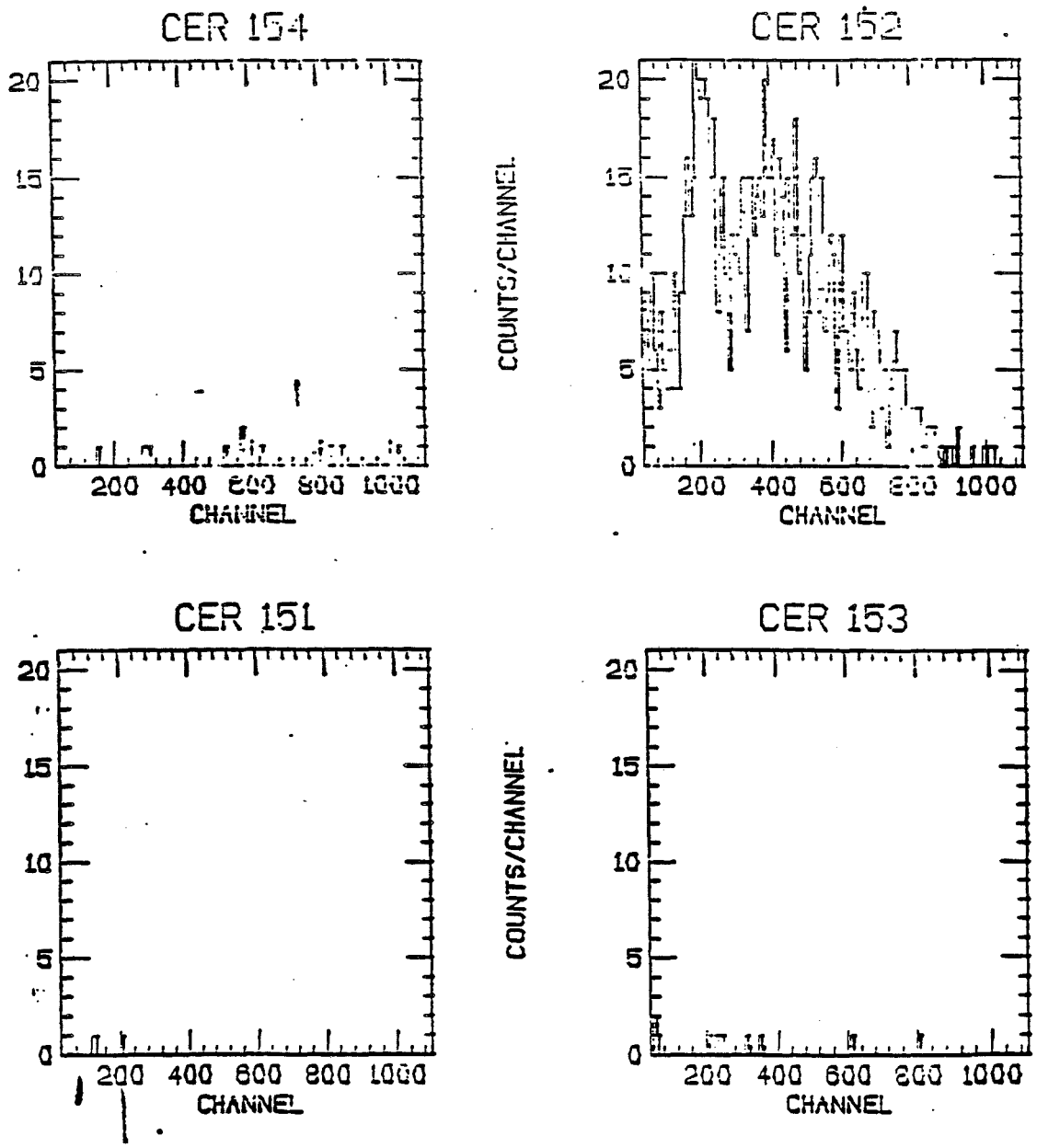

Fig.(5-14)- Helium Gas Pressure = 2.26 psi

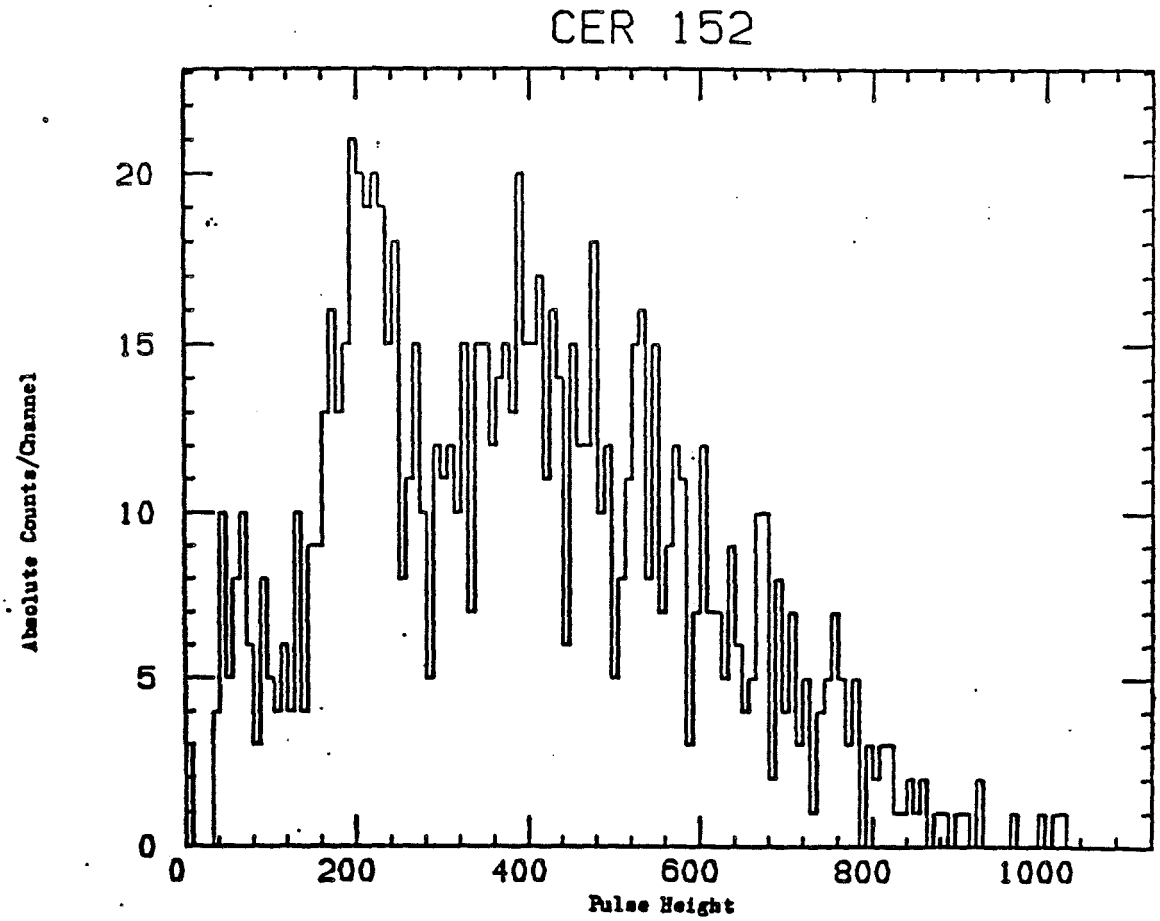

Fig.(5-15)- Helium Gas Pressure = 2.10 psi

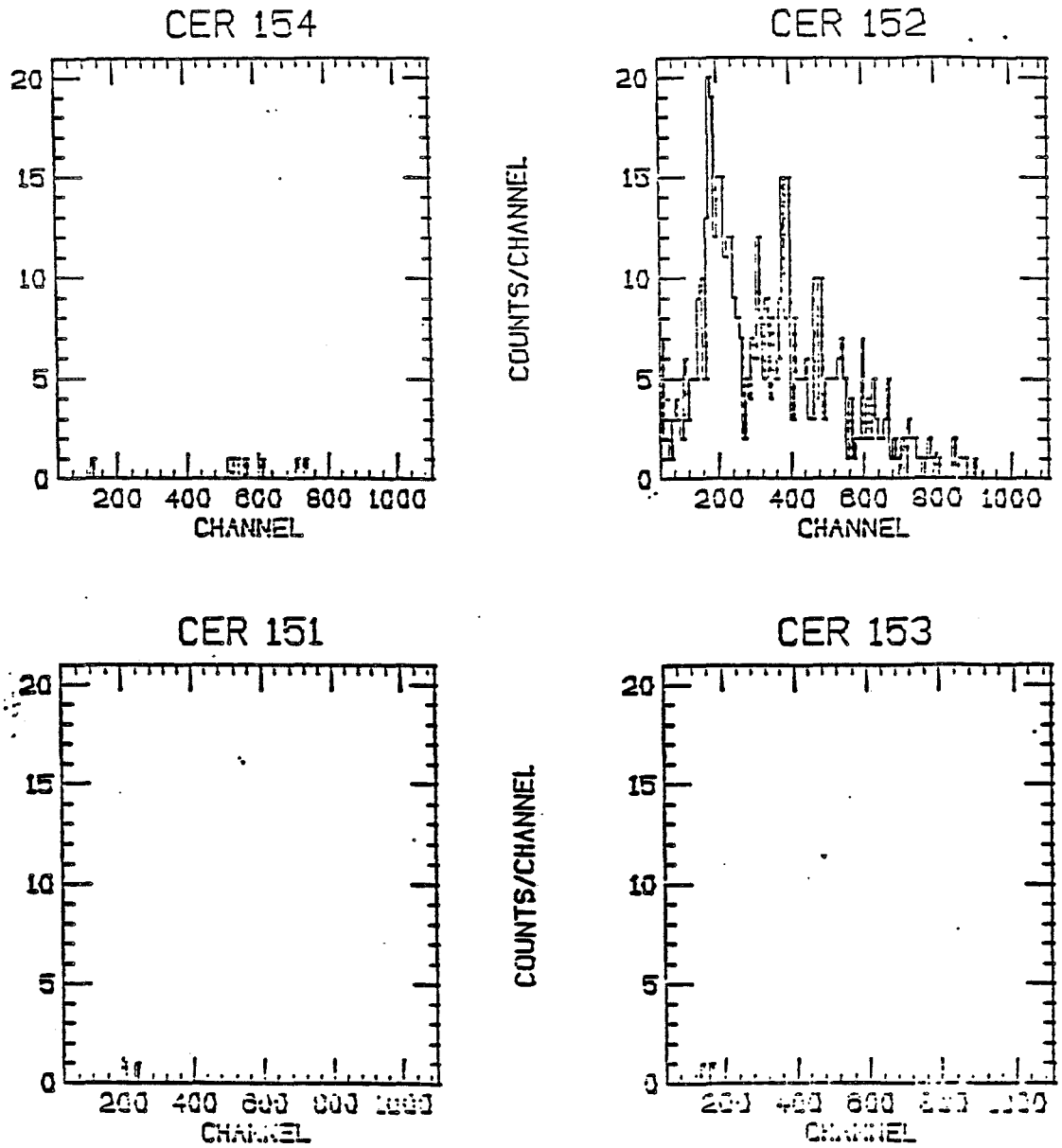

Fig.(5-16)- Helium Gas Pressure = 2.10 psi

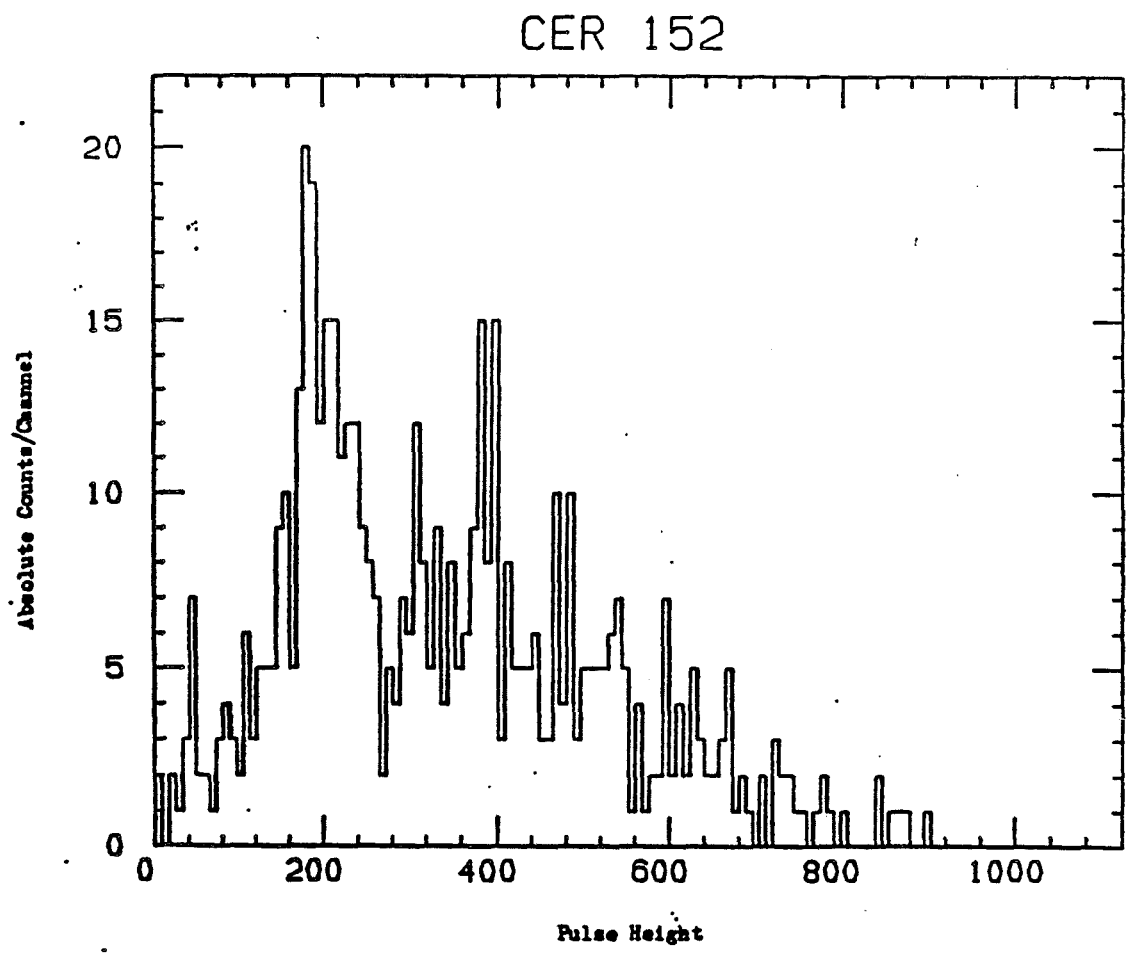

Fig.(5-17)- Helium Gas Pressure = 1.90 psi

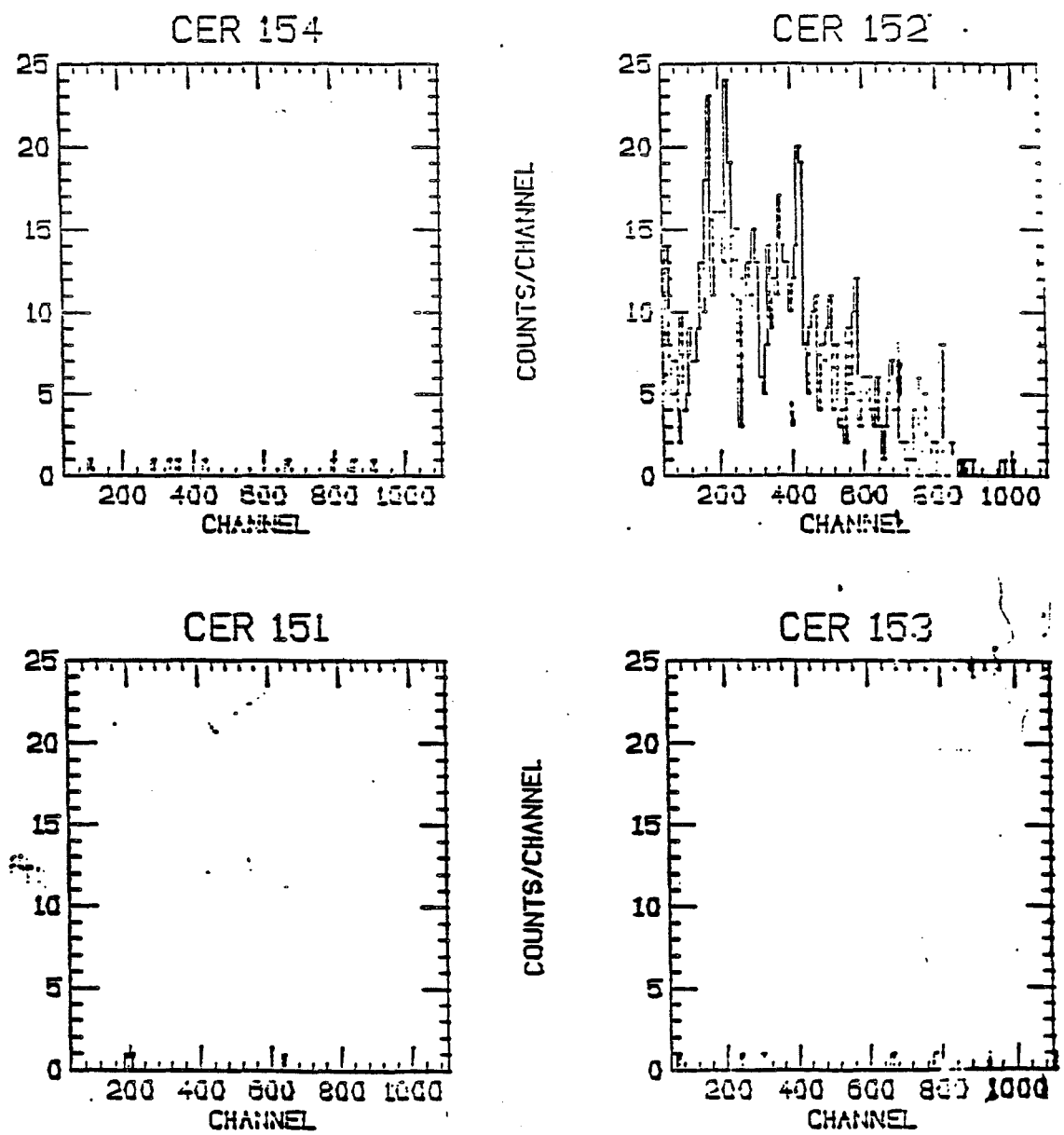

Fig.(5-18)- Helium Gas Pressure = 1.90 psi

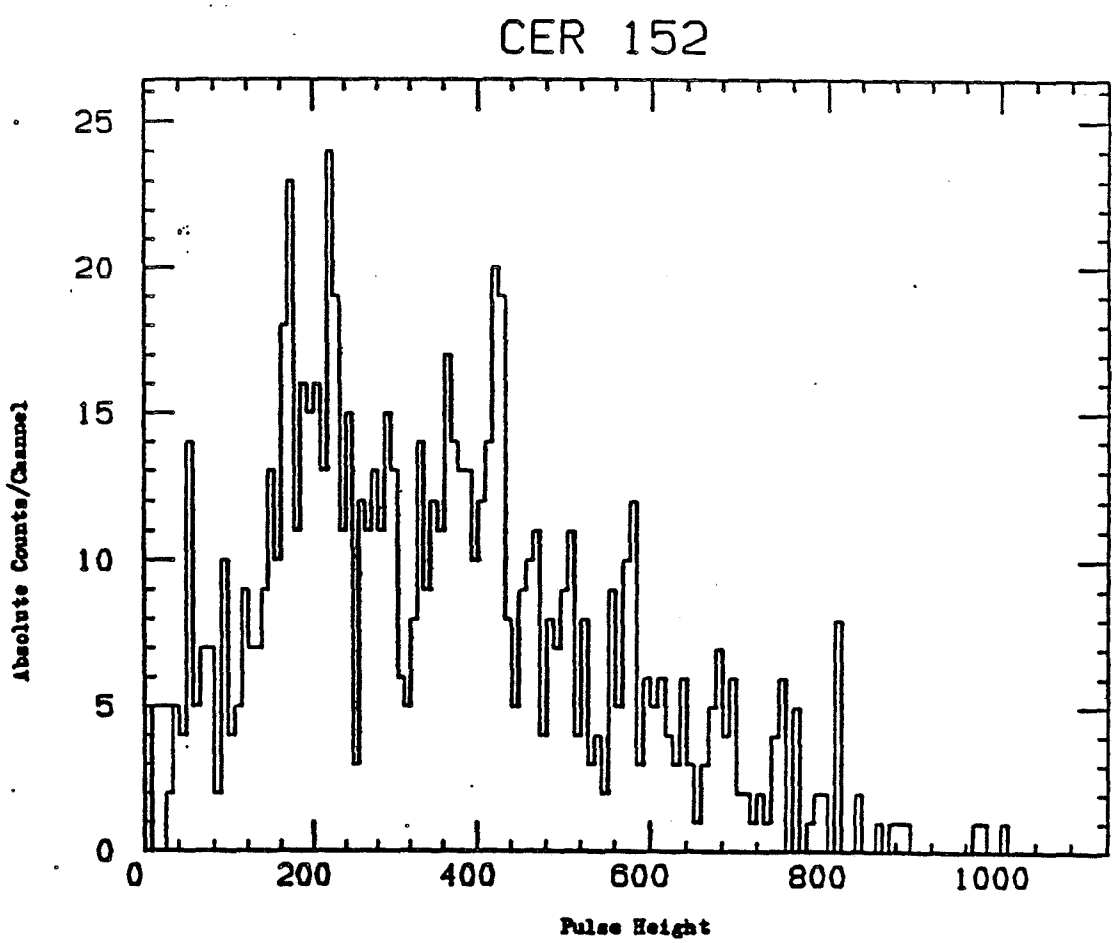

Fig.(5-19)- Helium Gas Pressure = 1.71 psi

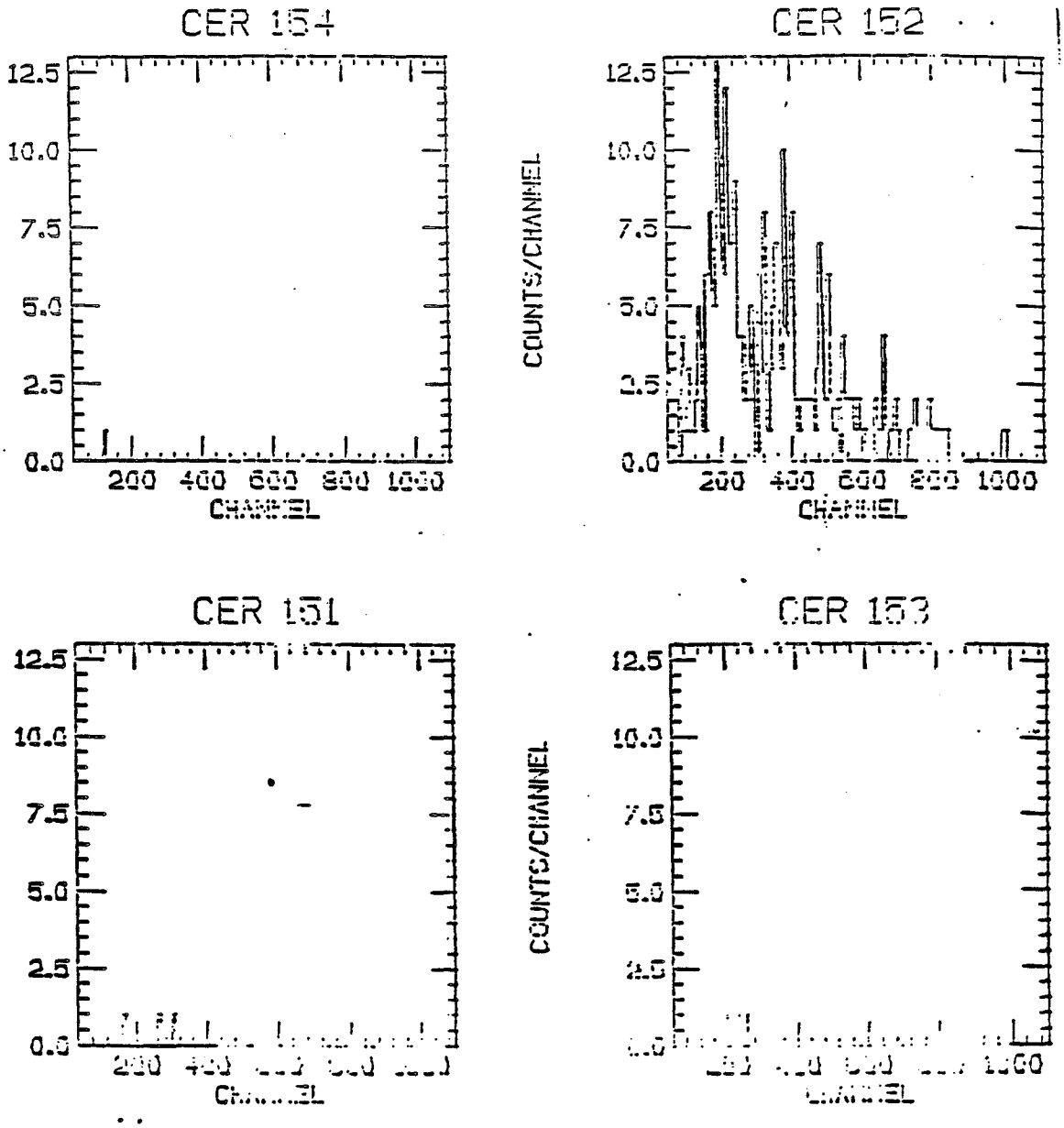

Fig.(5-20)- Helium Gas Pressure = 1.71 psi

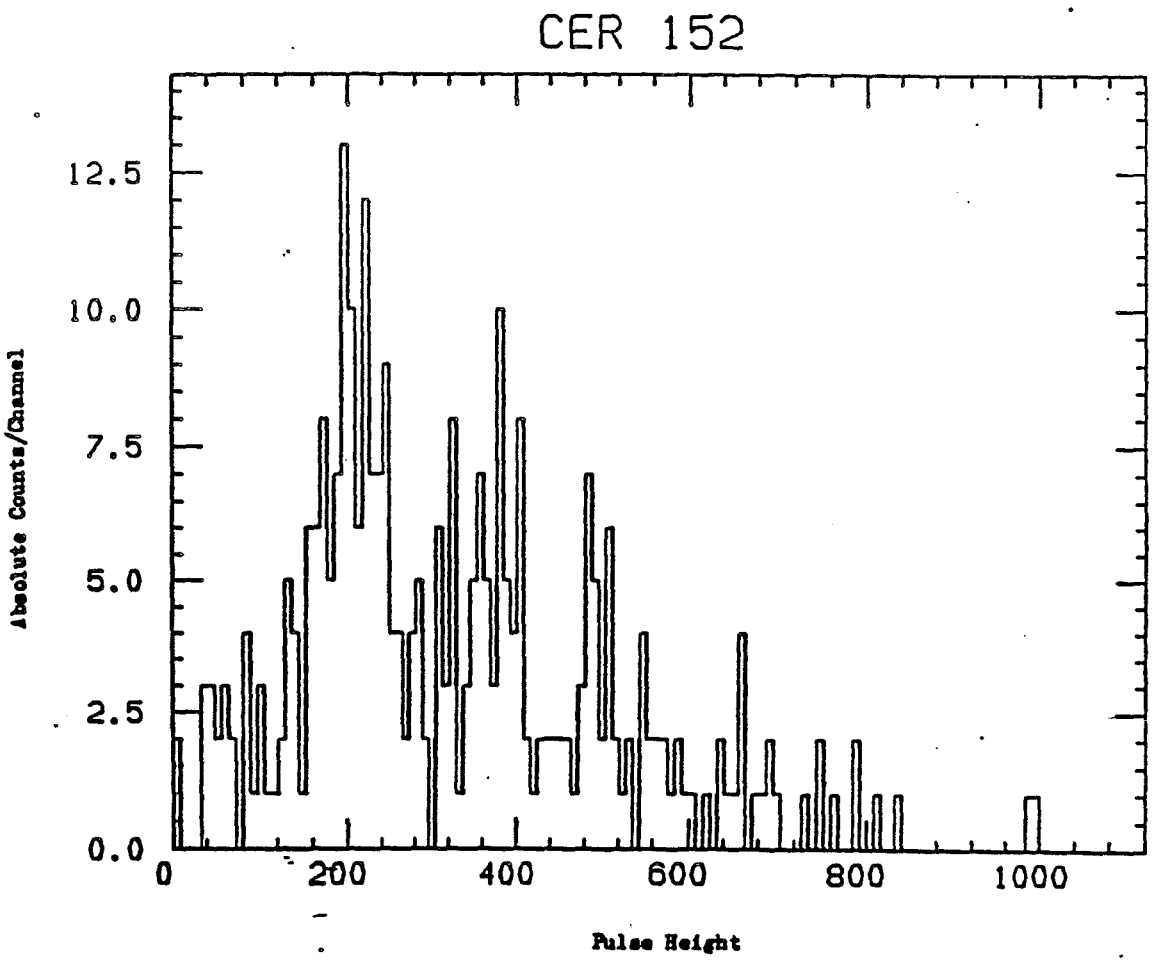

Fig.(5-21)- Helium Gas Pressure = 1.51 psi

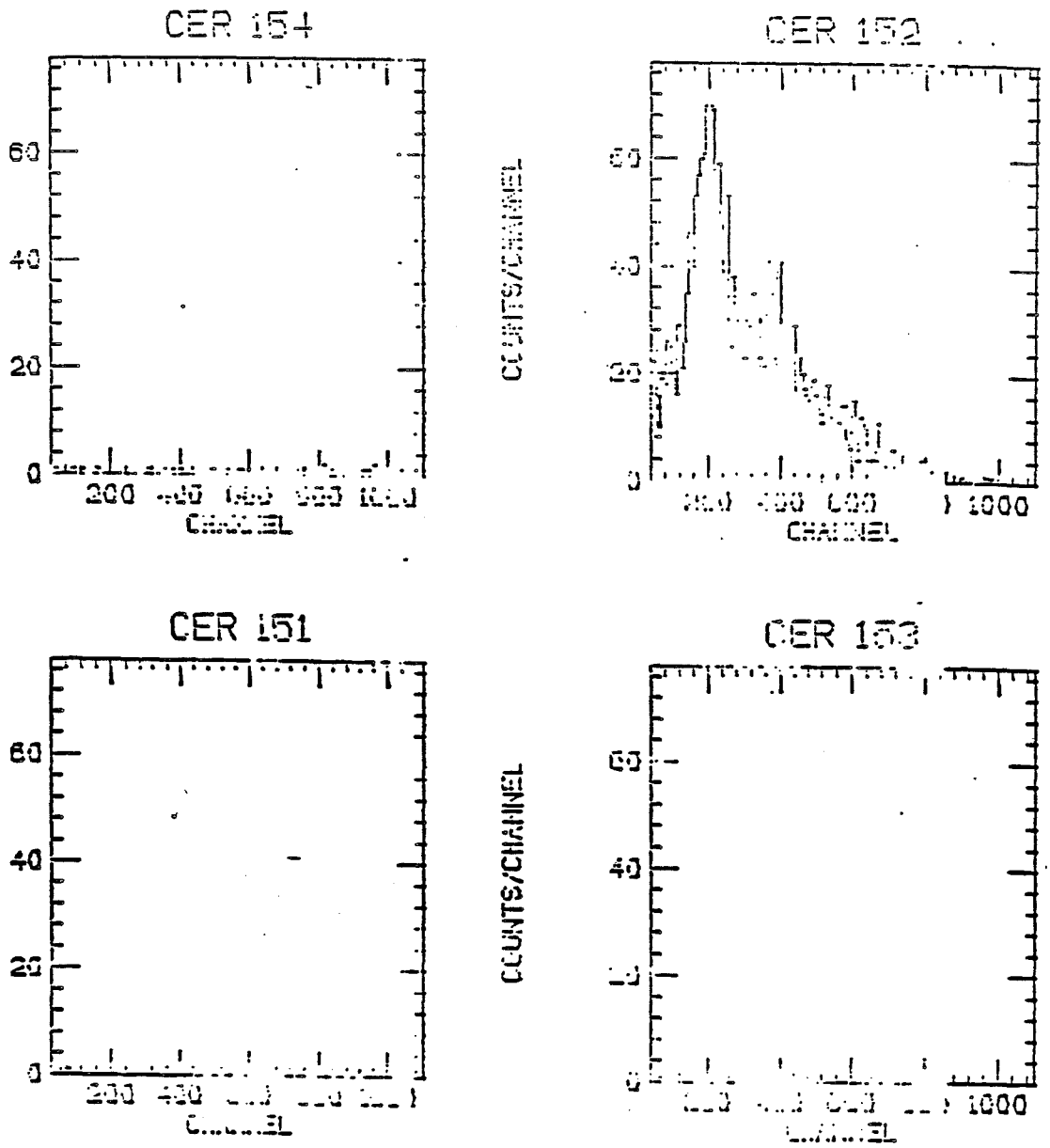

Fig.(5-22)- Helium Gas Pressure = 1.51 psi

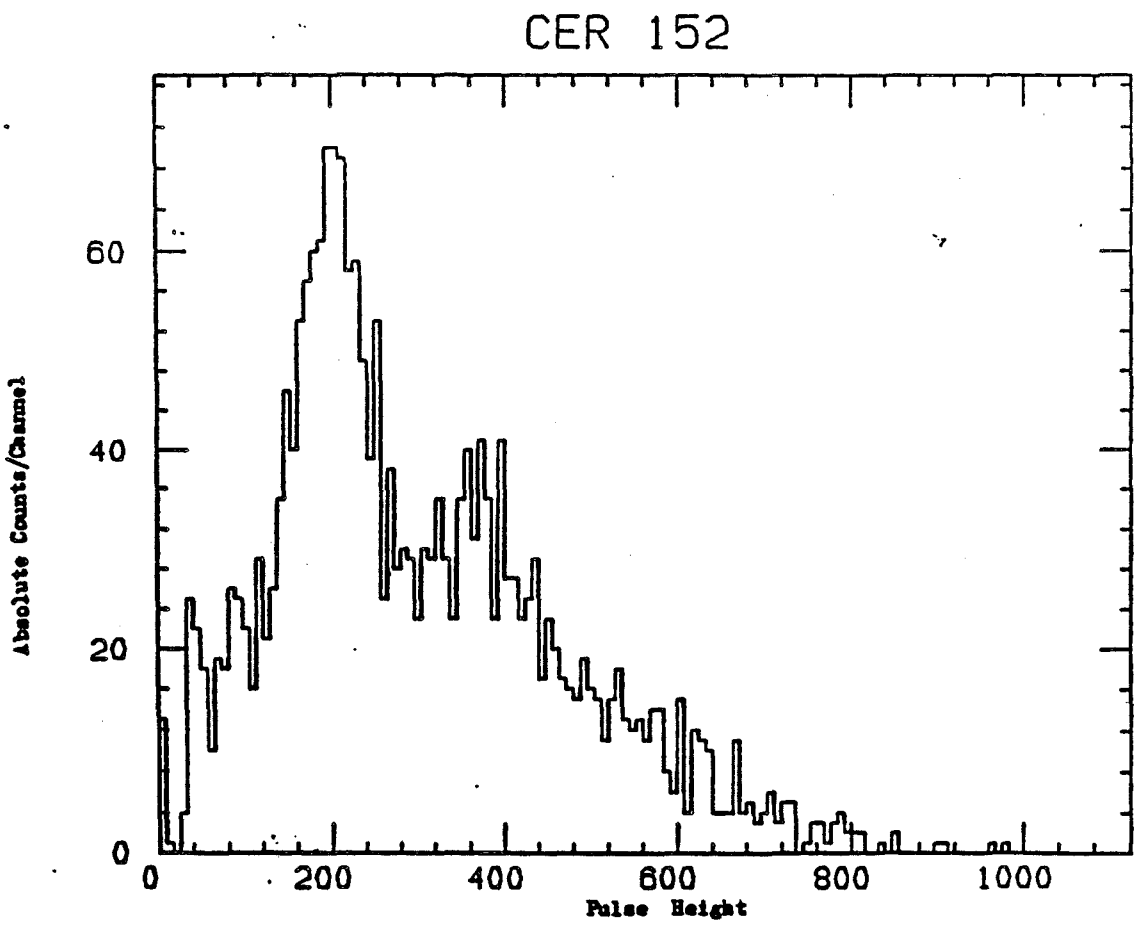

Fig.(5-23)- Helium Gas Pressure = 1.32 psi

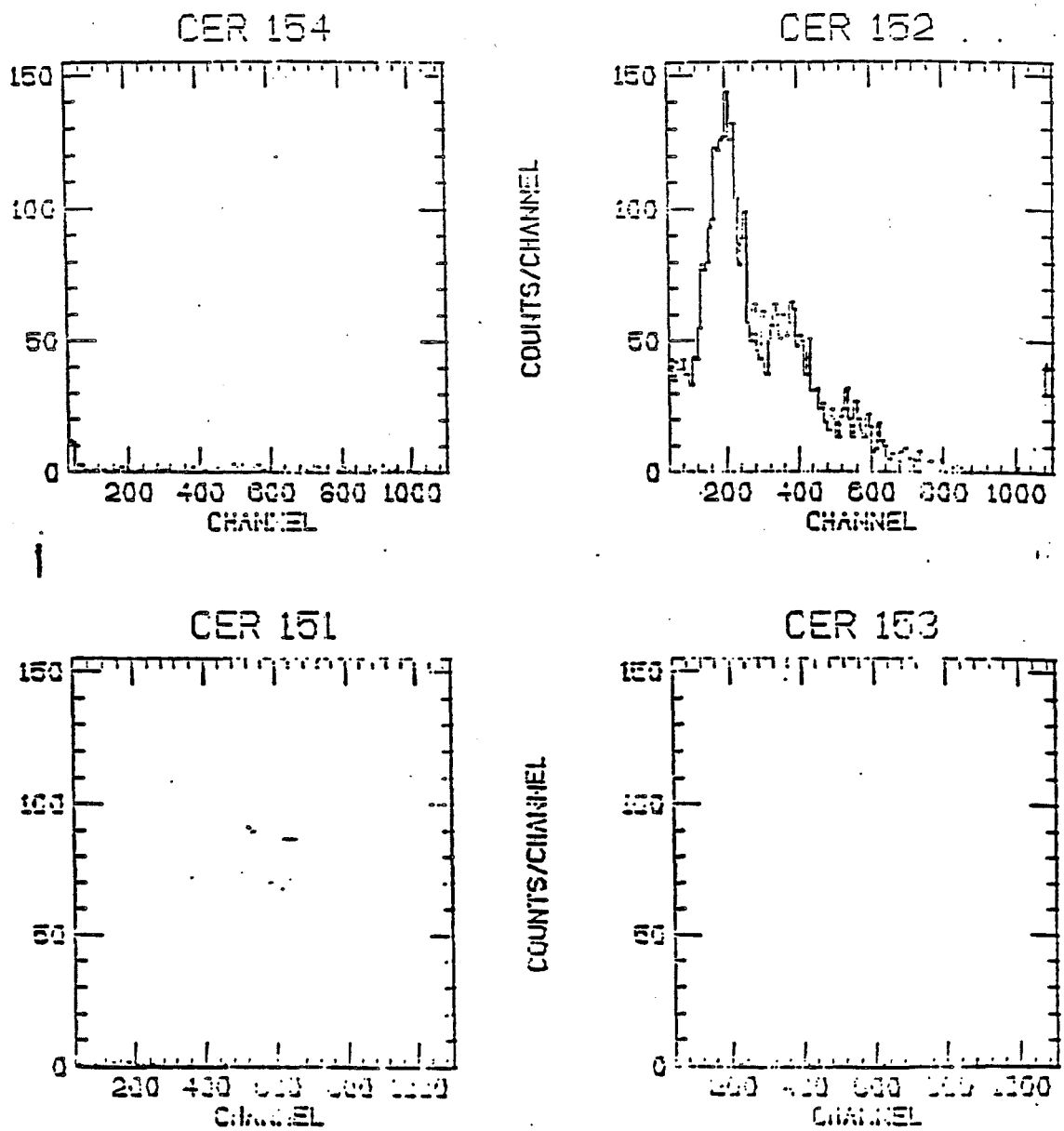

Fig.(5-24)- Helium Gas Pressure = 1.32 psi

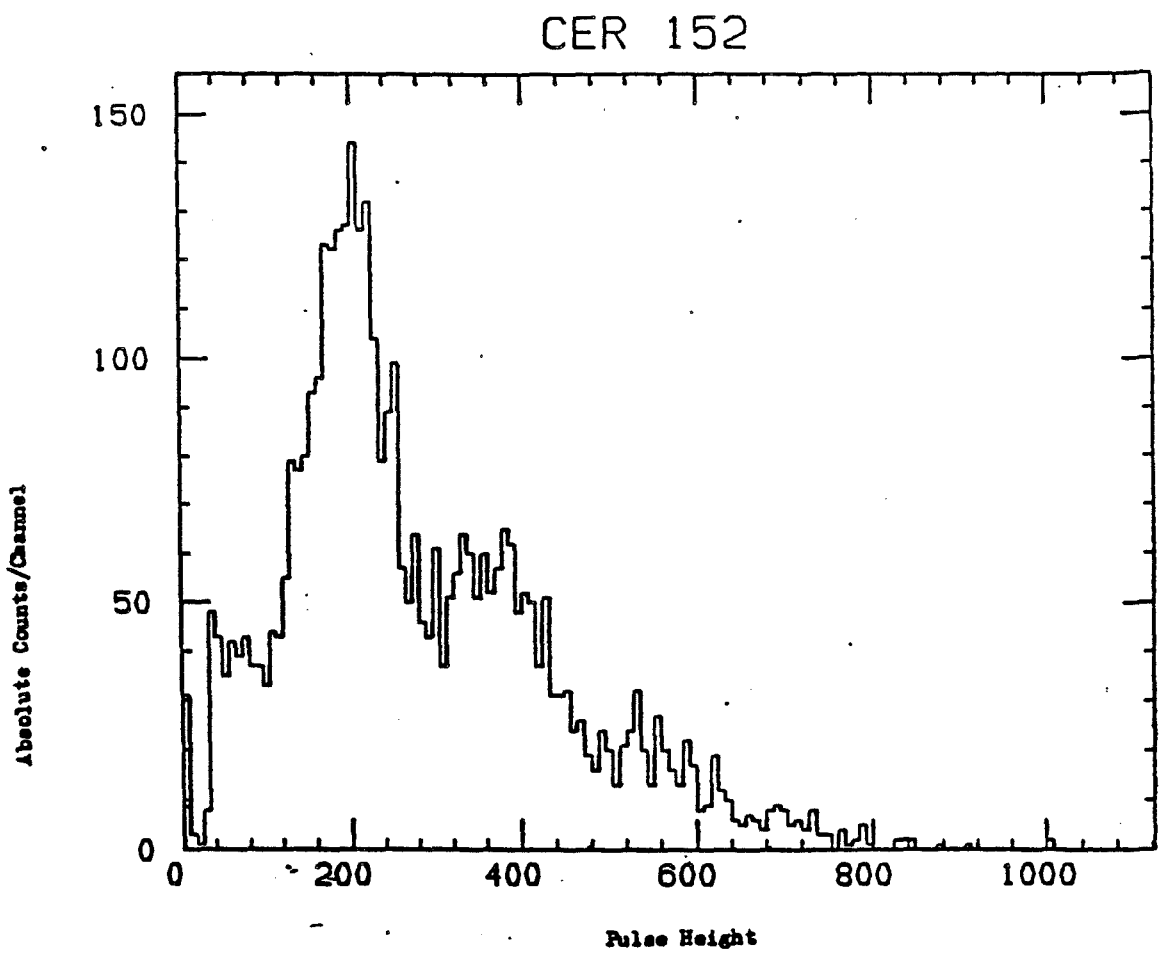

5.3 INTERPRETATION OF PULSE HEIGHT DISTRIBUTIONS

5.3.1 Motivation

To find the absolute efficiency of the Rice Cherenkov Counter we need to understand the Pulse Height Distributions (P.H.D.s), and to find the correspondence of the peaks seen in each spectrum to 1,2,3,...n photo-electrons.

5.3.2 Means of approach

To understand P.H.D.s we will compare three rather different ways to treat the same data. The first method uses the tagged beam measure of efficiency of Cherenkov to deduce the $\langle N_{p.e.} \rangle$. The second method uses the detailed P.H.D.'s which seem to show separate peaks, perhaps attributable to 1,2,3,..n photoelectrons, and have been used to confirm these interpretations. The third method treats the broad P.H.D.s as a broad Gaussian and derives the number of the photo-electrons also.

5.3.3 Analysis of the data

The P.H.D.s recorded during our runs can be roughly classified into the three categories of small, medium and large efficiencies. Figures (5-3), (5-12) and (5-24) show an example of each, respectively.

We define the photocathode inefficiency ϕ as the ratio of zero response to total triggers. One can use ϕ to calculate the average number, $\langle N_{p.e.}\rangle$, of emitted photoelectrons by recalling Poisson's law:

$$\phi = \mathrm{Exp}[-\langle N_{p.e.}\rangle] = 1-\varepsilon \qquad (5\text{-}1)$$

For finite statistics the value of $\langle N_{p.e.}\rangle$ calculated from eq. (5-1) is meaningful only if ϕ is sufficiently large. In practice this means that $\langle N_{p.e.}\rangle$ must be smaller than ~4 to provide a significant determination of ϕ. For larger values of $\langle N_{p.e.}\rangle$ the spectrum is similar to Gaussian. When $\langle N_{p.e.}\rangle \gtrsim 4$ the average pulse-height, μ, and the rms width, σ, are proportional to $\langle N_{p.e.}\rangle$ and $\sqrt{\langle N_{p.e.}\rangle}$ respectively (the proportionality constant is the gain of the P.M.). From this it follows that the ratio μ^2/σ^2 gives directly the value of $\langle N_{p.e.}\rangle$ (independent of the P.M. gain), thus we have

$$\langle N_{p.e.}\rangle = \mu^2/\sigma^2 \qquad (5\text{-}2)$$

For intermediate values of $\langle N_{p.e.}\rangle$, before distribution becomes Gaussian-like, we encounter cases like the one illustrated in Fig. (5-32). Here the Gaussian interpretation of μ^2/σ^2 and the measurement of ϕ are only marginally valid.

For interpretation and analysis of the P.H.D.s represented in sec. 5.2 we chose only those with enough statistics, namely Fig. (5-4), (5-6), (5-10), (5-22) and (5-24). We will use two different methods to determine the average number of photoelectrons for each spectrum, using Poisson and Gaussian statistics. This provides a useful consistency check between the two determinations of $\langle N_{p.e.}\rangle$.

METHOD (1): $\langle N_{p.e.}\rangle = -\ln \phi_{pe} = -\ln(1-\varepsilon(p))$ (5-3)

During our run the pressure and efficiency of each pulse height spectrum was recorded. This data is given in Table 1. Assuming Poisson statistics for the photomultiplier cathode, we use eq. (5-3) to calculate $\langle N_{p.e.}\rangle$ for the five different spectrums which are presented in Table 1.

METHOD (2): Estimating $\langle N_{p.e.}\rangle$ from P.H.D.s

For the three spectrum of Fig. (5-3), (5-12), and (5-24) we assume the observed pulse height distribution can be fitted by the convolution of a poisson and a Gaussian. The form used is

$$\sum \frac{(\langle N_{p.e.}\rangle)^2 \exp[-\langle N_{p.e.}\rangle]}{n!} (2\pi n\sigma^2)^{-1/2} \exp-(x-x)^2/2n\sigma^2$$

To estimate $\langle N_{p.e.}\rangle$ directly from the pulse-height distributions, we fitted Gaussian curves into each spectrum. The curves c_1, c_2, c_3...

are tentatively associated with 1,2,3... photoelectrons, respectively. To find $\langle N_{p.e.} \rangle$ under these assumptions, we multiply the efficiencies, of table 1, by the sum of the weighted integrals of each of the c_n's for the particular pulse height in question, thus;

$$\langle N_{p.e.} \rangle = \frac{\sum nA_n}{\sum A_n} \qquad (5\text{-}4)$$

Where A_n is the integral of the nth Gaussian.

In Table-1 the values of $\langle N_{p.e.} \rangle$ for the two methods,and A_n's for the three pulse-height distributions at different pressures are also presented. These integrals A_n will now be discussed.

To justify our method of approximate graph fitting, we consider the Gaussian fits in Fig. (5-29). First, we notice that the peaks for c_1, c_2, c_3 are at 185, 370, 555 of the ADC channel respectively. That is consistent with the assumption that the number of photoelectrons received from the photocathode must be proportional to the ADC Counts, thus

$$\langle N_{p.e.} \rangle = \frac{\langle ADC \rangle}{B} \qquad (5\text{-}6)$$

where B185 is the constant of proportionality between the number of photoelectrons and the observed ADC counts in the ratios 1:2:3.

Second, the rms width σ's of the Gaussians must be proportional to $\sqrt{\langle N_{p.e.}\rangle}$, therefore;

$$\sigma_{\langle N_{p.e.}\rangle} = sq6,1\langle N_{p.e.}\rangle \; \sigma_{\langle 1_{p.e.}\rangle} \qquad (5\text{-}7)$$

since for a Gaussian curve one has

$$\frac{1}{2.36}FWHM = \sigma \qquad (5\text{-}8)$$

we obtain the following relation between the widths of the Gaussian fits for each pulse-height distribution.

$$W_n = \sqrt{n}\, W_1 \qquad (5\text{-}9)$$

where W_n is the full width at half maximum of the nth Gaussian.

In order to make a consistency check clear, we define the parameter ν_n such that

$$\nu_n = \left(\frac{W_n}{W_1}\right)^2 \frac{1}{n} \qquad ,n>1 \qquad (5\text{-}10)$$

ν_n=1 represent the best possible fit. The calculated values of ν_n presented in Table-2 are indicative of good fits.

Third, using method 1, with the help of poisson's law (eq. 5-11 & 5-12), and efficiency ε, Table-1 we calculate $P_1(n)$'s, the probabilities of having 1,2,3,... photoelectrons, and compare it with the estimated $p_2(n)$'s, using method 2, which we obtain by using eq. (5-13)

$$\langle N_{p.e.} \rangle = -\ln(1-\varepsilon) \qquad (5\text{-}11)$$

$$P_1(n) = \frac{\exp-[\langle N_{p.e.} \rangle]\ (\langle N_{p.e.} \rangle)^n}{n} \qquad (5\text{-}12)$$

$$P_2(n) = \frac{A_n}{\sum A_n} \quad . \qquad (5\text{-}13)$$

For comparison, the ratios of P_1/P_2 are shown in Table-2. We notice that the agreement between $P_1(n)$ and $P_2(n)$ looks reasonable.

METHOD (3): Using eq. (5-2)

To estimate the $\langle N_{p.e.} \rangle$ for the pulse-height distributions of Fig. (5-28) and (5-29) we use equations (5-2) and (5-8) to get

$$\langle N_{p.e.} \rangle = (2.36\ \frac{\text{peak}}{\text{FWHM}})^2. \qquad (5\text{-}14)$$

The values of peaks and FWHMs are shown on each graph, and the average number of estimated photoelectrons are presented in Table-2.

Fig.(5-25)- Guassian curves fitted into the obtained pulse height distribution for helium gas at 1.32 psi. The three fitted curves, from the left to the right of the distribution are representing the one, two, and three photo-electron contributions to the pulse height distribution.

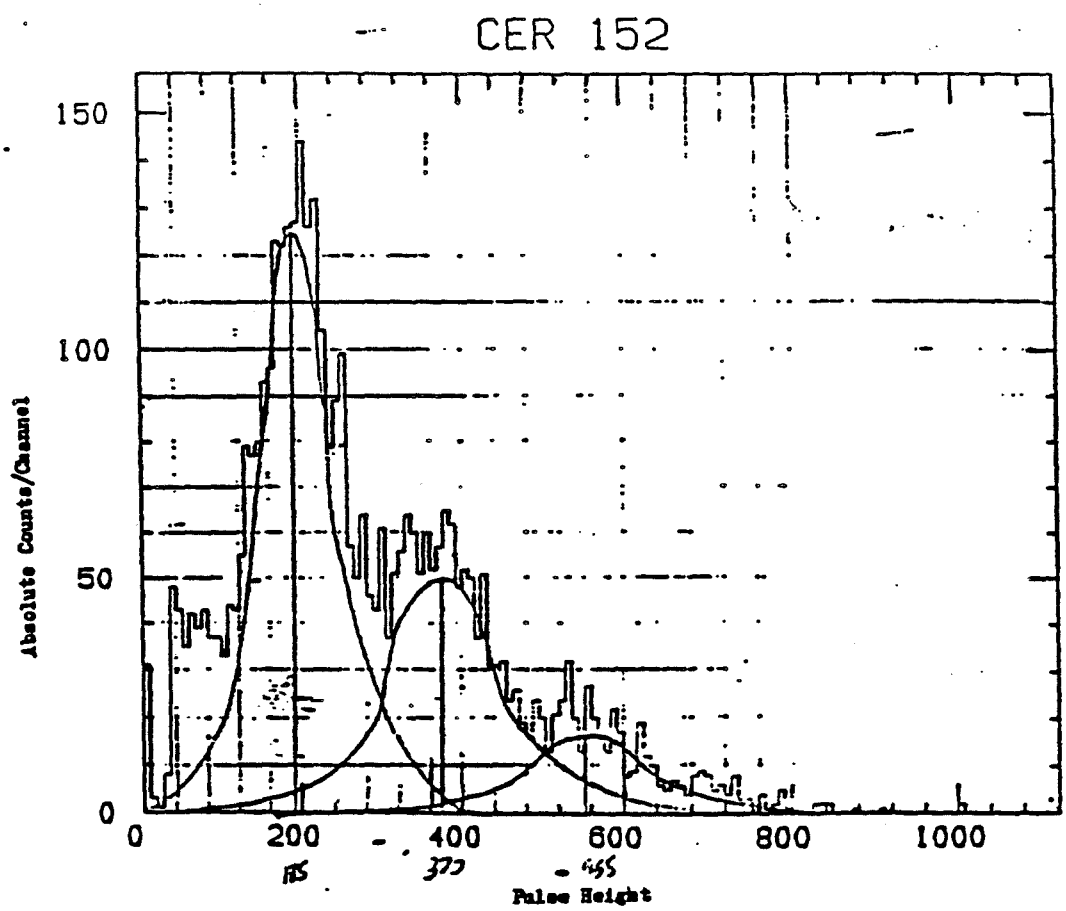

Fig.(5-26)- Guassian curves fitted into the obtained pulse height distribution for helium gas at 1.51 psi. The three fitted curves, from the left to the right of the distribution are representing the one, two, and three photo-electron contributions to the pulse height distribution.

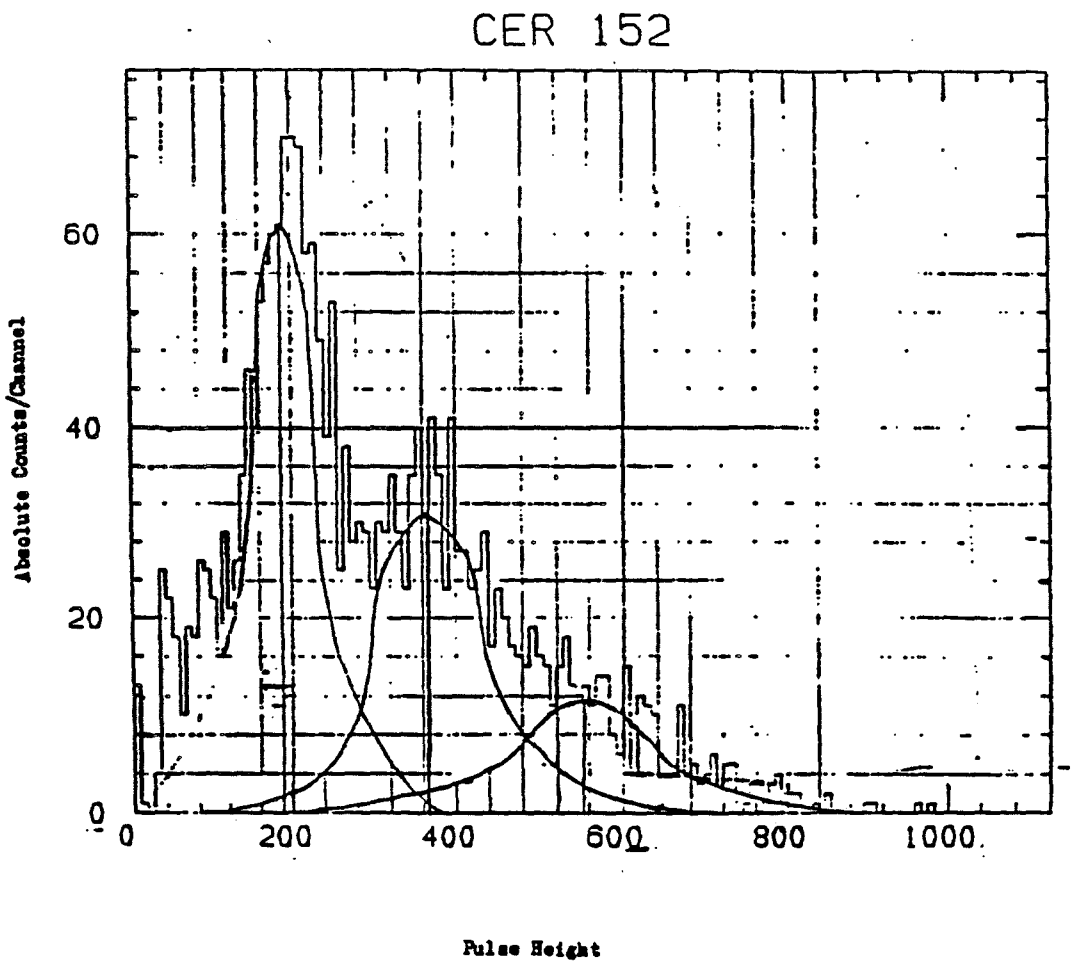

Fig.(5-27)- Guassian curves fitted into the obtained pulse height distribution for helium gas at 2.70 psi. The five fitted curves, from the left to the right of the distribution are representing the 1, 2, 3, 4, and 5 photo-electron contributions to the pulse height distribution.

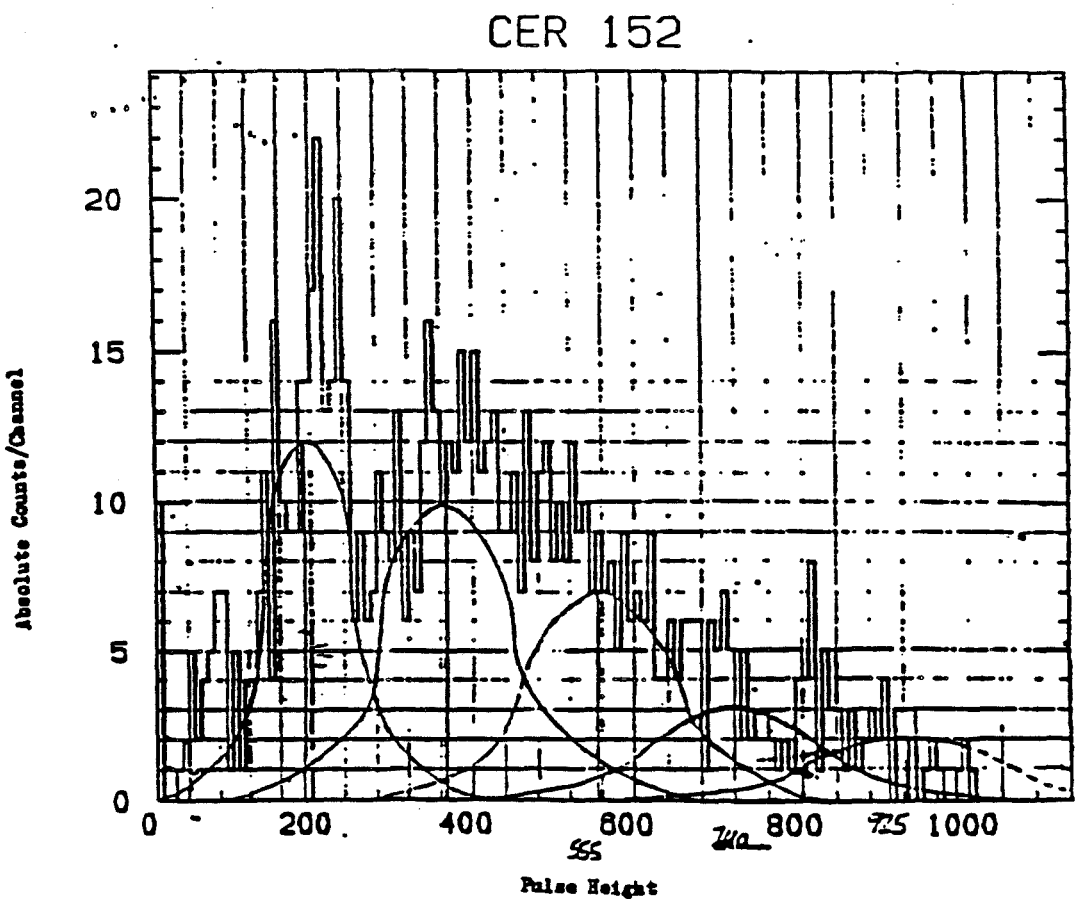

Fig.(5-28)- Guassian curve fitted into the obtained pulse height distribution for helium gas at 3.47 psi.

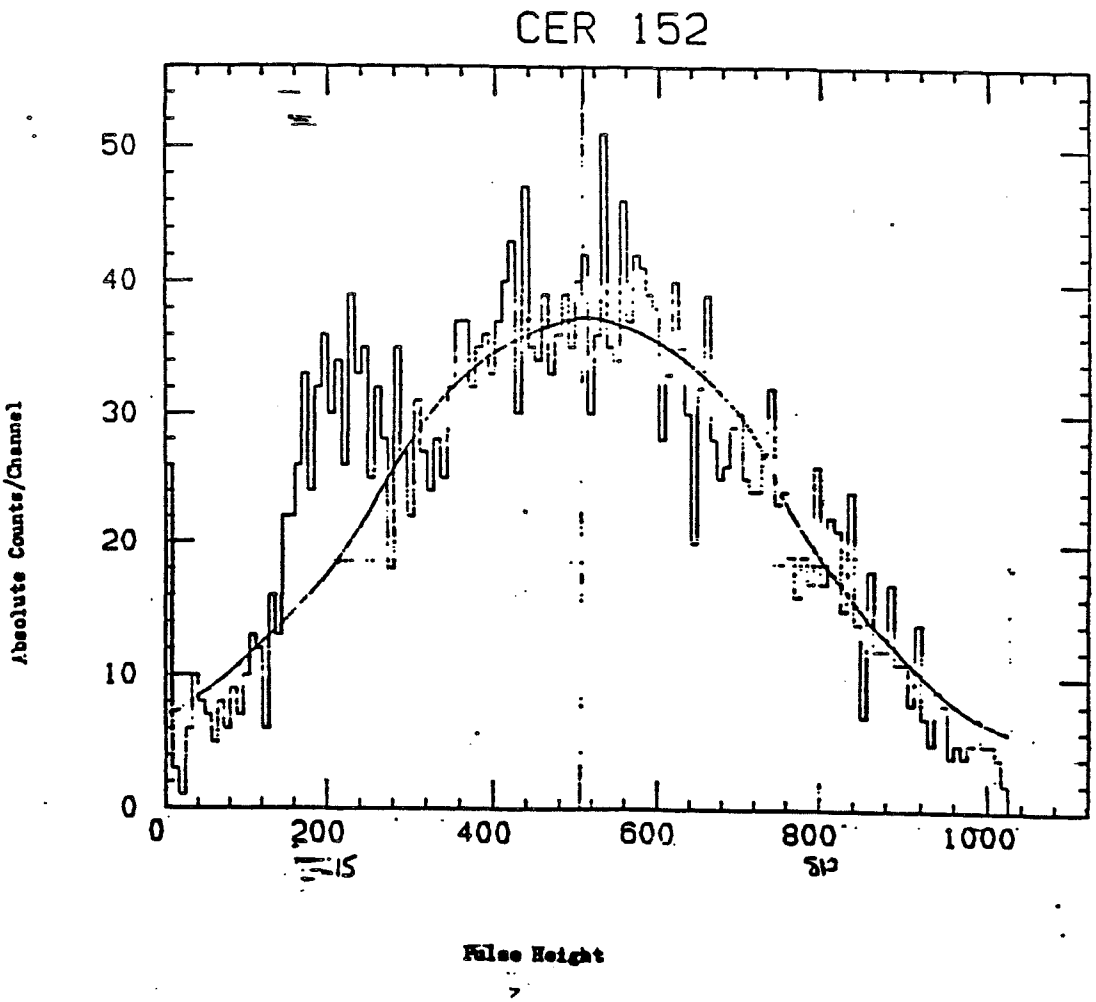

Fig.(5-29)- Guassian curve fitted into the obtained pulse height distribution for helium gas at 4.18 psi.

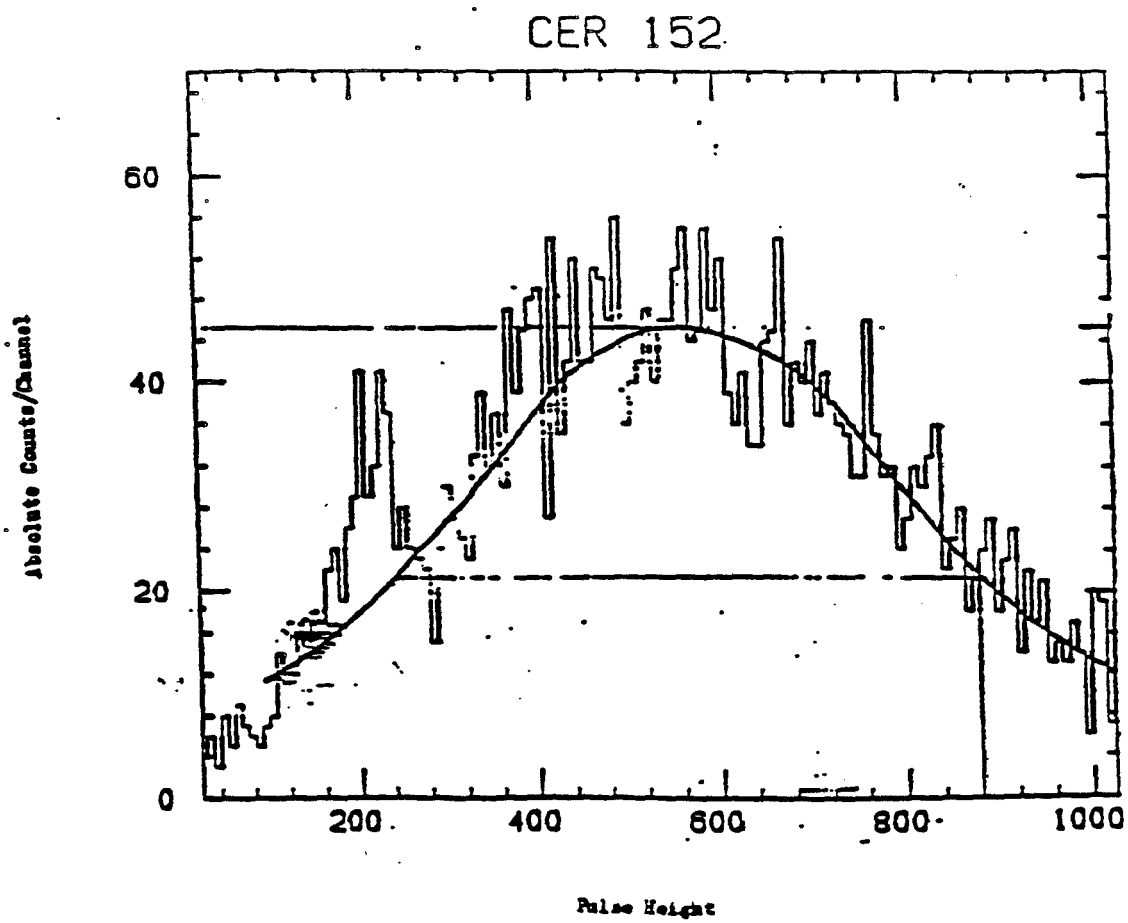

Table-I

Helium Gas Pressure (Psi)	Efficiency (ε) %	$\overline{N}_{p.e.}$ METH. I	METH. II	METH. III	λ_1	λ_2	λ_3	λ_4	λ_5
4.18	98.09	3.91		4.26					
3.47	96.56	3.37		4.01					
3.00	93.11	2.67							
2.70	89.48	2.25	2.15		42.0	51.5	37.5	19.0	10.0
2.50	91.15	2.42							
2.26	87.08	2.05							
1.90	82.11	1.72							
1.71	81.62	1.56							
1.51	76.33	1.44	1.28		46.0	33.5	15.5		
1.32	70.73	1.24	1.10		38.5	24.5	7.5		

Table- I

$\Delta\lambda_1$	$\Delta\lambda_2$	$\Delta\lambda_3$	$\Delta\lambda_4$	$\Delta\lambda_5$
±.5	±.5	±.5	±.5	±.5

EXPERIMENTAL RESULTS

Table II

Helium Gas Pressure (Psi)	W_1	W_2	W_3	W_4	W_5	2	3	4	5	$P_I(0)$	$P_I(1)$	$P_I(2)$	$P_I(3)$	$P_I(4)$	$P_I(5)$
1.32	0.6	0.9	1.0	-	-	1.13	0.93	-	-	0.29	0.36	0.22	0.09	-	-
1.51	0.6	0.8	1.1	-	-	0.89	1.12	-	-	0.24	0.34	0.25	0.12	-	-
2.70	0.7	1.0	1.2	1.4	1.5	1.02	0.98	1.0	0.92	0.11	0.24	0.27	0.20	0.11	0.05

Helium Gas Pressure (Psi)	$P_{II}(0)$	$P_{II}(1)$	$P_{II}(2)$	$P_{II}(3)$	$P_{II}(4)$	$P_{II}(5)$
1.32	0.29	0.39	0.25	0.08	-	-
1.51	0.24	0.37	0.27	0.12	-	-
2.70	0.11	0.23	0.29	0.21	0.11	0.06

Table- II

5.3.4 Conclusion of the P.H.D. study.

Based upon the checks discussed in the previous section, for the three methods investigated, we can calculate the average number of the photoelectrons for any going-through charged particle. This in turn enabled us to calculate the efficiency curve of the (Rice) Cherenkov Counter.

CHAPTER 6

CONCLUSIONS

We have built and successfully tested a large system of gas Cherenkov Counter, making use of low refractive index Helium. The average number of photoelectrons per event was obtained and recorded. This number results in a photo-electron yield of

$$N_o = 95 \text{ cm}^{-1}.$$

This has to be compared to the theoretical value, N_o 146.2, given by eq. (6.3).

We are pleased of the fact that for such a large system we achieved the average collection efficiency of $N_o = 95 \text{ cm}^{-1}$.

Additional tests need to be carried out in the following areas:

1. Comparisons of the response with and without wavelength shifter.

2. Measurements with high energy protons and pions to confirm the instrument's ability to effect their identification.

REFERENCES

[1] J.D. Jackson, Classical Electrodynamics, (1975).

[2] R.L. Anderson and J.D. Grant, Nuclear Instruments and Methods 135 (1976) 267-283.

[3] P.J. Carlson, Nuclear Instruments and Methods 158 (1979) 406.

[4] Richmond Tank Car Co., Houston, Texas.

[5] S&S Optical Co., New Haven, Indiana.

[6] Evaporated Metal Film Co., Ithaca, New York.

[7] Dell Optics Co.

[8] Makoto Takiue, Harwo Fujii, Hiroaki Ishikawa, Nuclear Instruments and Methods in Physics Research 227 (1984) 571-575.

[9] P.J. Carlson Nuclear Instruments and Methods 158 (1979).

[10] Gary Moss,

[11] J.P. O'Callaghan, R. Stanek and L.G. Hyman, Nuclear Instruments and Methods in Physics Research 225 (1984) 153-156.

[12] J.A. Grant and R.L. Carlson, Nuclear Instruments and Methods 135 (1976) 267-271.